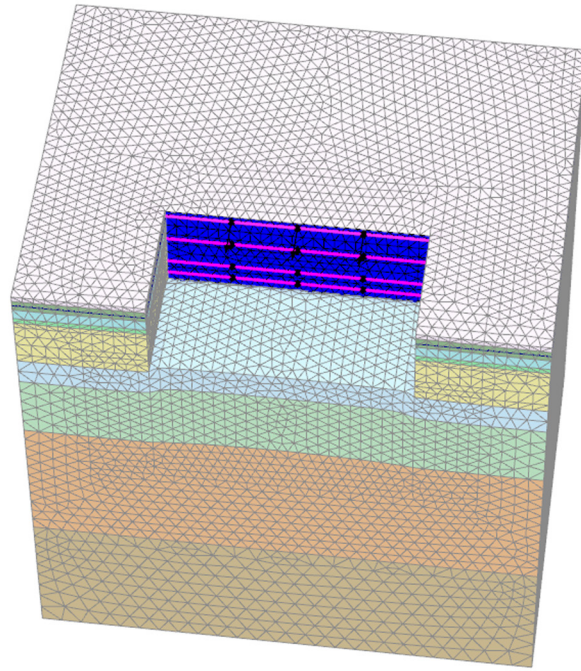




LUND
UNIVERSITY



3D-EFFECTS IN TOTAL STABILITY EVALUATIONS

ANTON KARLSSON and
STEFAN JARL WELLERSHAUS

Geotechnical
Engineering

Master's Dissertation

DEPARTMENT OF CONSTRUCTION SCIENCES

GEOTECHNICAL ENGINEERING

ISRN LUTVDG/TVGT--14/5051--SE (1-108) | ISSN 0349-4977

MASTER'S DISSERTATION

3D-EFFECTS IN TOTAL STABILITY EVALUATIONS

ANTON KARLSSON and STEFAN JARL WELLERSHAUS

Supervisors: Prof. **OLA DAHLBLOM**; Dept. of Construction Sciences, LTH, Lund
and **DANIEL BALTRÖCK**, MSc.

Examiner: Prof. **KENT PERSSON**, PhD; Dept. of Construction Sciences, LTH, Lund.

Copyright © 2014 Geotechnical Engineering,
Dept. of Construction Sciences, Faculty of Engineering (LTH), Lund University, Sweden.

Printed by Media-Tryck LU, Lund, Sweden, August 2014 (*PI*).

For information, address:

Geotechnical Engineering, Dept. of Construction Sciences,
Faculty of Engineering (LTH), Lund University, Box 118, SE-221 00 Lund, Sweden.

Homepage: <http://www.byggvetenskaper.lth.se/geoteknik>

Abstract

This master's dissertation has been performed in cooperation with *Tyréns* and the *Dept. of Construction Sciences, LTH*. We have investigated if it is possible to increase the total stability for excavations with retaining structures and if each side of an excavation could be treated as a separate 2D-case with additional theories to approximate its 3D-effects.

End-surface theories from the *Commission on slope stability (CSS) report 3:95* could possibly be used to consider 3D-effects although they are originally created for slopes without structural support. Neither is there any information regarding the interaction between these separated 2D-systems.

The intention of this master's dissertation is to validate that these theories mentioned can be used and that it is reasonable doing so.

It is done by evaluating three different kinds of systems namely

- Generalised sloped excavations where corners and thus interactions between sides are introduced into the model but without structure to examine end-surface- and additional 3D-effects where the applied theories are valid.
- Generalised excavation with retaining structure to determine corner-, end-surface- and structural effects.
- The theories evaluated are then applied to a real life case with material- and structural parameters evaluated from the *Västlänken* project. Here the possibility of excavating a 70x70x15 m (length, width, depth) is investigated.

For all of the modelling steps; analytical and numerical calculations have been performed, where *Slope/W* has been used to aid the analytical calculations and *Plaxis-2D* and *3D* have been used for 2D and 3D modelling.

Evident in the results assembled in this work is that 2D-analytical calculations underestimates the total stability (*FS*) for an excavation when compared to numerical calculations. Applying the end surface theory from *CSS report 3:95* generates results similar to the ones generated by 3D modelling, but on the safe side. This final comparison was made without considering the stabilising effect that can be accounted for due to the retaining structural connections in the corners.

Keywords: slope stabilization, geotechnical engineering, total stability, 3D-effects, factor of safety, *Plaxis*

Acknowledgements

This master's dissertation project was conducted at the Department of Construction Science at LTH, Lund University and in cooperation with Tyréns AB, from December 2013 until May 2014.

We want to thank everyone that has helped us during this time. Without the help from others this project would not have been possible to undertake.

There are however some key people that we want to express our thanks to, our supervisors; Daniel Baltrock (*Geotechnical engineer, PEAB*), who has guided us and answered our questions along the progression of this project with an undying interest and Prof. Ola Dahlblom (*Dept. of Construction Sciences, LTH*), for all the help with theoretical problems and interesting discussions.

Furthermore we want to express our thanks to Tyréns; especially Henrik Möller and Tim Björkmam for the aid with questions surrounding the *Västlänken* project and the material that has been provided to us.

With our time at LTH coming to an end with the completion of this dissertation, we want to thank all of our friends, family and others for their support during our time in Lund.

Lund, May 2014



Anton Karlsson



Stefan Jarl Wellershaus

Notations

Latin upper case letters

A	Area (cross-section)
$A_{Slip\ surface}$	Area of slip surface
I	Unit matrix
C	Stiffness matrix
C_c	Compression index
C_s	Swelling index or Reloading index
D	Material stiffness matrix
E	Young's modulus
E_1, E_2	Young's modulus one and two
EA	Axial stiffness
EI	Bending stiffness
E_{50}^{ref}	Secant stiffness at a reference stress level
E_{oed}^{ref}	Oedometer modulus at a reference stress level
E_{ur}^{ref}	Unloading/reloading stiffness at a reference stress level
FS_{2D}	2D factor of safety (standard analytical FS)
FS_p	Factor of Safety, 3:95 increase with planar end surfaces
FS_{3-Dim}	Reduced FS_p , due to non-planar end surfaces
$FS_{2D-Plaxis}$	2D factor of safety calculated in <i>Plaxis 2D</i>
$FS_{3D-Plaxis}$	Factor of safety calculated in <i>Plaxis 3D</i>
G	Shear modulus
H	Height of slope
H	Height of retaining structure
I	Moment of inertia
\bar{I}	Invariant
\bar{J}	Invariant
K_α	Hardening parameters
K_0	Coefficient for initial earth-pressure
K_{0NC}	Coefficient for normal consolidated soils at rest
$L_{Spacing}$	Spacing of supporting anchors
$M_{Resisting}$	Resisting moment
$M_{Activating}$	Activating moment
P	Normal force
R	Radius
S	Stress tensor
W	Weight

Latin lower case letters

b	Width of a slice
c	Cohesion
c_{inc}	Cohesion increase
c'	Effective cohesion
c_u	Undrained shear strength
h	Thickness (cross section)
l	Length of slice/slope
n	Unit vector
e	Deviatoric strain tensor
s	Stress invariant matrix
t	Thickness
u_i	Displacement
t_x, t_y, t_z	Body loads
w	Unit weight

Greek lower case letters

α	Inclination
α_{ij}	Kinematic hardening parameter
γ_{Soil}	Weight of soil
ε	Strain
λ	Eigen value
σ	Total stress
σ'	Effective stress
$\sigma_1, \sigma_2, \sigma_3$	Principal stresses
σ_n	Normal stress
σ_{y0}	Initial yield stress
σ_y	Yield stress
κ	Slope of unloading/reloading
τ	Shear stress
τ_{ij}	Shear stress
τ_{max}	Maximum shear stress (failure shear stress)
δ	Kronecker's delta
ν	Poisson's ratio
γ_{ij}	Shear strain
γ_s	Deviatoric strain
θ	Arc width
φ'	Internal friction angle

Abbreviations

<i>2D</i>	Two Dimensional
<i>3D</i>	Three Dimensional
<i>FS</i>	Factor of Safety
<i>FE</i>	Finite Element
<i>FEM</i>	Finite Element Method
<i>MS</i>	Method of Slices
<i>CSS</i>	Commission on Slope Stability
<i>IVA</i>	“Ingenjörsvetenskapsakademien”

Contents

1	Introduction	1
1.1	Background	1
1.2	Objective	2
1.3	Method	3
1.4	Disposition	3
1.5	Limitations	4
2	Theory	5
2.1	Analytical Calculation Theory	5
2.2	Strain invariants	11
2.3	Stress invariants	13
2.4	Various cases of stress	17
2.5	Plane Elasticity	18
2.6	Plasticity theory	19
2.7	Post yield	24
2.8	Hardening rule	27
3	Material Models	33
3.1	Mohr-Coulomb model	33
3.2	Hardening Soil model	36
4	Calculations and Modelling Methods	43
4.1	Software introduction	44
4.2	Generalised slope	50
4.3	Generalised excavation pit with retaining structure.....	53
4.4	Real-life case (<i>Västlänken</i> project)	58
5	Results	63
5.1	Generalised slope	63
5.2	Generalised excavation pit with retaining structure.....	68
5.3	Real-life case (<i>Västlänken</i> project)	74
6	Discussion and Conclusion	79

6.1 Discussion.....	79
6.2 Suggestions for further work.....	82
7 Bibliographies	85
Appendix.....	87
A - Material parameters.....	87
B - Slope results	90
C - Plaxis 2D Results	98
D - Real-life case (Västlänken project).....	100
E - Structural elements in Plaxis 3D.....	101

1 Introduction

1.1 Background

Tyréns and COWI are designing the future underground central station for the new railway system in Gothenburg, Sweden. The project is a huge undertaking with a large excavation planned where the new central station will be placed.

This large excavation in very soft clay has raised some concerns regarding the total stability of the entire excavation. Due to the circumstances it has been difficult to find a solution for a supporting structure that is possible to accomplish in reality with a satisfying factor of safety.

It is normal to use traditional 2D slope stability methods when calculating stability for vertical walls surrounding excavation pits, handling each side as a separate 2D-case. It has been proposed that it would be of great advantage to be able to account for 3D-effects when performing these 2-dimensional stability calculations. A method, described in the *Swedish commission of slope stability report 3:95*, is used to account for 3D-effects resulting from the shear strength of the end-surfaces for slope stability.

The method can be applied on slopes with variations in geometry and is especially efficient for slopes that have a limited length and a deep slip surface. It seems reasonable to think that this is also true for a square excavation where each side of the excavation can be seen as a single slope having a limited length.

If further investigations show that this model and these “3D-effects” is a reasonable approximation also for other types of systems i.e. systems with structural support, it would be of great advantage.

Studies have been performed in Singapore where estimated 3D effects around corners have been measured in terms of horizontal displacements ((Lee, et al. 1998) and (Ou and Shia 1989)). The deformations around and in the excavation have been compared to show that there are effects in the system making it more stable around the corners. Different relations for the magnitude of these effects that can be expected have been concluded from the experiments.

There is an indication that there is less deformation at the corners. If this is related to the 3D-effects (related to the end surfaces theory) is hard to say, but not unlikely.

1.2 Objective

This project has the objective to evaluate if it is reasonable, or at least on the safe side, to calculate the total stability for one single side in an excavation by using 2-dimensional analytical calculation methods with additional approximations of the 3D-effects, thereby giving a better approximation of the actual factor of safety.

In this dissertation, an attempt is made to answer the following questions:

Approximating the 3D-effect of a slope by adding the shear forces from the end areas of the sliding volume sounds reasonable but does it work if two sliding volumes interact as they do at the corner of a square excavation?

Is it a good approximation? Is it equally as good if constructions are inserted? Is the assumption and approximation on the safe side? To what extent is it on the safe side?

When modelling in a true 3D manner there are effects that in reality could influence the stability of the system (which are not accounted for in a two-dimensional calculation). The FE-programs (in this case *Plaxis 2D* and *3D*) accounts for all sorts of different phenomena that could increase/decrease the total stability. The exact reason for this increase/decrease is hard or even impossible to pinpoint.

To simplify for the readers and the authors of this report the objectives has been divided into three major parts.

- Part one is to investigate and evaluate the usage of 3D-effects in 2D-cases without supporting structures. Here the evaluation of how good this approximation is compared to the numerical 3D-systems factor of safety is made.
- Part two investigates and evaluates the usage of 3D-effects in 2D-cases with supporting structures. Here the evaluation of how good this approximation is compared to the numerical 3D-systems factor of safety is made.
- Part three will apply the same approach as for part one and two, but with a real life case to evaluate if similar increase in total stability can be accounted for. This system will have a different geometry and parameters evaluated from tests performed for the *Västlänken* project.

Our intention is not to evaluate exactly what is increasing the factor of safety for different geometries. It is rather to state that the numerical calculations are (in our cases with our geometries) higher than the analytical 2D cases with and without the approximation of additional 3D-effects. Neither is it our intension to evaluate the performance or accuracy of the FE-programs used.

1.3 Method

The work process for this master's dissertation project will be divided into three parts.

A thorough literature study will be conducted to enable the authors to obtain the necessary theoretical knowledge for the work that is going to be conducted. This study will also act as the foundation for the theoretical material.

The second part is an assembly of the theory chapters, which is a fairly large part of the report. This enables the readers to view and understand the underlying theoretical principles concerning a finite element analysis of geotechnical mechanics. This as well as how the different programs and calculations are conducted and what theories they are based on will also be presented.

Finally the report presents results from the calculations in *Slope/W*, *Plaxis 2D* and *Plaxis 3D* and evaluating the tasks stated in the objective.

1.4 Disposition

In the report the different chapters contain the following:

Chapter 2 – Main theory chapter, containing the theoretical knowledge needed to understand and conduct the analysis made.

Chapter 3 – Material models used in FE-programs are explained. These are the Hardening soil material model and the Mohr-Coulomb material model.

Chapter 4 – Contains a brief explanation into the programs used as well as the calculation and modelling methods conducted. Also the geometries, parameters and other inputs are described in detail.

Chapter 5 – Contains the results obtained for the two generalised excavation problems as well as for the real-life case.

Chapter 6 – Discussion, conclusions and suggestions for further work.

Chapter 7 – Contains the bibliography.

The chapters are followed by an appendix.

1.5 Limitations

The analysis is limited to cohesion material and with two different material models used in the FE-programs. These material models are Hardening soil and Mohr-Coulomb. The comparison between models will be in factor of safety and the failure mechanism analysed in this dissertation is total stability failure.

For the different stages of the modelling process a number of different geometries have been chosen and presented in Chapter 4. These models are used to analyse the impact of change in length which is the focus in the project.

The project will be limited to include modelling and calculations for analytical analysis concerning the factor of safety in slope stability with the help of the program *GeoStudio Slope/W*. For the numerical calculations the programs *Plaxis 2D* and *Plaxis 3D* will be used. The accuracy or performance of these programs will not be investigated.

2 Theory

In this chapter the underlying theory for the analytical calculations and the numerical calculations applied to soil mechanics will be discussed. The basic FE-theory will however not be presented and for these basics the reader is referred to other literature such as Ottosen and Ristinmaa (2005).

2.1 Analytical Calculation Theory

Method of slices

The *method of slices* is a method for calculation of slope stability in two dimensions. The method does not account for any changes in the topography along the length of the specific section that is modelled. For slopes with variations though, this type of model can be used due to the fact that the calculations can be performed for an infinite number of sections. Thereby the calculations have the ability to deal with changes in material, topography and geometry.

The traditional method of slices was pioneered by *Fellenius* in 1927-1936. Since then it has been modified and further developed to extend the range of application and usability for today's usage and demands (Chowdhury, et al. 2010).

For the traditional *method of slices* the circular slip surface viewed below (Figure 2:1) is divided into vertical slices. Each slice has its own weight, tangential components and normal component acting upon it.

True for the calculation is that the forces on each slice and forces acting on the entire sliding mass must satisfy the conditions of equilibrium (Chowdhury, et al. 2010).

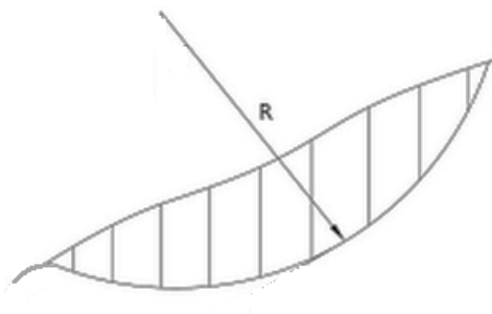


Figure 2:1 –Traditional method of slices method with circular slip surface (Chowdhury, et al. 2010)

For each slice there are individual parameters, geometrical data and forces acting upon the different slices. These can be viewed in Figure 2.2 below.

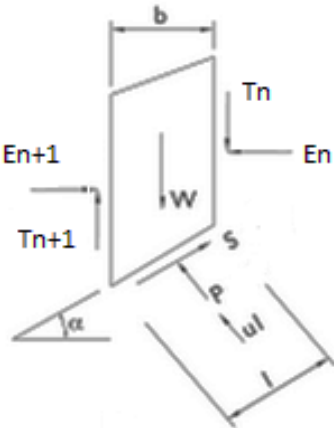


Figure 2:2 – Parameters, Geometrical data and forces acting on a slice (Chowdhury, et al. 2010)

Symbol explanation:

- b* – Width of the slice
- W* – Weight
- T* – Tangential components
- E* – Normal components
- α* – Inclination
- l* – Length of the sloped side
- S* – Shear resistance
- P* – Normal force
- R* – Radius
- θ* – Arc length

The evaluation of the forces *E* and *T* is proven to be difficult due to the dependencies on many different parameters. To simplify the calculations the forces perpendicular and tangential to the base are used to obtain the Normal stress. This means that the inter-slice forces *T* and *E* are assumed to be zero which yields

$$\sum \tan(\phi) \{ (T_n - T_{n+1}) \cos \alpha - (E_n - E_{n+1}) \sin \alpha \} = 0 \tag{2:1}$$

for the overall equilibrium (Chowdhury, et al. 2010).

This assumption is an underestimation of the factor of safety i.e. the error is on the safe side (Chowdhury, et al. 2010).

To solve the moment equation a cent of rotation equal to zero is used where the activating moment is compared to the retaining moment.

$$F = \frac{\sum(cl + \tan\phi(W\cos\alpha - ul))}{\sum W\sin\alpha} \quad (2:2)$$

$$F = \frac{\sum(cl + (W\cos\alpha - ul\cos^2\alpha)\tan\phi)}{\sum W\sin\alpha} \quad (2:3)$$

Assuming that the angle $\phi = 0^\circ$ gives:

$$F = \frac{\sum(cl)}{\sum W\sin\alpha} = \frac{c_u R\theta}{\sum W\sin\alpha} \quad (2:4)$$

From here the slope stability is found by searching the most critical centre and radius of the slope. This can be done through experience or more likely software designed to test a large number of different variations to find the location of the critical circle (Chowdhury, et al. 2010).

The method of slices is a good method for fast and preliminary calculations for the stability of a certain slope. The user of the method should however be aware of the errors that can arise due to the simplifications. Even though the errors should be on the "safe side" there is a possibility of large errors up to 60 % (Chowdhury, et al. 2010).

Commission on Slope Stability (3D - effects)

The CSS is a committee of the IVA (*Ingenjörsvetenskapsakademien*) founded in 1988 with the tasks of handling research, development and information concerning landslides.

Commission on slope stability report 3:95

In 1995 the Commission released *report 3:95* called *Instructions for slope stability calculations* where the calculations and methods for different parameters and testing methods in slope stability are explained. This is a complete guide for slope stability evaluations with detailed information and help for anyone that are evaluating the subject. Even though the guide was published in 1995 it is still used in the Swedish Geotechnical industry for analytical 2D calculations.

3-Dimensional effects

When the slope geometry is highly variable, or if its width is small and the slip surface is deep, it may be interesting to account for three-dimensional effects. If the length of the slope is short the stability can be calculated with the method of slices described above (FS_{2-dim}) plus adding the additional resisting shear force in the end surfaces. This gives a 3-dimensional factor of safety FS_p based on the assumption that the end surfaces are plane.

According to other surveys mentioned in Skredkommisionen (1995), the critical slip surface refers to when the end surfaces have a certain curvature. Therefore a standard reduction F_{3-Dim} is made to modify the 3-dimensional factor of safety given when assuming plane surfaces. Below follows the equations with related illustrations.

$$FS_{2-dim} = \frac{M_{(\tau_{fu} * l * r)}}{M_{(W * a + Q * b)}} \tag{2:5}$$

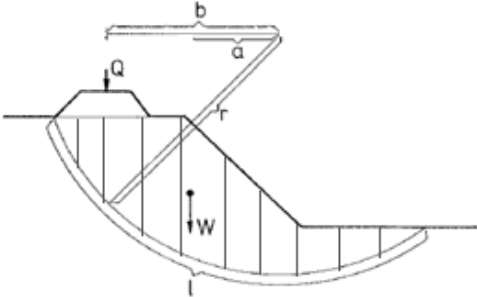


Figure 2:3 – Illustration of slope with plane end surfaces, FS_{2-Dim} is the normal factor of safety (Skredkommisionen 1995)

$$FS_P = \frac{M_{\tau_{fu} * l * r * L} + 2M_{(\tau_{fu} * A * c)}}{M_{(W * a + Q * b)L}} \quad (2:6)$$

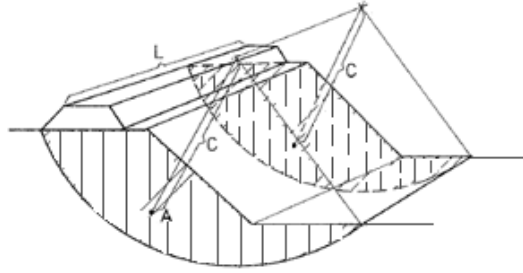


Figure 2:4 - Illustration of slope with plane end surfaces, FS_P is the factor of safety including increase from 3D-effects (Skredkommesjonen 1995)

$$FS_{3-Dim} = FS_{2-Dim} + 0,75 \left(\frac{FS_P}{FS_{2-Dim}} - 1 \right) \quad (2:7)$$

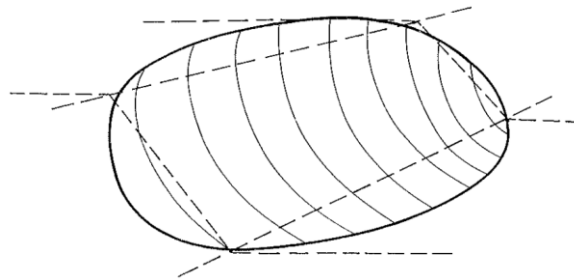


Figure 2:5 - Illustration of slope with curved end surfaces, FS_P is the factor of safety including increase from 3D-effects but with reduction due to non-planar end surfaces (Skredkommesjonen 1995)

For full insight into the theory surrounding 3-dimensional effects on 2D calculations the reader is referred to other literature.

It should be noted that Skredkommesjonenens (1995) suggestions for 3-dimensional effects only can be considered for cohesive soil materials. Furthermore the entire theory is based on the assumption that the surrounding material has the ability to withstand the transferred forces from the end surface. When performing these calculations it is possible to calculate the maximal length for which the end surfaces can absorb excess moment. Thereby the maximum length for a specified FS can be calculated.

The calculations should always be verified to assure that the 3D influenced security factor is the lowest of all the calculated 3D-security factors for the entire system. Otherwise an overestimate of the actual failure strength of the model may be chosen and the factor of safety might not be representable for some areas.

Morgenstern-Price model

This method is based in the previously described *method of slices* and is the method used when performing calculation for critical slip surface in *GeoStudio – Slope/W*.

The Morgenstern-Price method bases the variation in *factor of safety* on the summation of tangential and normal forces on each slice. The *Newton-Rhapson* method is used to solve the moment and force equation for lambda and the factor of safety in the equation described below.

The function describing the direction of the interslice forces

$$\lambda f(x) = X/E. \quad (2:8)$$

λ is a constant and $f(x)$ is functional variation with x (Fredlund and Krahn 1977)

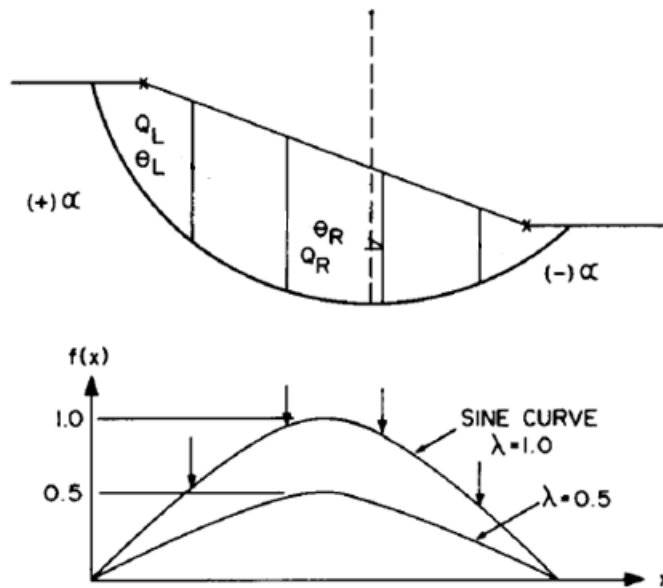


Figure 2:6 – Side force designation, Morgenstern-Price method (Fredlund and Krahn 1977).

2.2 Strain invariants

There are different invariants, common for all is that the invariants have the same value in every coordinate system. This fact is the criterion for the invariants and it is crucial for the calculations that they are used in. Therefore it is strategic to use the invariants when describing the constitutive relations and the yield criteria (Ottosen and Ristinmaa 2005).

The principal strains

The principal strains describe the maximum and minimum elongation of the elements. These occur when the shear strains are equal to zero. Finding them is therefore a matter of finding a coordinate system ($\mathbf{n}_1, \mathbf{n}_2, \mathbf{n}_3$) where this occurs. One can describe the principal strains using (Ottosen and Ristinmaa 2005)

$$(\boldsymbol{\varepsilon} - \lambda \mathbf{I})\mathbf{n} = \mathbf{0} \quad (2:9)$$

For this eigenvalue problem to exist with a nontrivial solution; \mathbf{n} has to exist and therefore requires the following to be true

$$\det(\boldsymbol{\varepsilon} - \lambda \mathbf{I}) = 0 \quad (2:10)$$

The cubic characteristic equation provided by the expression is fulfilled by the three *eigenvalues*, λ . When these have been determined this provides the solution in which these eigenvalues determines the principal strains.

$$\boldsymbol{\varepsilon} = \begin{bmatrix} \lambda_1 & 0 & 0 \\ 0 & \lambda_2 & 0 \\ 0 & 0 & \lambda_3 \end{bmatrix} = \begin{bmatrix} \varepsilon_1 & 0 & 0 \\ 0 & \varepsilon_2 & 0 \\ 0 & 0 & \varepsilon_3 \end{bmatrix} \quad (2:11)$$

Equation 2:10 can be rewritten as the *Characteristic equation*:

$$-\lambda^3 + \theta_1 \lambda^2 - \theta_2 \lambda + \theta_3 = 0 \quad (2:12)$$

where,

$$\begin{aligned}\theta_1 &= \varepsilon_{11} + \varepsilon_{22} + \varepsilon_{33} = \varepsilon_{ii} \\ \theta_2 &= \varepsilon_{11}\varepsilon_{22} + \varepsilon_{22}\varepsilon_{33} + \varepsilon_{11}\varepsilon_{33} - \varepsilon_{23}^2 - \varepsilon_{12}^2 - \varepsilon_{13}^2 = \frac{1}{2}\theta_1^2 - \frac{1}{2}\varepsilon_{ij}\varepsilon_{ji} \\ \theta_3 &= \varepsilon_{11}\varepsilon_{22}\varepsilon_{33} - \varepsilon_{11}\varepsilon_{23}^2 - \varepsilon_{22}\varepsilon_{13}^2 + \varepsilon_{33}\varepsilon_{12}^2 + 2\varepsilon_{12}\varepsilon_{13}\varepsilon_{23} = \det(\varepsilon_{ii})\end{aligned}$$

Generic strain and Cauchy strain invariants

From the characteristic equation for the principal stresses (2:12) the Cauchy invariants can be described with

$$\theta_1 = \varepsilon_{ii} \quad (2:13)$$

$$\theta_2 = \frac{1}{2}\theta_1^2 - \frac{1}{2}\varepsilon_{ij}\varepsilon_{ji} \quad (2:14)$$

$$\theta_3 = \det(\varepsilon_{ii}) = \varepsilon_1\varepsilon_2\varepsilon_3 \quad (2:15)$$

The Cauchy invariants follow a systematic way in their definition and have a unique relation to the *generic invariants*. These generic invariants are defined for their systematic manner and are described as

$$\bar{I}_1 = \varepsilon_{ii} = \varepsilon_1 + \varepsilon_2 + \varepsilon_3 \quad (2:16)$$

$$\bar{I}_2 = \frac{1}{2}\varepsilon_{ij}\varepsilon_{ji} = \frac{1}{2}(\varepsilon_1^2 + \varepsilon_2^2 + \varepsilon_3^2) \quad (2:17)$$

$$\bar{I}_3 = \frac{1}{3}\varepsilon_{ij}\varepsilon_{jk}\varepsilon_{ki} = \frac{1}{3}(\varepsilon_1^3 + \varepsilon_2^3 + \varepsilon_3^3) \quad (2:18)$$

where the relation between the Cauchy and the generic invariants can be derived from (2:5-2:7) and (2:8-2:10), resulting in

$$\bar{I}_1 = \theta_1 \quad (2:19)$$

$$\bar{I}_2 = \frac{1}{2}\theta_1^2 - \theta_2 \quad (2:20)$$

$$\bar{I}_3 = \frac{1}{3}\theta_1^3 - \theta_1\theta_2 + \theta_3 \quad (2:21)$$

The deviator strain invariants can be formed in a matter similar to the form in which the generic strains were constructed earlier. In the same way as the generic invariants were formed, we start with the strain tensor and for the deviator invariants the deviator strain tensor is used (Ottosen and Ristinmaa 2005).

$$e_{ij} = \varepsilon_{ij} - \frac{1}{3} \varepsilon_{kk} \delta_{ij} \quad (2:22)$$

where e_{ij} is the deviatoric strain tensor.

This gives that e_{ij} and ε_{ij} have identical principal direction

There is a relation between $\theta_1, \theta_2, \theta_3$ and $\bar{I}_1, \bar{I}_2, \bar{I}_3$ where a defined analogy with the help of the *generic invariants*; is defined (Ottosen and Ristinmaa 2005)

$$\bar{J}_1 = e_i = e_1 + e_2 + e_3 \quad (2:23)$$

$$\bar{J}_2 = \frac{1}{2} e_{ij} e_{ji} = \frac{1}{2} \mathbf{tr}(\mathbf{e}^2) = \frac{1}{2} (e_1^2 + e_2^2 + e_3^2) \quad (2:24)$$

$$\bar{J}_3 = \frac{1}{3} e_{ij} e_{jk} e_{ki} = \frac{1}{3} \mathbf{tr}(\mathbf{e}^3) = \frac{1}{3} (e_1^3 + e_2^3 + e_3^3) = e_1 e_2 e_3 \quad (2:25)$$

From the above stated invariants we get the octahedral normal and shear strains which can be simplified into (Ottosen and Ristinmaa 2005)

$$\varepsilon_0 = \frac{1}{3} \bar{I}_1 \quad \text{Octahedral normal strain} \quad (2:26)$$

$$\gamma_0 = 2 \sqrt{\frac{2}{3} \bar{J}_2} \quad \text{Octahedral shear strain i.e. Engineering shear strain} \quad (2:27)$$

2.3 Stress invariants

In the same manner as the invariants were described in the previous section for the strains the invariants can be described for the stresses.

The stress tensor is symmetric and is defined as

$$\boldsymbol{\sigma}_{ij} = \begin{bmatrix} \mathbf{t}_1^T \\ \mathbf{t}_2^T \\ \mathbf{t}_3^T \end{bmatrix} = \begin{bmatrix} \sigma_{11} & \sigma_{12} & \sigma_{13} \\ \sigma_{21} & \sigma_{22} & \sigma_{23} \\ \sigma_{31} & \sigma_{32} & \sigma_{33} \end{bmatrix} = \begin{bmatrix} \sigma_{11} & \sigma_{12} & \sigma_{13} \\ \sigma_{12} & \sigma_{22} & \sigma_{23} \\ \sigma_{13} & \sigma_{23} & \sigma_{33} \end{bmatrix} \quad (2:28)$$

where the traction vector \mathbf{t} is described as

$$t_i = \lim_{\Delta A \rightarrow 0} \frac{\Delta P_i}{\Delta A} \quad (2:29)$$

With this symmetry proven the traction vector for an arbitrary surface \mathbf{t} , can be resolved as a component parallel and perpendicular to \mathbf{n} (normal vector) through a certain point (Ottosen and Ristinmaa 2005).

Parallel component i.e. *Normal stress*

$$\sigma_n = n_i t_i \Rightarrow t_i = \sigma_{ij} n_j \quad (2:30)$$

Perpendicular component i.e. *Shear stress*

$$\tau_n = m_i t_i \Rightarrow t_i = \sigma_{ij} m_j \quad (2:31)$$

Principal stresses

From the previously given equations (2:30 and 2:31) the following can be stated

$$\tau_n^2 = t_i t_i - \sigma_n^2 \quad (2:32)$$

This gives a preliminary result, a physical interpretation of the eigenvalue problem for the stress tensors were the solution of the described problem results in the stress tensors (Ottosen and Ristinmaa 2005).

$$(\sigma_{ij} - \lambda \delta_{ij}) n_j = 0$$

or

$$(\boldsymbol{\sigma} - \lambda \mathbf{I}) \mathbf{n} = \mathbf{0} \quad (2:33)$$

When comparing the solution to the derived eigenvalue problem for the strain tensor (Equation 2:9) there is complete equivalence, therefore the same derivation as previously can be used for the stress invariant which gives the characteristic equation

$$\det(\boldsymbol{\sigma} - \lambda \mathbf{I}) = 0$$

From this the three principal stresses are determined and for each λ a corresponding principal direction is given.

Finally we arrive at a similar solution for the stress tensor as for the strain tensor in previous derivations (Ottosen and Ristinmaa 2005)

$$\boldsymbol{\sigma}' = \mathbf{A}\boldsymbol{\sigma}\mathbf{A}^T = \begin{bmatrix} \sigma_1 & 0 & 0 \\ 0 & \sigma_2 & 0 \\ 0 & 0 & \sigma_3 \end{bmatrix}$$

where,

$$\mathbf{A}^T = [\mathbf{n}_1 \ \mathbf{n}_2 \ \mathbf{n}_3] \quad (2:34)$$

Generic stress invariants

In correlation with the generic strains the stress tensor satisfies the *Cayley-Hamilton* theorem (Ottosen and Ristinmaa 2005); therefore the same calculations are performed in the stress case. The coefficients in the characteristic equation are the Cauchy-stress invariants and have the following *generic stress invariants* (Ottosen and Ristinmaa 2005)

$$I_1 = \sigma_{ii} \quad (2:35)$$

$$I_2 = \frac{1}{2}\sigma_{ij}\sigma_{ji} \quad (2:36)$$

$$I_3 = \frac{1}{3}\sigma_{ij}\sigma_{jk}\sigma_{ki} \quad (2:37)$$

Deviator stress invariants

Similar to the deviatoric strain invariants the deviatoric stress tensor forms the stress invariants. In the below stated deviatoric stress tensor the term $\frac{\sigma_{kk}}{3}$ ($b = \frac{\sigma_{kk}}{3}$) is referred to as the hydrostatic stress. For the yield criteria in rocks, soils and similar materials the hydrostatic stress has a major impact on the calculations while the influence is close to nothing for other materials such as steel. Therefore it is crucial to take into account when modelling and performing calculations with soils (Ottosen and Ristinmaa 2005).

$$s_{ij} = \sigma_{ij} - \frac{1}{3}\sigma_{kk}\delta_{ij} \quad (2:38)$$

The deviatoric stress invariants are given by

$$J_1 = s_{ii} = 0 \quad (2:39)$$

$$J_2 = \frac{1}{2} s_{ij} s_{ji} \quad (2:40)$$

$$J_3 = \frac{1}{3} s_{ij} s_{jk} s_{ki} \quad (2:41)$$

Finally the octahedral normal and shear stresses are defined as (Ottosen and Ristinmaa 2005)

$$\sigma_0 = \frac{1}{3} I_1 \quad \text{Octahedral normal stress} \quad (2:42)$$

$$\tau_0 = \sqrt{\frac{2}{3} J_2} \quad \text{Octahedral shear stress} \quad (2:43)$$

2.4 Various cases of stress

Illustrated below are some of the stress states which will be discussed in the theory chapter.

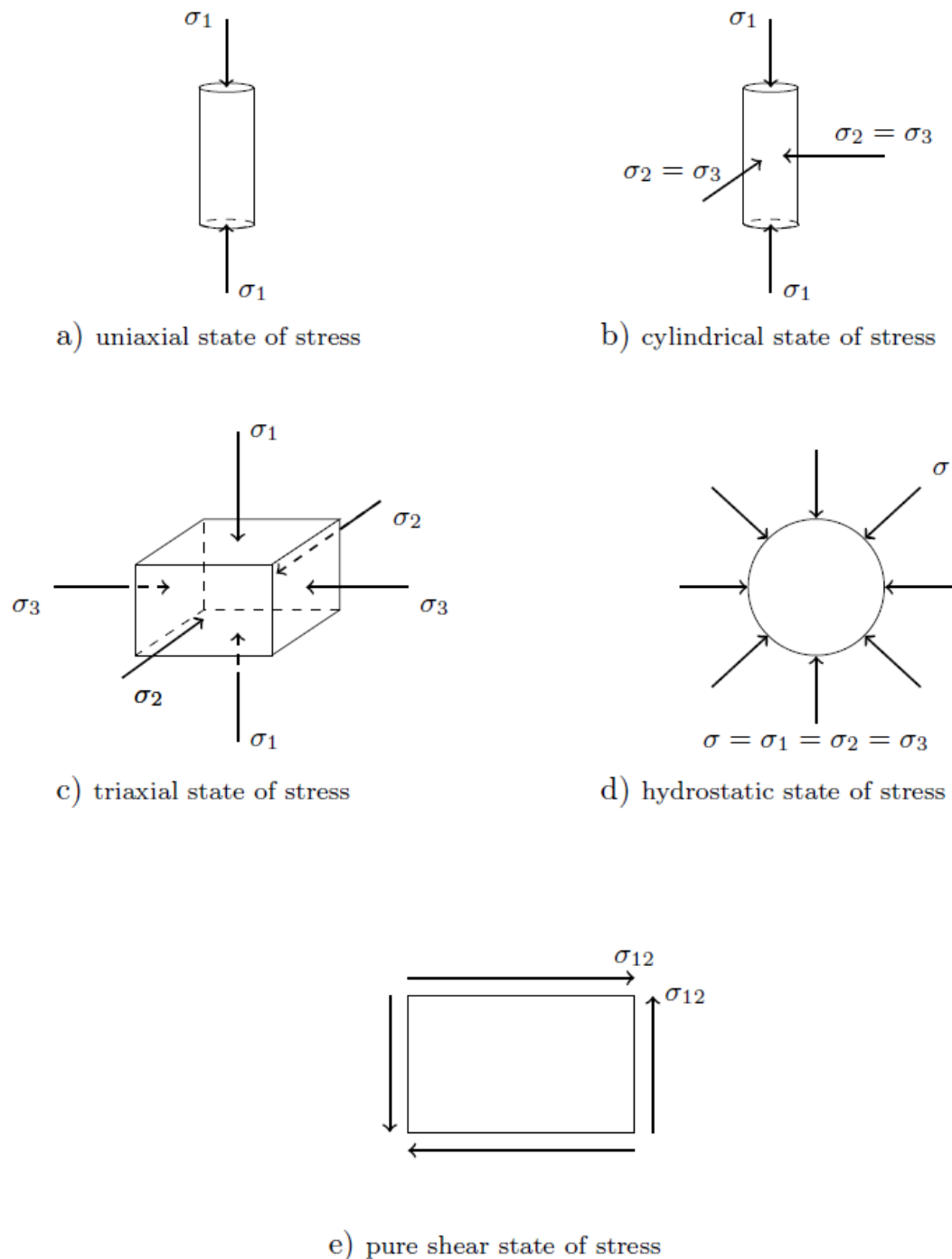


Figure 2:7 - Illustration of different states of stress (Spetz, 2010)

2.5 Plane Elasticity

Plane elastic strain

When performing analytical calculations for geotechnical problems it is often of great benefit for computer modelling to reduce the three-dimensional problem into two-dimensions. For the plane strain case the simplification into a two-dimensional calculation (xy -plane) means that no deformations occur out-of-plane in the z -direction and nothing in the model is affected by the z -coordinate (Ottosen and Ristinmaa 2005) i.e.

$$\begin{aligned}u_1 &= u_1(x, y) \\u_2 &= u_2(x, y) \\u_3 &= 0\end{aligned}$$

All z -direction dependent deformations are zero and therefore;

$$du_1 = \frac{\partial u_1}{\partial x} dx + \frac{\partial u_1}{\partial y} dy \quad (2:44)$$

and

$$du_2 = \frac{\partial u_2}{\partial x} dx + \frac{\partial u_2}{\partial y} dy \quad (2:45)$$

Similar to the three-dimensional strain case the plane elastic strain case has the following relations derived from the kinematic equation:

$$\boldsymbol{\varepsilon} = \begin{bmatrix} \varepsilon_{11} \\ \varepsilon_{22} \\ \gamma_{12} \end{bmatrix} \quad (2:46)$$

$$\tilde{\nabla} = \begin{bmatrix} \frac{\partial}{\partial x} & 0 \\ 0 & \frac{\partial}{\partial y} \\ \frac{\partial}{\partial y} & \frac{\partial}{\partial x} \end{bmatrix} \quad (2:47)$$

$$\mathbf{u} = \begin{bmatrix} u_1 \\ u_2 \end{bmatrix} \quad (2:48)$$

For the elastic strain case Hooke's generalised law for linear elasticity is used and therefore the following is given for an isotropic material (Ottosen and Ristinmaa 2005).

$$\begin{bmatrix} \sigma_{11} \\ \sigma_{22} \\ \sigma_{12} \end{bmatrix} = \frac{E}{(1+\nu)(1-2\nu)} \begin{bmatrix} 1-\nu & \nu & 0 \\ \nu & 1-\nu & 0 \\ 0 & 0 & \frac{1}{2}(1-2\nu) \end{bmatrix} \begin{bmatrix} \varepsilon_{11} \\ \varepsilon_{22} \\ \gamma_{12} \end{bmatrix} \quad (2:49)$$

$$\sigma_{33} = \frac{E\nu}{(1+\nu)(1-2\nu)} (\varepsilon_{11} + \varepsilon_{22}) \quad (2:50)$$

$$\sigma_{13} = \sigma_{23} = 0 \quad (2:51)$$

2.6 Plasticity theory

This section will clarify plastic deformations. Loading and unloading may leave the material with plastic strains ε^P if the stresses exceed the initial yield stress σ_{y0} , shown with the uniaxial stress-strain curve in Figure 2:8.

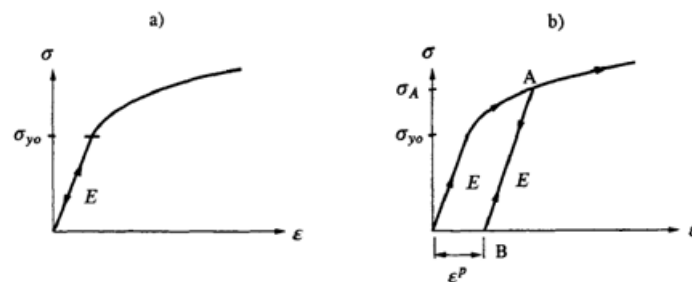


Figure 2:8 – a) Loading without exceeding the initial yield stress; b) Loading, exceeding the initial yield stress (Ottosen and Ristinmaa 2005).

The material is assumed to behave linear elastic, with Young's modulus E (Figure 2:8a), below the initial yield stress as well as when loading and unloading between A and B in the Figure 2:8b. When reloading from B to A the yield stress has changed due to a *hardening effect*. This means that the material retains some of its deformation after a loading cycle i.e. the material has sustained plastic deformation. For elaboration into post-yield behaviour the initial yield stress needs some further explanation (Ottosen and Ristinmaa 2005).

Yield criteria

The failure and initial yield stress in a uniaxial stress state refers to the stress level where the material breaks respectively starts to plasticise, Figure 2:8b. The general stress state is not as simple as the uniaxial state described above, and is defined by the stress tensor (Equation 2:38). We seek an expression, i.e. a function F , which is zero when yielding occurs. F has to be invariant meaning the following expressions hold in an arbitrary coordinate-system.

$$F(\sigma_{ij}) = \sigma - \sigma_{y0} \quad (2:52)$$

$$F(\sigma_{ij}) < 0 \quad \text{Elastic} \quad (2:53)$$

$$F(\sigma_{ij}) = 0 \quad \text{Yielding starts} \quad (2:54)$$

$$F(\sigma_{ij}) > 0 \quad \text{Above yield or failure} \quad (2:55)$$

We consider the isotropic case where the stresses can be expressed without the directions n . Therefore the following relation is generated where the stresses do not depend on chosen coordinate system

$$F(\sigma_{ij}) = F(\sigma_1, \sigma_2, \sigma_3) = 0 \quad (2:56)$$

It is of great advantage to express the criterion using invariants. This way the eigenvalue problem that has to be solved when determining the principal stresses can be avoided. The failure criterion can be expressed using the invariants explained in section (2.1, 2.2). The failure criterion is according to Ottosen and Ristinmaa (2005) especially convenient to express as

$$F(I_1, J_2, \cos(3\theta)) = 0 \quad (2:57)$$

This set of invariants also gives a useful geometrical interpretation separating the hydrostatic stress, $I_1/3$, from the amount of deviatoric stresses J_2 , and the direction of the deviatoric stress $\cos 3\theta$.

To simplify the geometrical interpretation we introduce the Cartesian coordinate system so-called *Haigh-Westergaard coordinate system*. Consider a point, P , in the stress space σ_1, σ_2 and σ_3 and the unit vector \mathbf{n} , diagonal in space.

$$\mathbf{n} = \frac{1}{\sqrt{3}}(1,1,1) \quad (2:58)$$

Along the unit vector \mathbf{n} all stresses are equal meaning, $\sigma_1 = \sigma_2 = \sigma_3$, and it is a *hydrostatic state*. The plane perpendicular to the hydrostatic axis is the deviatoric plane, Figure 2:9 (Left). Projecting σ_1, σ_2 and σ_3 is a common way to visualise these on the deviatoric space, also called the π – *plane* Figure 2:9 (Right).

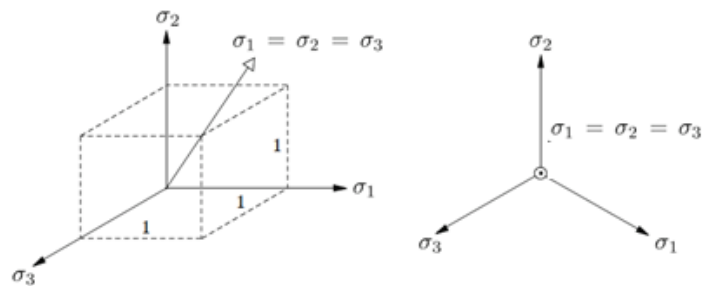


Figure 2:9 - Diagonal space (Left) and the π -plane (Right) (Ottosen and Ristinmaa 2005)

The cos-function is periodic with a period of 360° and concludes the failure/yield curve in the deviatoric plane which is periodic with a period of 120° . Therefore it can be shown that the curve-function in the deviatoric plane is symmetric around $\cos x = 60^\circ, 180^\circ$ and 300° . From this follows that all states of stress in the deviatoric space is known if $0 \leq \theta \leq 60^\circ$ is determined. In Figure 2:10, a possible shape of the failure and yield curve is showed as a convex curve (Ottosen and Ristinmaa 2005)

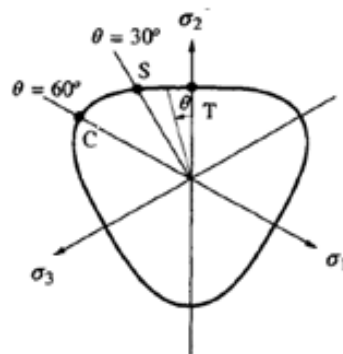


Figure 2:10 - Possible shape of the failure/yield curve in the deviatoric plane. T=tensile meridian, C=compressive meridian, S=Shear meridian (Ottosen and Ristinmaa 2005)

The Figure 2:10 shows three meridians, which are of special interest. The meridian of the initial yield or failure surface is the curve obtained from the intersection between a plane containing the hydrostatic axis and the yield/failure surface, while θ is kept constant. It is presented in the *meridian plane*, as a $\frac{I_1}{\sqrt{3}}, \sqrt{2J_2}$ -coordinate system, illustrated in Figure 2:11.

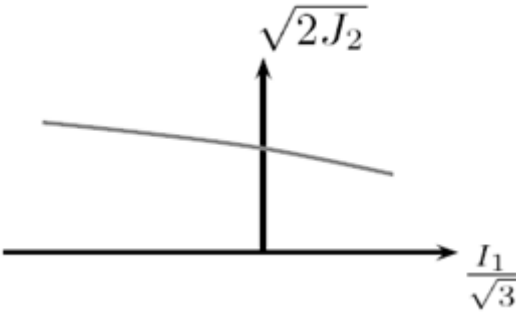


Figure 2:11 – Meridian plane, θ is kept constant (Ristinmaa n.d)

We arrange the principal stresses, with positive quantity denoted as tension, according to: $\sigma_1 \geq \sigma_2 \geq \sigma_3$.

The points T, C and S intersecting the deviatoric plane, Figure 2:10

- $\sigma_1 > \sigma_2 = \sigma_3$ $\theta = 0$ *tensile meridian*
- $\sigma_1 > \sigma_2 = \frac{\sigma_1 + \sigma_3}{2} > \sigma_3$ $\theta = 30$ *shear meridian*
- $\sigma_1 = \sigma_2 > \sigma_3$ $\theta = 60$ *compressive meridian*

To identify points of intersection between the deviatoric plane, for a certain meridian in a multi-axial stress state, a triaxial test can be performed. In the triaxial tests it is only possible to test the material along two of the meridians, the tensile and compressive meridian (Figure 2:10) (Ottosen and Ristinmaa 2005).

Presentation of the stress state can be done in different ways; in general geotechnical calculations it is presented in the MIT-plane where relation between shear and effective mean stress is denoted. For more advanced material models like the ones

used in FE-analyses the relations between deviatoric and effective mean stress are used. This is called the Cambridge-plane (Triax SGF, 2012).

Due to the fact that the different planes have the same input parameters σ_1 , σ_2 and σ_3 theoretical relations make it possible to evaluate the corresponding strength parameters between the planes. Normally the evaluations are made under the assumption that the Mohr-Coulomb failure criterion is valid (Equation 3.1).

Two specimens with different pre-consolidation are tested (hydrostatic stress) and are then inserted into the diagram from the Mohr-circles. The strength parameters are then evaluated from the theoretical relations.

Before going into specific material models it is convenient to separate friction materials from non-friction materials since experimental evidence indicate they behave differently. Initial yield of metals and steel is for an example characterised to be uninfluenced of the hydrostatic stress compared to friction materials such as concrete, soil and rocks where it has a strong influence. These materials also have a smooth stress-strain curve making it hard to determine the initial yield stress (Ottosen and Ristinmaa 2005).

As this report is focusing on geotechnical calculations a summation of the friction materials experimental evidences is listed below. In Chapter 3 the relevant material models for this work are treated further.

- Hydrostatic stress has a strong influence
- $\cos 3\theta$ is important to include.
- The failure surface is convex in the deviatoric plane.

2.7 Post yield

Having discussed the initial yield criteria i.e. the conditions when plastic effect first occurs, and before discussing the general plasticity theory further, some idealized stress-strain curves for the uniaxial case are introduced. This is to characterise a number of known responses.

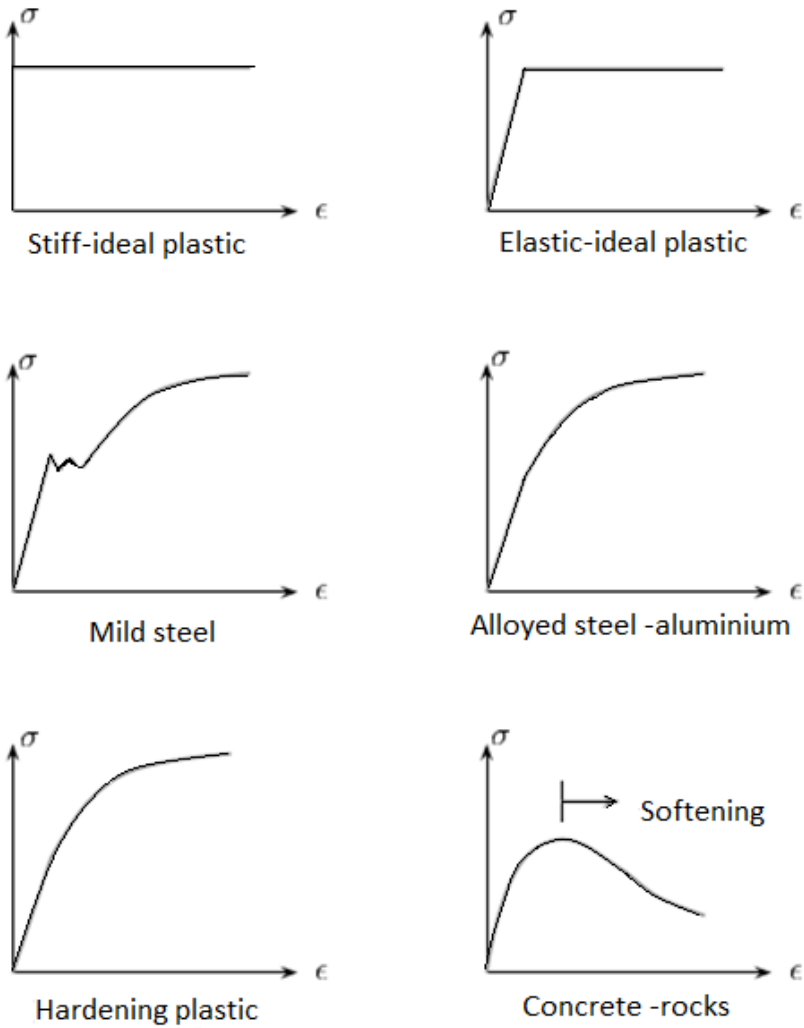


Figure 2:12 – Illustration of a known number of plasticity responses (Ristinmaa n.d)

Plane plastic strain

As for the elastic case described earlier the plane plastic strains has to be derived to get some insight into the function and behaviour of the strain.

For the plane strain case the deformations out of plane are equal to zero and the incremental strains therefore also have to be zero.

$$\dot{\epsilon}_{33} = \dot{\epsilon}_{13} = \dot{\epsilon}_{23} = 0$$

The relation between the incremental stresses and strains are described below (Ottosen and Ristinmaa 2005).

$$\dot{\sigma}_{\alpha\beta} = D_{\alpha\beta\gamma\delta}^{ep} \dot{\epsilon}_{\gamma\delta} \quad (2:59)$$

$$D_{\alpha\beta\gamma\delta}^{ep} = D_{\alpha\beta\gamma\delta} - \frac{1}{A} D_{\alpha\beta st} \frac{\partial g}{\partial \sigma_{st}} \frac{\partial f}{\partial \sigma_{mn}} D_{mny\delta} \quad (2:60)$$

The out of plane stresses are not necessarily equal to zero only because the strains are. Therefore the out of plane stresses and strain relations are described. Furthermore the below stated relations are components in the calculation of the yield function and are sometimes used in the calculation of hardening parameters, which will be described later on.

$$\dot{\sigma}_{i3} = D_{i3\gamma\delta}^{ep} \dot{\epsilon}_{\gamma\delta} \quad (2:61)$$

$$\dot{\epsilon}_{i3} = \dot{\lambda} \dot{\sigma}_{i3} \quad (2:62)$$

$$\dot{\lambda} = \frac{1}{A} \frac{\partial f}{\partial \sigma_{kl}} D_{kl\gamma\delta} \dot{\epsilon}_{\gamma\delta} \quad (2:63)$$

The stiffness tensor of the isotropic elasticity for the plane plastic strain case is described as (Ottosen and Ristinmaa 2005)

$$D_{\alpha\beta\gamma\delta} = 2G \left[\frac{1}{2} (u_{\alpha\gamma} u_{\beta\delta} + u_{\alpha\delta} u_{\beta\gamma}) + \frac{1}{1-2\nu} u_{\alpha\beta} u_{\gamma\delta} \right] \quad (2:64)$$

Hardening and Softening

For understanding the Hardening/Softening phenomenon it is illustrated in Figure 2:13 and hardening will be discussed in greater detail in Section 2.9.

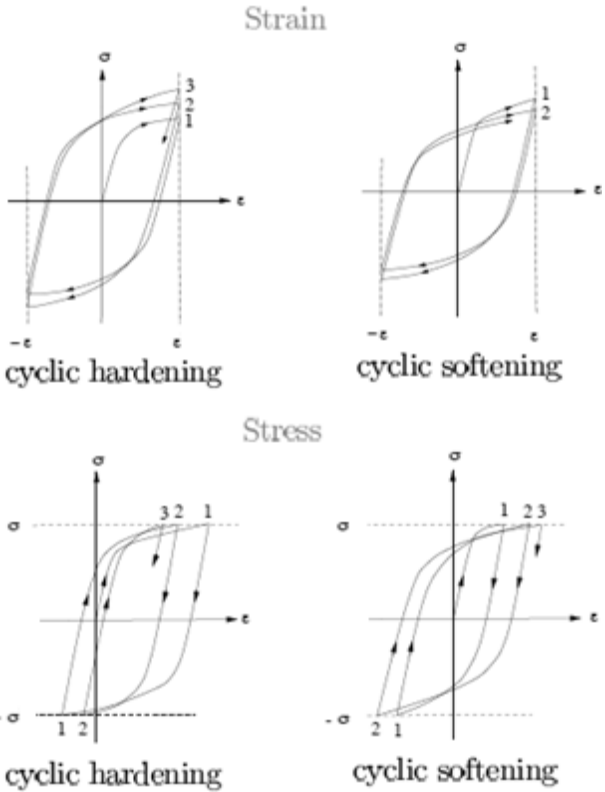


Figure 2:13 – Hardening and Softening behaviour (Ristinmaa n.d)

Post yielding

Having discussed the stresses in Section 2.5, the current conditions (Post yielding) are presented below and illustrated in Figure 2:14.

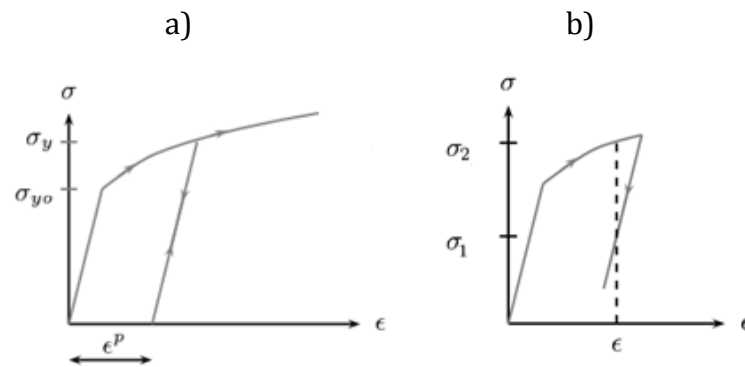


Figure 2:14 –Loading and reloading, σ_{y0} =initial yielding stress, σ_y =current yielding stress, ϵ^p =plastic strain (Ristinmaa n.d)

When plastic loading is being applied plastic strains develop and the yielding criterion changes. Consider one load-cycle as in Figure 2:14a and it becomes evident that the yield stress has changed from its initial value σ_{y0} to σ_y with the plastic deformations. As mentioned before the initial yield stress is generalised and described with the initial yielding surface. How the current surface evolves with the plastic loading is called the *hardening rule*. What can also be seen in Figure 2:14b is that there is no unique relation between σ and ϵ . Information is missing and the material is said to be *history dependent*.

2.8 Hardening rule

The initial yield surface is fundamental for the plasticity theory and we will in this section describe the mathematical expressions for how the yield surface evolves with the plastic strains.

In general the initial yield surface for isotropic materials is described as

$$F(\sigma_{ij}) = 0 \quad (2:65)$$

The current yield surface can be described by (Ottosen and Ristinmaa 2005)

$$F(\sigma_{ij}, K_1, K_2, \dots) = 0 \quad (2:66)$$

or

$$F(\sigma_{ij}, K_\alpha) = 0 \quad (2:67)$$

Here the so-called hardening parameters $K_\alpha = K_1, K_2$ are introduced to characterise the changes of the yield surface, such as shape, size and position of the surface.

The number of hardening parameters varies and it is therefore convenient to collect them in K_α . Before yielding occurs the hardening parameters K_α are by definition zero.

To model the fact that K_α varies with the plastic loading it is assumed that there are internal parameters κ_α that characterise the *state* of the elastic-plastic material. It is also appropriate to assume that the hardening parameters depend on the internal variables.

The internal variables memorize the plastic loadings and by which follows that it also holds true for $\kappa_\alpha = 0$ *initially* and since the hardening parameters are also zero, due to that no plastic strains have developed.

$$K_\alpha = K_\alpha(\kappa_\beta) \quad (2:68)$$

where,

$$\begin{aligned} \beta &= 1, 2, \dots \\ \kappa_\alpha &= 0 \text{ initially and for the elastic case} \end{aligned}$$

To keep a unique relation between hardening parameters and internal variables it is reasonable to assume that the numbers of parameters are equal. We get the relation

$$\dot{K}_\alpha = \frac{\partial K_\alpha}{\partial \kappa_\beta} \dot{\kappa}_\beta \quad (2:69)$$

Let us now exemplify some of the different types of hardening, starting with the ideal plasticity where the yield surface is unaffected by the plastic deformation.

No hardening occurs and therefore no hardening parameters exist. As illustrated in Figure 2:15 the yield surface remains fixed in the stress space. And as stated below the initial- and the current yield surface coincide (Ottosen and Ristinmaa 2005).

$$f(\sigma_{ij}, K_\alpha) = F(\sigma_{ij}) = 0 \quad (2:70)$$

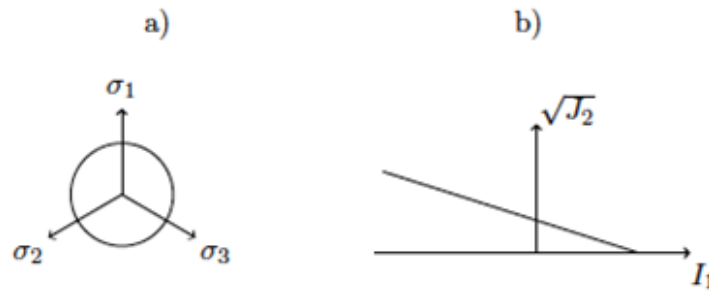


Figure 2:15 – Yield surface positioning with no hardening, a) Deviatoric plane ($f(\sigma_{ij}, K_\alpha) = F(\sigma_{ij}) = 0$), b) Meridian plane (Ristinmaa n.d)

For materials that show *isotropic hardening* where the current yield surface evolves with the plastic strains, the change of yield surface is described with the hardening function $K(\kappa)$.

$$f(\sigma_{ij}, K_\alpha) = F(\sigma_{ij}) - K = 0 \quad (2:71)$$

The yield surface holds the same position and shape but differs in size as illustrated in Figure 2:16.

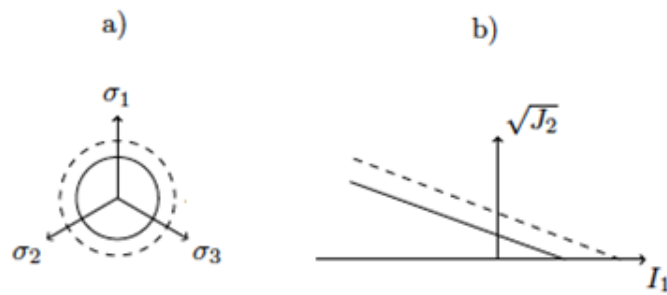


Figure 2:16 – Yield surface positioning with hardening, a) Deviatoric plane, b) Meridian plane (Ristinmaa n.d)

Due to the uniform expansion of the yield surface the yield stress is predicted to be the same for both tension and compression as illustrated in Figure 2:17 (Left). This prediction has been proven to be rather inaccurate for steel and metal where the plastic strains seem to occur earlier in performed experiments. The Figure 2:17 (Right) illustrate this phenomenon called the *Baushinger effect* (Ottosen and Ristinmaa 2005).

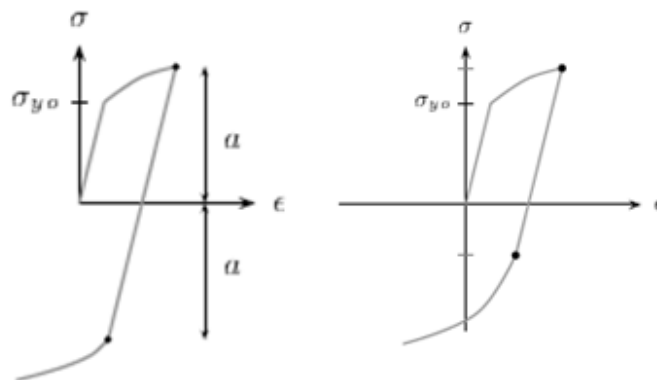


Figure 2:17 – Uniform expansion of the yield surface (current yield stress in tension = current yield stress in compression) (Left), Baushinger effect (Right), (Ristinmaa n.d)

Kinematic hardening

Kinematic hardening is a way of trying to approximate this effect where the size and shape are assumed to be constant but instead the position of the yield surface is changed with the plastic loadings.

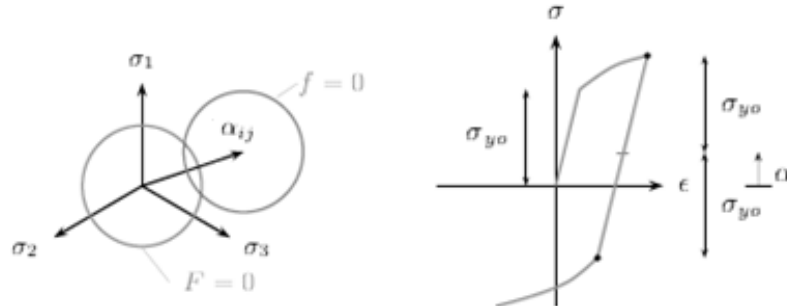


Figure 2:18 – Current yield surface depending on plastic history (Left), Size of current yield surface is constant i.e. Kinematic hardening (Right), (Ristinmaa n.d)

The so-called *back-stress* tensor α_{ij} describes the position of the current yield surface. Having the hardening parameters expressed in terms of α_{ij} we can model the kinematic hardening as

$$f(\sigma_{ij}, K_\alpha) = F(\sigma_{ij} - \alpha_{ij}) = 0 \quad (2:72)$$

In the last rule, the *mixed hardening rule*, the set of hardening parameters K_α depends on both the hardening parameters from isotropic hardening, K , and kinematic hardening, α_{ij} .

The mixed hardening rule can then be described by

$$f(\sigma_{ij}, K_\alpha) = F(\sigma_{ij} - \alpha_{ij}) - K = 0 \quad (2:73)$$

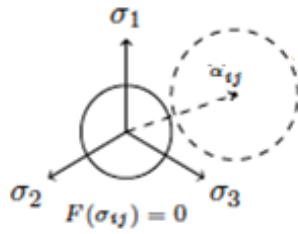


Figure 2:19 - Current yield surface moves and expands i.e. mixed hardening (Spetz 2012)

For the mixed hardening the yield surface has the same shape but changes position and/or size with the plastic loading.

3 Material Models

To accurately model different types of soil material a soil model must be used.

It is possible to choose and create your own material models in *Plaxis* but to simplify the calculations and modelling, *Plaxis* have in its software created a number of different soil-models that are based on traditional models (Plaxis 3Db 2013). The models chosen in this dissertation are presented below.

3.1 Mohr-Coulomb model

When modelling soil mechanics the Mohr-Coulomb yield criterion is the most used. The model is based on the Coulomb criterion established in 1773 by Charles-Augustin de Coulomb. The Mohr-Coulomb failure criterion is the first to account for hydrostatic stresses and it describes that the maximum shear stress τ_{max} varies with the normal stresses σ_n (Ronaldo 2013).

$$\tau_{max} = c - \sigma_n \tan \phi \quad (3:1)$$

Mohr-Coulomb yield criterion

If yielding is assumed to be analogous with failure then the Mohr-Coulomb yield criterion becomes analogous with Equation 3:1 above. Figure 3:1 illustrates the relation between the shear strength τ_{max} , the normal stresses σ_n . ϕ is the angle of the envelope, c the cohesion that can be evaluated as the intercept of the τ -axis and the envelope (Ronaldo 2013).

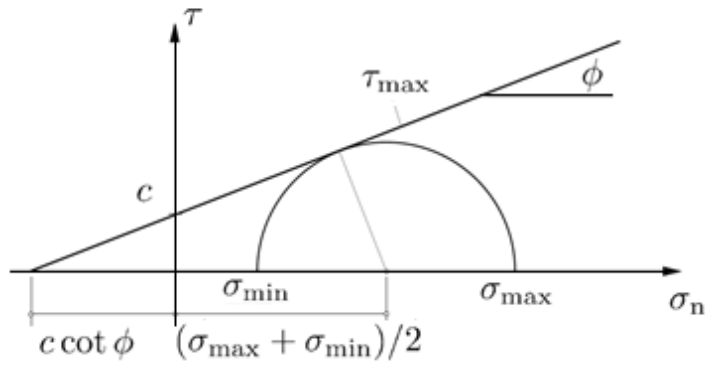


Figure 3:1 - Mohr-Coulomb failure envelope (Ronaldo 2013)

To be able to apply the yield criterion in three dimensions Equation 3:1 needs to be reformulated in terms of an isotropic yield function. Using $F(\sigma_1, \sigma_2, \sigma_3)$ with the same convention as in Section 2.7, it is possible to express the yield function as

$$-(\sigma_{max} - \sigma_{min}) = 2c \cos\phi - (\sigma_{max} + \sigma_{min})\sin\phi \quad (3:2)$$

In *Plaxis* the Mohr-Coulomb yield condition consists of six yield functions (Plaxis 2Db 2013):

$$f_{1a} = \frac{1}{2}(\sigma'_2 - \sigma'_3) + \frac{1}{2}(\sigma'_2 + \sigma'_3)\sin\phi - c \cos\phi \leq 0 \quad (3:3)$$

$$f_{1b} = \frac{1}{2}(\sigma'_3 - \sigma'_2) + \frac{1}{2}(\sigma'_3 + \sigma'_2)\sin\phi - c \cos\phi \leq 0 \quad (3:4)$$

$$f_{2a} = \frac{1}{2}(\sigma'_3 - \sigma'_1) + \frac{1}{2}(\sigma'_3 + \sigma'_1)\sin\phi - c \cos\phi \leq 0 \quad (3:5)$$

$$f_{2b} = \frac{1}{2}(\sigma'_1 - \sigma'_3) + \frac{1}{2}(\sigma'_1 + \sigma'_3)\sin\phi - c \cos\phi \leq 0 \quad (3:6)$$

$$f_{3a} = \frac{1}{2}(\sigma'_1 - \sigma'_2) + \frac{1}{2}(\sigma'_1 + \sigma'_2)\sin\phi - c \cos\phi \leq 0 \quad (3:7)$$

$$f_{3b} = \frac{1}{2}(\sigma'_2 - \sigma'_1) + \frac{1}{2}(\sigma'_2 + \sigma'_1)\sin\phi - c \cos\phi \leq 0 \quad (3:8)$$

Appearing in the yield functions are friction angle ϕ and cohesion c (Equations 3:3-3:8). The condition ($f_{ii} = 0$) represents a hexagonal cone illustrated in Figure 3:2 (Plaxis 3Db 2013).

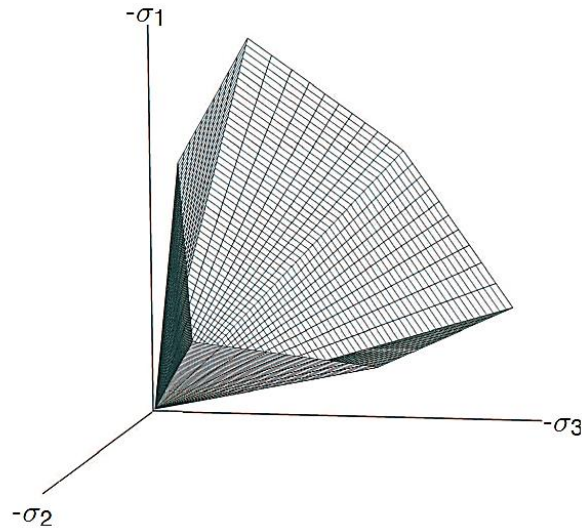


Figure 3:2 – Illustration of the failure surface in the principal stress space for a non-cohesive soil (Plaxis 3Db 2013)

For the Mohr-Coulomb material model in addition six plastic potential functions are used (Plaxis 3Db 2013).

$$g_{1a} = \frac{1}{2}(\sigma'_2 - \sigma'_3) + \frac{1}{2}(\sigma'_2 + \sigma'_3)\sin\psi \quad (3:9)$$

$$g_{1b} = \frac{1}{2}(\sigma'_3 - \sigma'_2) + \frac{1}{2}(\sigma'_3 + \sigma'_2)\sin\psi \quad (3:10)$$

$$g_{2a} = \frac{1}{2}(\sigma'_3 - \sigma'_1) + \frac{1}{2}(\sigma'_3 + \sigma'_1)\sin\psi \quad (3:11)$$

$$g_{2b} = \frac{1}{2}(\sigma'_1 - \sigma'_3) + \frac{1}{2}(\sigma'_1 + \sigma'_3)\sin\psi \quad (3:12)$$

$$g_{3a} = \frac{1}{2}(\sigma'_1 - \sigma'_2) + \frac{1}{2}(\sigma'_1 + \sigma'_2)\sin\psi \quad (3:13)$$

$$g_{3b} = \frac{1}{2}(\sigma'_2 - \sigma'_1) + \frac{1}{2}(\sigma'_2 + \sigma'_1)\sin\psi \quad (3:14)$$

The plastic potential function contains the parameter dilatency angle (ψ) which is required in order to model positive plastic volumetric strain increments. It should be mentioned that clay soils tend to show very low dilatency angles ($\psi \approx 0$) (Plaxis 3Db 2013).

3.2 Hardening Soil model

The Hardening soil model is an elasto-plastic model which takes into account isotropic hardening. To be able to understand the inner workings of this model, a more thorough description will be presented.

The hardening soil model is compared to the Mohr-Coulomb model not fixed in the principal stress space but the yield surface can be expanded due to plastic straining. The model is based on the *hyperbolic* model (Ottosen and Ristinmaa 2005) and the model takes into account two different types of hardening, namely shear and compression hardening.

The shear hardening is a result of irreversible strains due to primary deviatoric loading and the compression hardening is a result of primary compression in oedometer and isotropic loading.

Due to the very complex nature and calculations performed in the Hardening soil model the number of input variables is high. Therefore it should be mentioned that even if the model is strong and is a good way of describing real life materials it is still dependent of inputs. Without access to these input parameters a different model should be used.

A list of parameters is given in Table 3:1

Table 3:1 -Parameter specification for the hardening soil model (Plaxis 3Db 2013)

c'_{ref}	Effective cohesion	kN/m ²
φ'	Effective angle of internal friction	°
ψ	Angle of dilatancy	°
E_{50}^{ref}	Secant stiffness at a reference stress level	kN/m ²
E_{oed}^{ref}	Oedometer modulus at a reference stress level	kN/m ²
E_{ur}^{ref}	Unloading/reloading stiffness at a reference stress level	kN/m ²
m	Power for stress-level dependency of stiffness	-
ν_{ur}	Poisson's ratio for unloading/reloading	-
p_{ref}	Reference stress for stiffness's	kN/m ²
K_0^{nc}	K_0 -value for normal consolidation	-
R_f	Failure ratio	-
z_{ref}	Reference level	m
c'_{inc}	As for Mohr-Coulomb model	kN/m ³
C_c	Compression index	-
C_s	Swelling index or reloading index	-
e_{init}	Initial void ratio	-

From the list of parameters in Table 3:1 we can easily distinguish the ones used for the linear-elastic case and the ones that are specific for this method. Due to the fact that some of the parameters are the same as in the earlier described model, only the new parameters will be presented.

Hardening Soil

The basics of the model lie in the stress dependencies of soil stiffness and for this particular model the oedometer conditions are described through the relation:

$$E_{oed} = E_{oed}^{ref} \left(\frac{\sigma}{p^{ref}} \right)^m \quad (3:15)$$

For the cases of soft soils were $m \approx 1$ the equation is modified (Plaxis 3Db 2013) into

$$E_{oed}^{ref} = \frac{p^{ref}}{\lambda^*} \quad (3:16)$$

where,

$$\lambda^* = \frac{\lambda}{1+e_0} \quad (3:17)$$

and

$$E_{oed}^{ref} = \frac{2p^{ref}}{\kappa^*} \quad (3:18)$$

where,

$$\kappa^* = \frac{2p^{ref}}{1+e_0} \quad (3:19)$$

Hyperbolic relationship and approximation

The formulation of the relationship between the vertical strain and the deviatoric stress (Hyperbolic relationship) is in primary triaxial-loading described as

$$-\varepsilon_1 = \frac{1}{E_i} \frac{q}{1 - \frac{q}{q_a}} \quad (3:20)$$

for $q < q_f$

$$E_i = \frac{2E_{50}}{2-R_f} \quad (3:21)$$

This relation between E_i and E_{50} is plotted in Figure 3:3 and is described with the following function (Plaxis 3Db 2013)

$$E_{50} = E_{50}^{ref} \left(\frac{c \cos \varphi - \sigma'_3 \sin \varphi}{c \cos \varphi + p^{ref} \sin \varphi} \right)^m \quad (3:22)$$

where the E_{50}^{ref} is the reference stiffness modulus. The stiffness modulus is corresponding to the pressure p_{ref} in *Plaxis* (Plaxis 2013).

The ultimate deviatoric stress is derived through the Mohr-Coulomb criterion

$$q_f = (c \cot \varphi - \sigma'_3) \frac{2 \sin \varphi}{1 - \sin \varphi} \quad (3:23)$$

When $q=q_f$ the failure criterion is obtained and plastic yielding occurs.

For the case of unloading and reloading stress paths however, another stiffness-model is used. This is visualised in Figure 3:3 below and is obtained through the equation

$$E_{ur} = E_{ur}^{ref} \left(\frac{c \cos \varphi - \sigma'_3 \sin \varphi}{c \cos \varphi + p^{ref} \sin \varphi} \right)^m \quad (3:24)$$

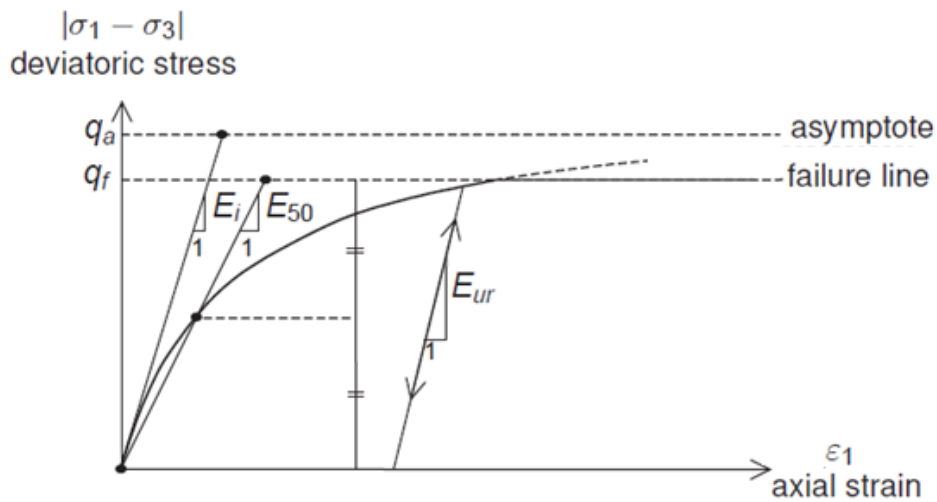


Figure 3:3 - Unloading and reloading stress paths (Plaxis 3Db 2013)

With Hooke's law for isotropic elasticity the conversion between E and G is described by $E=2(1+\nu)G$, this gives us

$$E_{ur} = 2(1 + \nu)G_{ur} \quad (3:25)$$

For convenience a restriction to triaxial loading is made to approximate the hyperbola by the hardening soil model.

The approximation of the hyperbola is restricted to $\sigma'_2 = \sigma'_3$, and σ'_1 as the compressive stress. The approximation originates in the shear hardening yield function (Plaxis 3Db 2013)

$$f = \bar{f} - \gamma^p \quad (3:26)$$

Where \bar{f} and γ^p is described by

$$\bar{f} = \frac{2}{E_j} \frac{q}{1 - \frac{q}{q_a}} - \frac{2q}{E_{ur}} \quad (3:27)$$

$$\gamma^p = -(2\varepsilon_1^p - \varepsilon_v^p) \approx -2\varepsilon_1^p \quad (3:28)$$

This means that

$$\varepsilon_1^p \approx \frac{1}{E_i} \frac{q}{1 - \frac{q}{q_a}} - \frac{q}{E_{ur}} \quad (3:29)$$

Through further derivation of the previously presented equations it is concluded that

$$-\varepsilon_1 = -\varepsilon_1^e - \varepsilon_1^p \approx \frac{1}{E_i} \frac{q}{1 - \frac{q}{q_a}} \quad (3:30)$$

The hardening soil model enables infinite compressive stresses but with the introduction of a yield cap these can be limited (Plaxis 3Db 2013).

Introduction of yield surface cap for the hardening soil model

To explain and include the plastic volume strains in isotropic compression a second type of yield surface is introduced to enclose the elastic region for compressive stress paths. This cap ensures the possibility to model with independent input from E_{50}^{ref} respectively E_{oed}^{ref} . These parameters control the shear yield surface and the oedometer modulus.

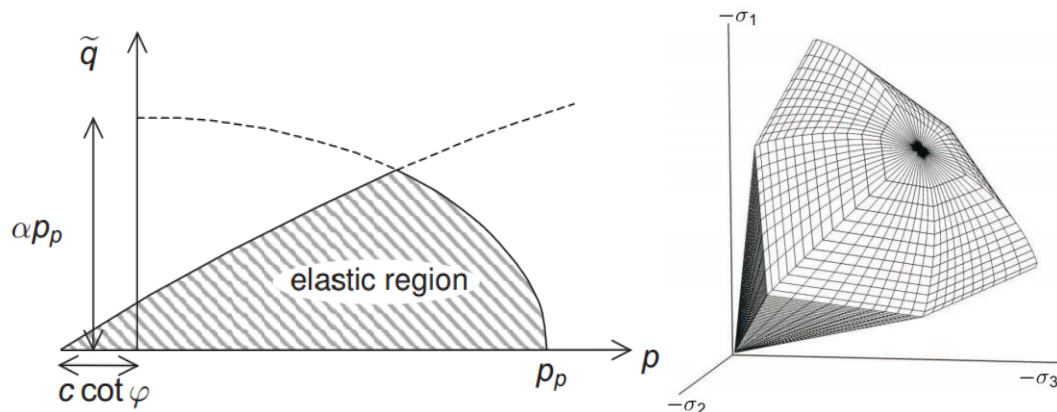


Figure 3:4 - Illustration of the yield surface cap (Plaxis 3Db 2013)

From the Figure 3:4 one can formulate a deeper understanding of the yield surface for the hardening soil model. With the yield lines and the yield surface in principal stress space visualising that the yield cap has a hexagon shape much like the Mohr-Coulomb failure criterion. The cap expands in relation to p_p (pre-consolidation stress) and is described by the function 3:31 (Plaxis 3Db 2013).

$$f^c = \frac{\bar{q}^2}{\alpha^2} + p'^2 - p_p^2 \quad (3:31)$$

For full derivations for the equations presented for the hardening soil model the reader is referred to the *Plaxis Material Model Manual* (Plaxis 3Db 2013).

4 Calculations and Modelling Methods

To evaluate the outcome, when approximating 3D-effects, two generalised cases (one model with no retaining structure, and one with retaining structure) are applied. They are both analysed analytically with and without the use of end-surface effects and also analysed numerically in *Plaxis 2D* and *3D*. The calculations and modelling for each case are performed for a number of different geometries, described later in this chapter.

Neither the 2D-calculations for calculating total stability or the approximation used for 3D-effects are originally made for problems involving constructions (such as a retaining wall). It is therefore of interest to model and compare the results between the two generalised cases.

The sloped excavations, where corners and thus interactions between sides are introduced into the model, are used to compare the analytical and numerical calculations on a case that is valid in accordance with the *CSS report 3:95*. It is also used to evaluate what happens around the corners and the interaction between sides.

The excavations with retaining structures are modelled and compared to the sloped excavation. In this model there are stabilising effects from the structures as well. It has also been noticed that *Plaxis* is limited to model the retaining structure with a linear-elastic material model. In this model, which we call the boxed excavation, the retaining structures are connected between sides and allowed to take unreasonably big moment (due to the fact that they don't plasticise), which is making the calculated *FS* misleadingly high.

To cope with this limitation in *Plaxis 3D* the same model has been analysed but with the retaining structure along one side and prescriptions in the material illustrating retaining structures along the other sides without the connections in the structure corners.

The goal of the created models is to enable generalised cases for which the total stability failure can be studied for different lengths of the longest side in the excavation. For all of the different models the *Factor of Safety* is compared for

respective calculation-method. This is done to determine how and if they differ from each other.

After the generalised models have been created, a similar work process is applied to a real-life case to see if a case with real-life parameters and structures behave in accordance with the generalised models.

This work investigates behaviour in total stability and it is important that the calculated FS can be traced to this type of failure mechanism. For example excavations with a width smaller than the length of the critical slip surface at the bottom of the excavation can therefore no longer be compared in terms of total stability. Here the failure mechanism is thought to be bottom heave and is therefore not included in this project.

4.1 Software introduction

Slope/W

Slope/W is a part of the *Geostudio*-series alongside a number of different analytical geotechnical calculation software used for different problems. *The Geostudio-software* is created by *Geo Slope International* (Geo-Slope International 2012).

Slope/W is designed to calculate slope stability; it uses moment and force equilibrium equations to calculate the stability. For the calculations in *Slope/W* the different slip surfaces evaluated are split into a number of slices (see Section 2.1) and then calculated. The program then evaluates a number of slip surfaces to find the most critical one (Geo-Slope International 2012). With the aid of *Slope/W* the user has the possibility to find and calculate a huge number of different slip surfaces much faster than possible by hand calculations.

Slope/W includes a number of different methods for calculations; the one used in this work is the *Morgenstern-Price* method. This method is explained further in Section 2.1.

From the calculations performed in *Slope/W* the user gets useful and necessary results. In this work the following results are used from *Slope/W*: factor of safety, activating moment, retaining moment, area of slip surface and radius of slip surface.

Depending on how the retaining structure is constructed i.e. how the wailing beams is supported, different assumptions of the acting force at each level can be made.

If the wailing beam is anchored between the retaining structure and the slip surface (internally supported) it should in the opinion of the authors have no influence on the total stability. If the sliding body on the other hand is externally supported with for example beams against the wailing beams it seems reasonable to include these forces in the analytical equilibrium equations. This is later verified by comparing the analytical calculations to the numerical calculations in *2D-Plaxis*.

Plaxis 2D and Plaxis 3D

Introduction

Plaxis is one of the most used numerical programs for performing analyses of deformation, stability and of water flow in geotechnical engineering.

In this work two versions of *Plaxis* are used, the 2D version (*Plaxis 2D*) and the 3D version (*Plaxis 3D*). *Plaxis 2D* includes methods for calculating static elastic-plastic deformations, stability analysis, consolidation, safety-analysis and steady-state groundwater flow.

Plaxis 3D is similarly equipped with several features to deal with various aspects of complex geotechnical structures and construction processes. The workflow in *Plaxis* enables the user to model the real workflow in different phases meaning, for example, that different parts of the excavation and activation of retaining structures can be modelled in accordance with the actual workflow.

In this work *Plaxis 2D* is mainly used for modelling the total stability. This is done to be able to verify that the FE-calculations generate the same *FS* out of the same conditions as the analytical 2D calculation does.

With *Plaxis 3D* complex 3D-geometries of soil can be defined for soil modelling. With a wide variety of different material models it is able to give a good representation of the real materials. The material models used in this work are the Mohr-Coulomb model and the Hardening soil model. These material models and how they are handled by *Plaxis* are explained more thoroughly in Chapter 3. Information regarding which material model the different cases are modelled in is presented in respective sections in Sections 4.2-4.4.

Mesh

In order to perform FE-calculations the geometry has to be divided into finite elements. A short introduction to the different elements available follows below. The

composition of these elements is called the mesh and it is automatically generated by *Plaxis*.

The resolution of the mesh should be sufficiently fine to obtain accurate finite element calculations (Plaxis 3Da 2013). *Plaxis* recommended mesh is not always sufficient and the meshing is of great importance when determining the *FS*. This has become apparent during the modelling process, as well as for other users (Persson and Sigström 2010). Therefore the mesh should be created in various levels of resolution to ensure that the *Factor of Safety* in the end does not change with a finer setting of the mesh. Examples of meshing for the models conducted in this work can be seen in Appendix B.

Elements

The default and recommended element used for soil and volume clusters in *Plaxis 2D* is the 15-node element. The elements provide a fourth order interpolation for displacements and the numerical integration involves twelve *Gauss Points* as illustrated below. Simplified elements are available; they do not give as good results as the 15-node element but require less memory (Plaxis 2D 2013).

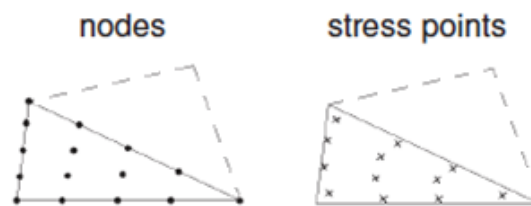


Figure 4:1 - Illustration of the node and stress points positions in a 15-node element (Plaxis 2D, 2013)

Structural elements used will by *Plaxis* automatically be assigned elements to be compatible with the chosen soil element (Plaxis 2D 2013).

Fixed end anchor

A point element fixed in the structure in one point and “fixed in space” on the other side. The fixed end anchors are used to simulate the shoring supporting the retaining structure.

Plate Elements

Plates are structural elements used for modelling slender constructions with material parameters EI , EA and d_{eq} (d_{eq} is the equivalent thickness). The plates are used to simulate the retaining wall, influence from walls and other similar constructions.

The 5-node plate elements are compatible with the 15 node soil elements. The bending moments and axial forces are possible to evaluate from the stresses at the stress points shown in Figure 4:2.

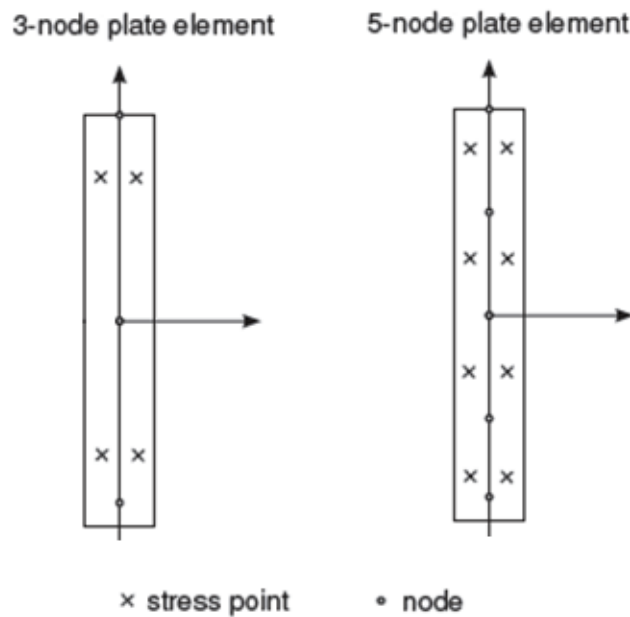


Figure 4:2 – Illustration of the node and Gaussian stress point positions at the plate elements (Plaxis 2D 2013)

Plaxis 3D elements

The default soil elements in the FEM mesh is 10-node tetrahedral elements Figure 4:3. The elements that interact with these soil elements are; *beam elements* that fit the 3-node of the soil elements edges, *interface elements* that are 12-node element for simulation of the interaction between soil and structural elements and 6-node plate and *geogrid elements* for plates and geogrid respectively.

For further information about the elements in *Plaxis 3D* the reader is referred to the *Plaxis* reference and scientific manuals (Plaxis 3D 2013), (Plaxis 3Db2013).

When modelling the constructions for this work the additional element when modelling in 3-dimensions is wailing beams supporting the retaining wall in-between the supporting shoring.

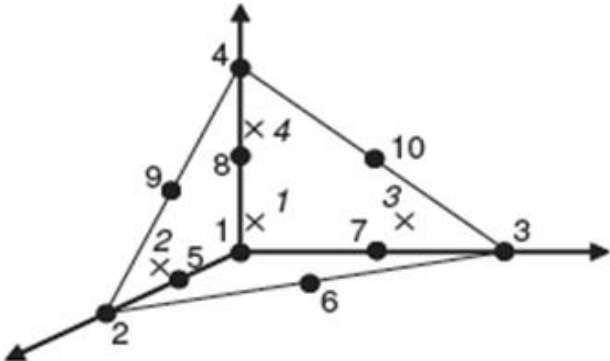


Figure 4:3 – Tetrahedral 10-node soil element (Plaxis 3Db 2013)

Safety calculation

The safety calculation mode in *Plaxis* successively reduces the parameters ϕ , S_u or C over a certain number of steps until failure occurs. The structural strength is not influenced by the reduction process.

The safety calculation is performed with the *Load advancement number of steps* procedure in *Plaxis*. The multiplier M_{fs} specifies the incremental strength reduction at the first step. At the start of the calculation it is set to 1.0 and the increments is by default set at 0.1.

The strength parameters are reduced successively until failure occurs. Then it recalculates the last step in the same manner until the target value of $\sum M_{fs}$ is reached exactly (Plaxis 3D 2013).

$$\sum M_{fs} = \frac{\tan\phi_{input}}{\tan\phi_{reduced}} = \frac{C_{input}}{C_{reduced}} = \frac{S_{u,input}}{S_{u,reduced}} \tag{4:1}$$

When the last step has resulted in failure the factor of safety is given by;

$$FS = \frac{available\ strength}{strength\ at\ failiure} = \sum M_{fs} \tag{4:2}$$

Boundary conditions

Plaxis 2D automatically sets the deformations along the bottom boundary to fully fixed and fixes the deformation in the X-direction $U_x = 0$ along the symmetry line. The corresponding is done for each of the vertical model boundaries in *Plaxis 3D* as shown in Figure 4:4;

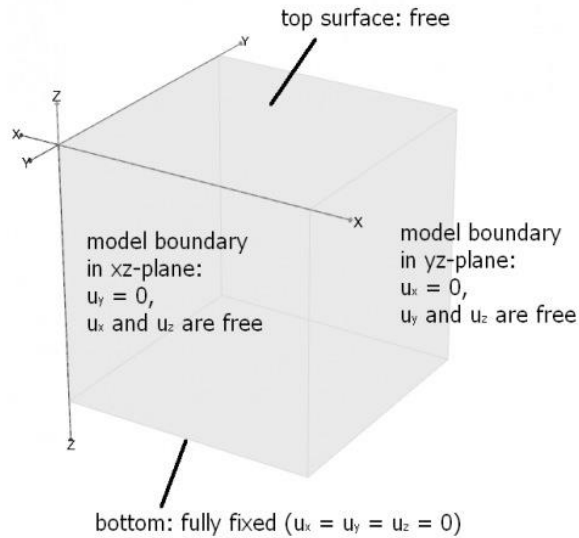


Figure 4:4 – Illustration of the outer boundaries of the geometry (Plaxis Tips n.d)

Regardless of the symmetry the slope and excavation in this work are modelled with sufficient lengths prior to and after itself so that these lengths do not affect the determination of the critical slip surface. The depth of the soil layer is also modelled to such depth that the critical slip surface is not affected by chosen boundaries. A simple test performed in *Plaxis 2D* is made to verify that the thought symmetry line works in a satisfying manner. This is presented in Appendix C.

Boundary conditions between the retaining structures and the soil are modelled with interfaces. Interfaces are joint elements that enable control of the soil-structure interaction. For the models in this work the strength of the interface is to be full, meaning $R_{inter} = 1$ (Plaxis 3Da 2013). Therefore no interface elements have been used.

The assumption of full interaction between soil and structure is based on a survey made 2002 at Götatunneln (the same site as for the Västlänken project). Pull-out tests were performed showing that the interaction is 98% for diaphragm walls performed in bentonite slurry and full interaction for other solutions (Engelstad 2002).

Drainage situations

Plaxis offers a number of different ways to perform the FE-analysis; drained analysis, undrained analysis and partially drained analysis. In this work the analysis is performed assuming undrained conditions for the clay material and drained for the fill material. Undrained analysis suits clay material in short-term perspective, which is suitable when calculating total stability for the excavations.

There are three ways of evaluating undrained behaviour in *Plaxis*; undrained A, B and C. In *Plaxis 2D* and *3D*, undrained B is chosen due to the fact that the friction angle in the clay is zero and the cohesion is equal to the undrained shear strength S_u in the models. The authors used *Plaxis* to generate the pore pressure (Plaxis 3Db 2013). For our models the excavations are considered to be time limited and the undrained shear strength is the parameter best known for the real-life case.

Initial stress generation

Initial stress generation can be modelled in two ways in *Plaxis*, either by the K_0 procedure or by *gravity loading*. The initial stress generation in the models for this work is done with the K_0 procedure which is a direct input method used when $K_0 = \frac{\sigma_h}{\sigma_v}$, the ratio between horizontal and vertical stresses is known and defined for each soil layer.

4.2 Generalised slope

The input parameters, geometrical data and other generalisations will be presented in this section of the report. It enables the recreation of the results that are presented later on.

The goal when creating this generalised slope has been to choose such geometry and material parameters that the generated slope will fail due to its own weight and therefore have a *Factor of Safety* less than one ($FS < 1$) for the 2D-calculations. The parameters, simplifications and generalisations made follows below with comments on why and how these are made.

Geometry

The slope chosen for the generalised model has a height of four meters and a length of six meters. This gives a slope at a 1:1.5 ratio. The height, length and width of the soil surrounding the slope are set to values which ensure that the slope itself is not affected by the size of the surrounding model.

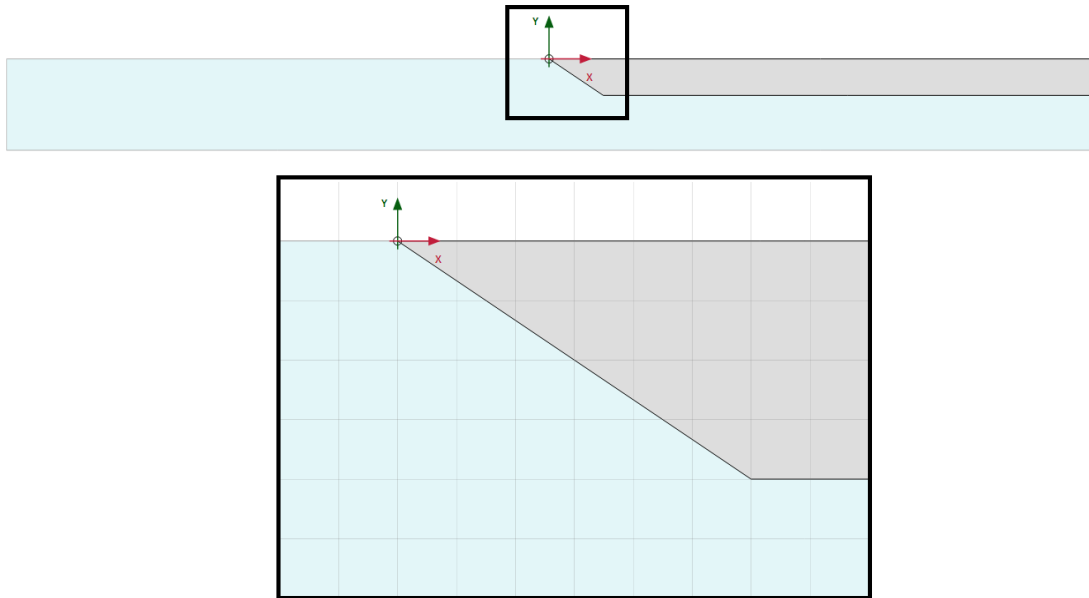


Figure 4:5 – Illustration of the geometry modelled in Plaxis 2D, for the generalised slope, height=4 m, width=6 m. The model shown above is cropped and does not show the total depth.

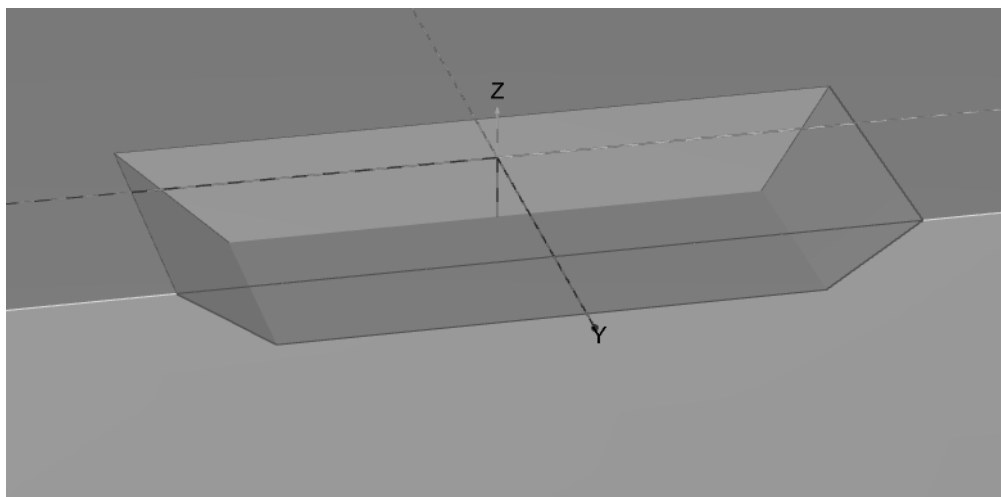


Figure 4:6 – Illustration of the geometry modelled in 3D, height=4 m, width=6 m. The model shown above is cropped and does not show the total depth.

To calculate the critical slip surfaces for the analytical calculations, *Slope/W* is used. The input-parameters used are specified in Section 4.2.

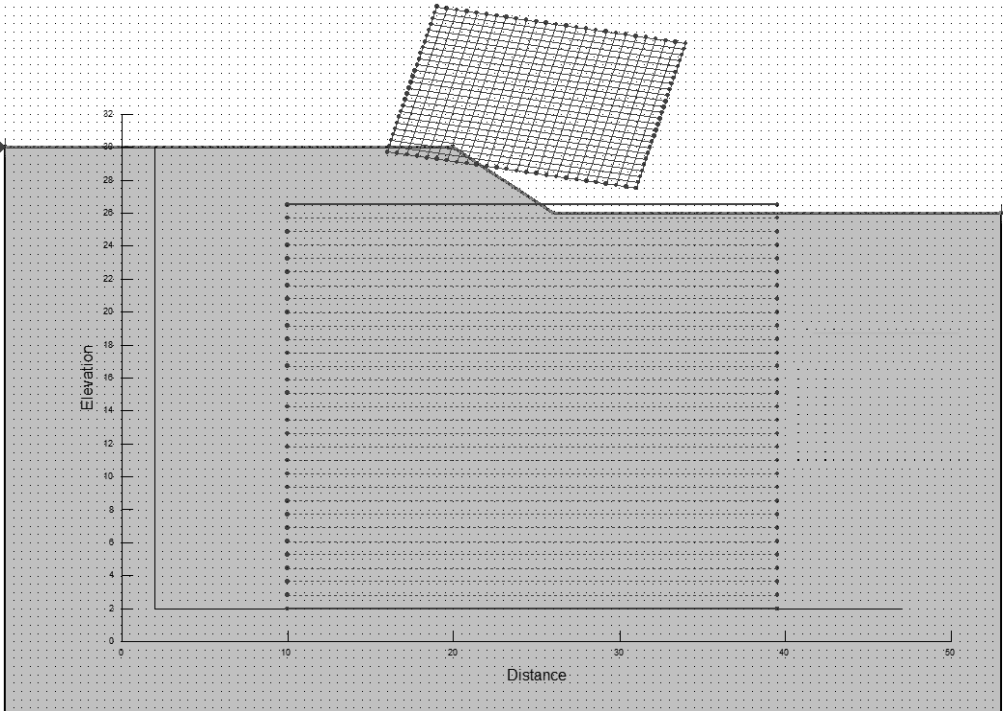


Figure 4:7 – Illustration of geometry used for calculations in *Slope/W*, height=4 m, width=6 m

Water

Due to the fact that the model is defined for cohesion materials the water level is set to follow the ground level. This means that the soil is always fully saturated. The drainage type used in *Plaxis 2D* and *Plaxis 3D* is *Undrained B*. After the excavation phase the area excavated is considered pumped dry (light area).

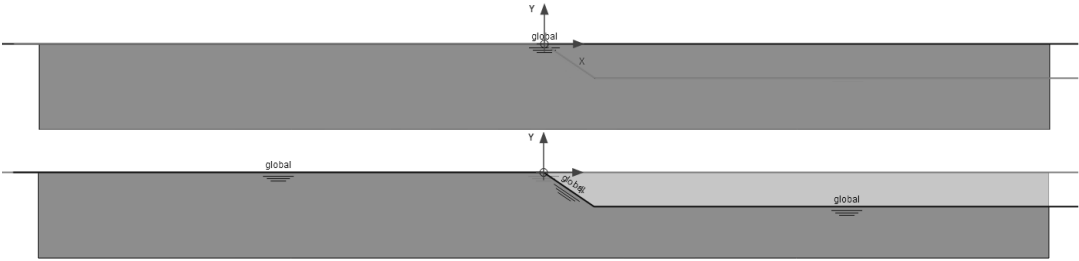


Figure 4:8 – Positioning of water level

Parameters

The parameters used for the soil model are presented in the table below (Table 4:1). The *Mohr-Coulomb* material model is chosen for *Plaxis 2D- and 3D*-analyses and the *Morgenstern-Price* method for the analytical calculations in *Geostudio – Slope/W*.

Table 4:1 –Parameter specification for the generalised slope

Input Parameters			
Name	Variable	Value	Unit
Height of slope	h	4	m
Length of slope	l	6	m
Water level is equal to ground level. i.e. Fully saturated			
Material			
Unit Weight of soil	γ_{soil}	16	kN/m ³
Cohesion	c	9	kPa
Cohesion increase	c_{inc}	0.3	kPa/m
E-modulus	E	7500	kPa
Poisson's ratio	ν	0.2	-
Initialising K	K_0	0.6650	-

Mesh

The meshing is of great importance when determining the *Factor of Safety*. Therefore the mesh is done in accordance with the software introduction Section 4.1.

4.3 Generalised excavation pit with retaining structure

Similar as for the generalised slope without retaining structures this model has parameters chosen to achieve a *Factor of Safety* that is less than one ($FS < 1$) in 2D-calculations. The length and type of the retaining structure is determined based on calculation methods from Ryner, et al. (1996). The material parameters for the anchors and beams have also been calculated according to theory stated by Ryner, et al. (1996).

Geometry

This model has the geometry of an excavation pit. The depth of the excavation is four meters and the retaining structure continues down another three meters below the bottom of the pit. The retaining structure is supported by wailing beams and shoring.

The supporting structure is attached at one meter from the top of the wall and the shoring is attached every five meters along the sides see Figure 4:9. In the 2D-figure the shoring is placed in the z-direction (into the paper).

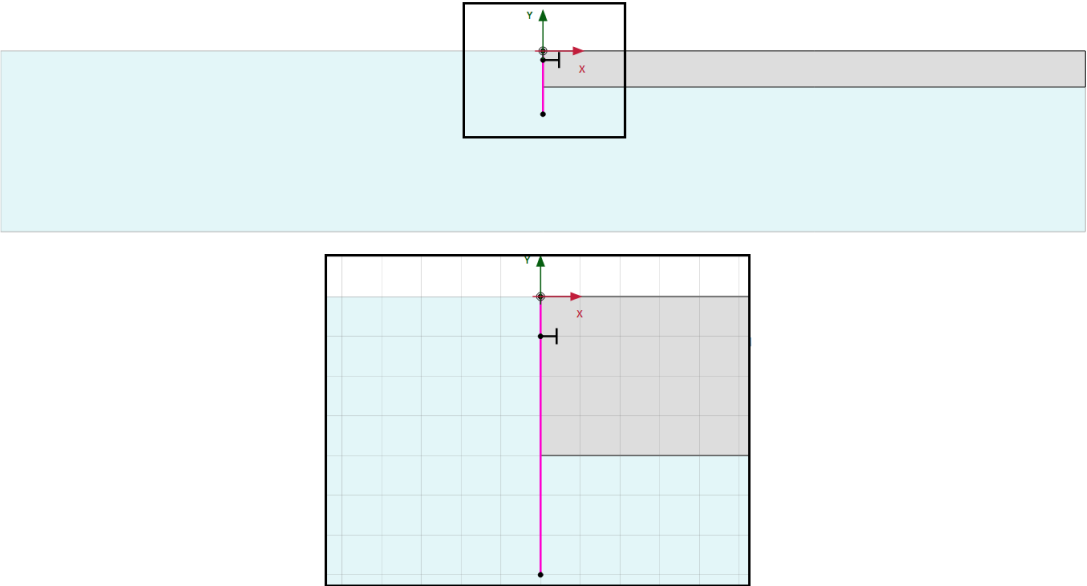


Figure 4:9 – Illustration of the geometry modelled in Plaxis 2D, for the generalised slope with retaining structure, height=4 m, height of retaining structure=7 m. The model shown above is cropped and does not show the total depth.

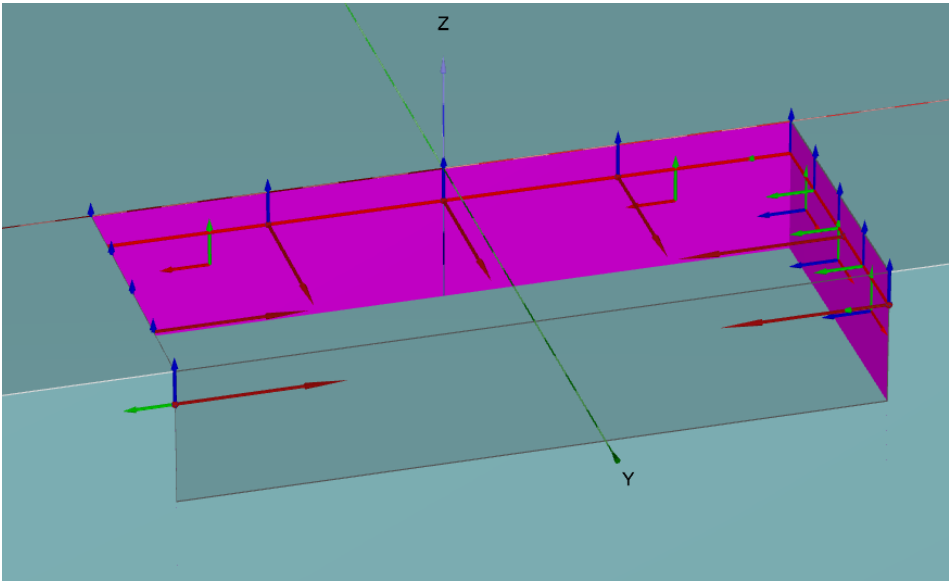


Figure 4:10 – Illustration of the geometry modelled in 3D, for the generalised slope with retaining structure, height=4 m, height of retaining structure=7 m. The model shows the boxed system

To cope with the limitation of just being able to model structures in linear elastic material in *Plaxis 3D* the same model has been modelled but with the retaining structure along one side and prescriptions in x-directions in the material simulating retaining structures along these sides. This enables the models to be created without the problematic structural connections in the corners but the effects of the surrounding materials and length limitation is still enabled. The difference can be seen by comparing Figure 4:10 and Figure 4:11.

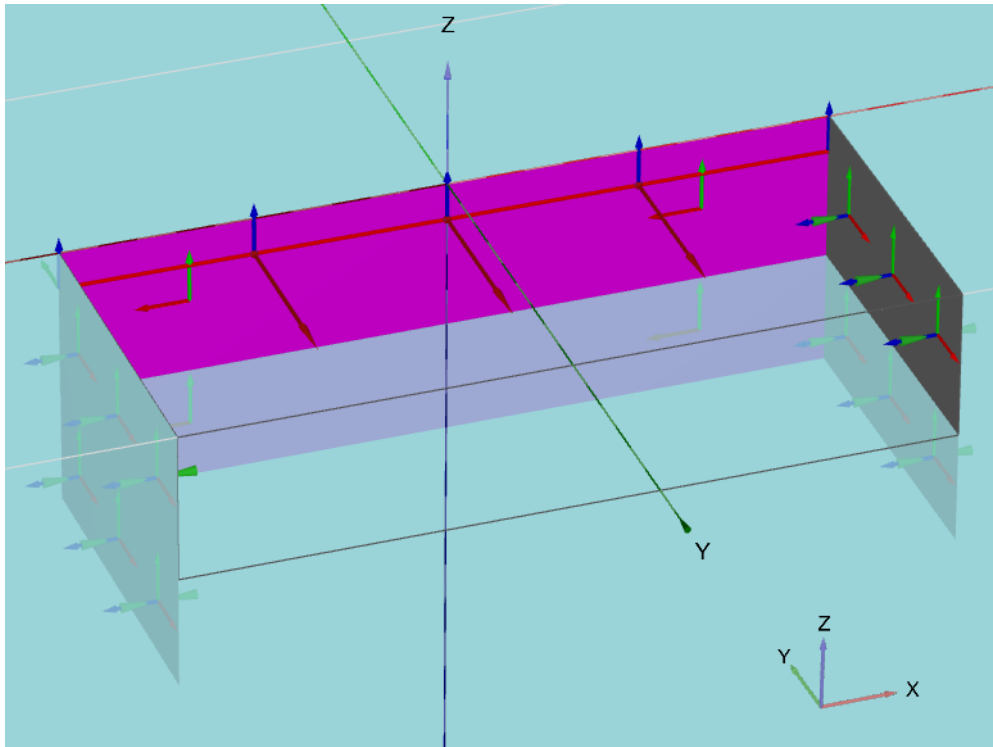


Figure 4:11 – Illustration of the geometry modelled 3D, for the generalised slope with retaining structure, height=4 m, Prescribed height and height of retaining structure =7 m. The figure shows the model with retaining structure on one side and prescriptions on the other two.

To find and calculate the critical slip surfaces *Geo Studio – Slope/W* is used. The input-parameters used are the ones specified in the parameters section. The wailing beam force levelled at -1 m has a minor influence in this calculation and is therefore left out.

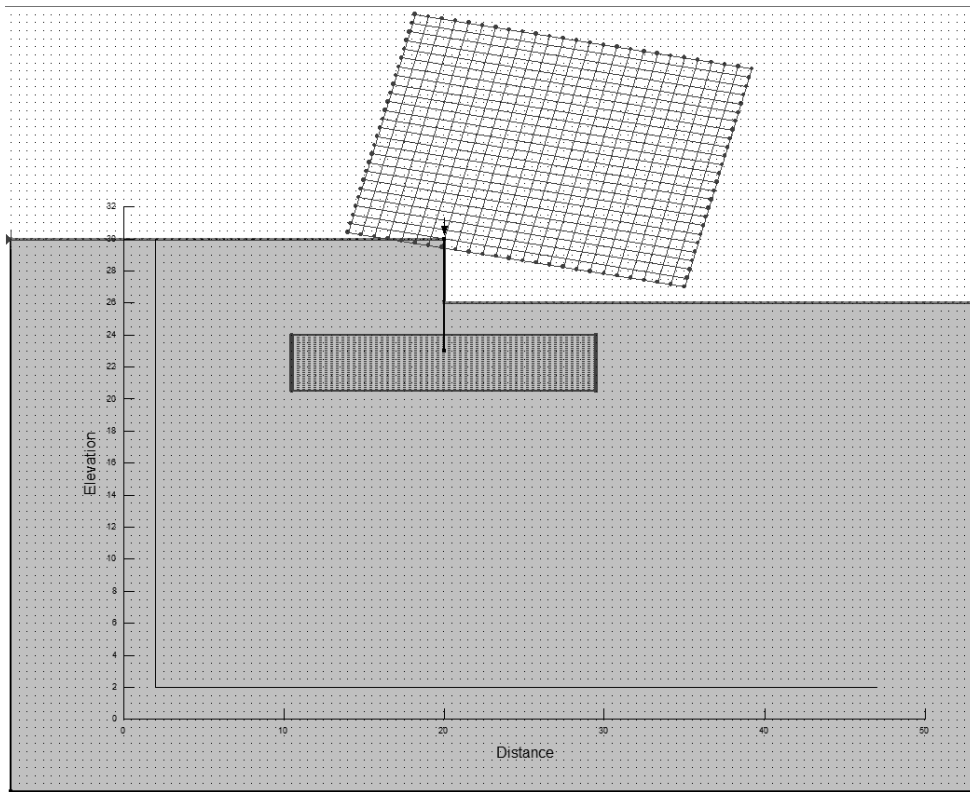


Figure 4:12 - Illustration of geometry used for calculations in Slope/W, height=4 m, height of retaining structure = 7 m

Water

Due to the fact that the model is defined for cohesion materials the water level is set to follow the ground level. This means that the soil is always fully saturated. The drainage type used in *Plaxis 2D* and *Plaxis 3D* is *Undrained B*. After the excavation phase the area excavated is considered pumped dry (light area in Figure 4:13).

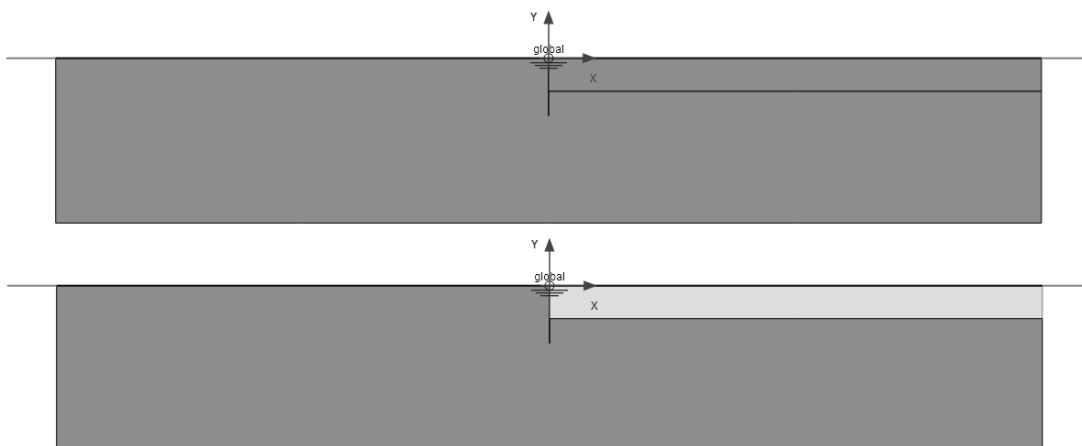


Figure 4:13 - Positioning of water level, before and after excavation

Parameters

The parameters used for the soil model are presented in Table 4:2. The material is the same as for the generalised slope. The *Mohr-Coulomb* material model is chosen for the *Plaxis 2D and 3D* FE-analysis and the *Morgenstern-Price* method for the analytical calculations in *Geostudio – Slope/W*.

Table 4:2 - Parameter specification for the generalised slope with retaining structure

Input parameters			
Name	Variable	Value	Unit
Height of slope	H	4	m
Height of retaining structure	H_{sp}	7	m
Height of prescribed sides	H_p	7	m
Water level is equal to ground level. i.e. Fully saturated			
Soil		Clay	
Unit weight of soil	γ_{soil}	16	kN/m ³
Cohesion	c	9	kPa
Cohesion increase	c_{inc}	0.3	kPa/m
E-modulus	E	7500	kPa
Poisson's ratio	ν	0.2	-
Initial K	K_0	0.6650	-
Plate			
Thickness	t	0.006	m
Thickness (cross section)	h	0.22	m
Elasticity modulus	E_{steel}	210*10 ⁹	kPa
Area (cross-section)	A	0.00101	m ² /m
Moment of inertia	I	6.6*10 ⁻⁵	m ⁴ /m
Unit weight steel	γ	78.50	kN/m ³
Beam			
Elasticity modulus	E	210	GPa
Area (cross-section)	A	0.01314	m ²
Unit weight	γ	78.50	kN/m ³
Moment of inertia	I_2	0.06595*10 ⁻³	m ⁴
Moment of inertia	I_3	0.1927*10 ⁻³	m ⁴
Anchor			
Elasticity modulus	E	210	GPa
Area (cross-section)	A	0.002124	m ²
Anchor spacing	$L_{spacing}$	5	m

Mesh

The meshing is of great importance when determining the *Factor of Safety*. Therefore the mesh is done in accordance with the software introduction in Section 4.1. Example of meshing quality can be seen in Appendix B.

4.4 Real-life case (*Västlänken* project)

As for the generalised case with retaining structure this model is conducted in a similar fashion as explained previously but with parameters and structures from a real-life project. The parameters and geometry used in this model are listed below.

Another task for this particular case is to evaluate how big sections with a 70 meter wide excavation (with retaining walls) that can be dug-out and still satisfy the factor of safety used in the *Västlänken* project ($FS > 1.56$).

Geometry

The model has the geometry of an excavation. The depth of the excavation is 15 m and the retaining structure continues down an additional 23 m below the bottom of the pit. The retaining structure is supported by four wailing beams with shoring every 10 m. The levels where the wailing beams are installed are at 1, 6, 11 and 13.5 m beneath the surface.

To find and calculate the critical slip surfaces *Slope/W* is used. The input-parameters used are specified in the parameters section.

On the right hand side in Figure 4:14 the length of the excavated area is 35 meters from the retaining wall to the symmetry line i.e. the width of the excavation is constantly kept to 70 meters. This is done due to the fact that this is the sought length of the sections for the project. Also true for this model is that, the conditions for this failure mechanism must be allowed in accordance with previous statements.

In this case the same method as for the generalised case with retaining structure is used to deal with the limitations in *Plaxis 3D*. The 3D-models therefore contain one side with retaining structure and prescriptions on the other two.

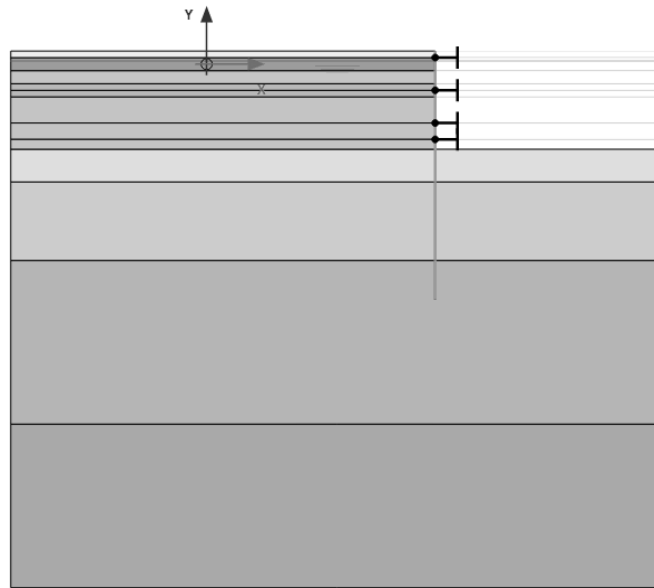


Figure 4:14 – Geometry illustration for Plaxis 2D-model

The model is in correlation with previous models, defined with sufficient length on the left hand side of Figure 4:14 so that the placement of the critical slip surface is not affected. The depth of the soil layer is also modelled to such a depth that the slip surface is not affected.

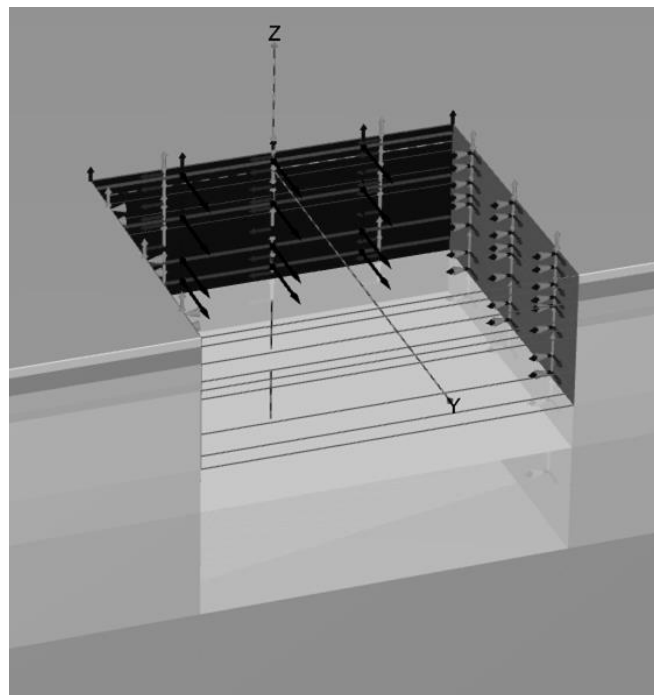


Figure 4:15 – Illustration of the geometry modelled 3D. The figure shows the model with retaining structure on one side and prescriptions on the other two.

For the calculations performed in Slope/W the geometry is modelled as can be seen in Figure 4:16. In the analytical calculations the method does not allow for a symmetry line and the length is therefore set to the full width of 70 meters to allow the critical slip surface inside the excavation.

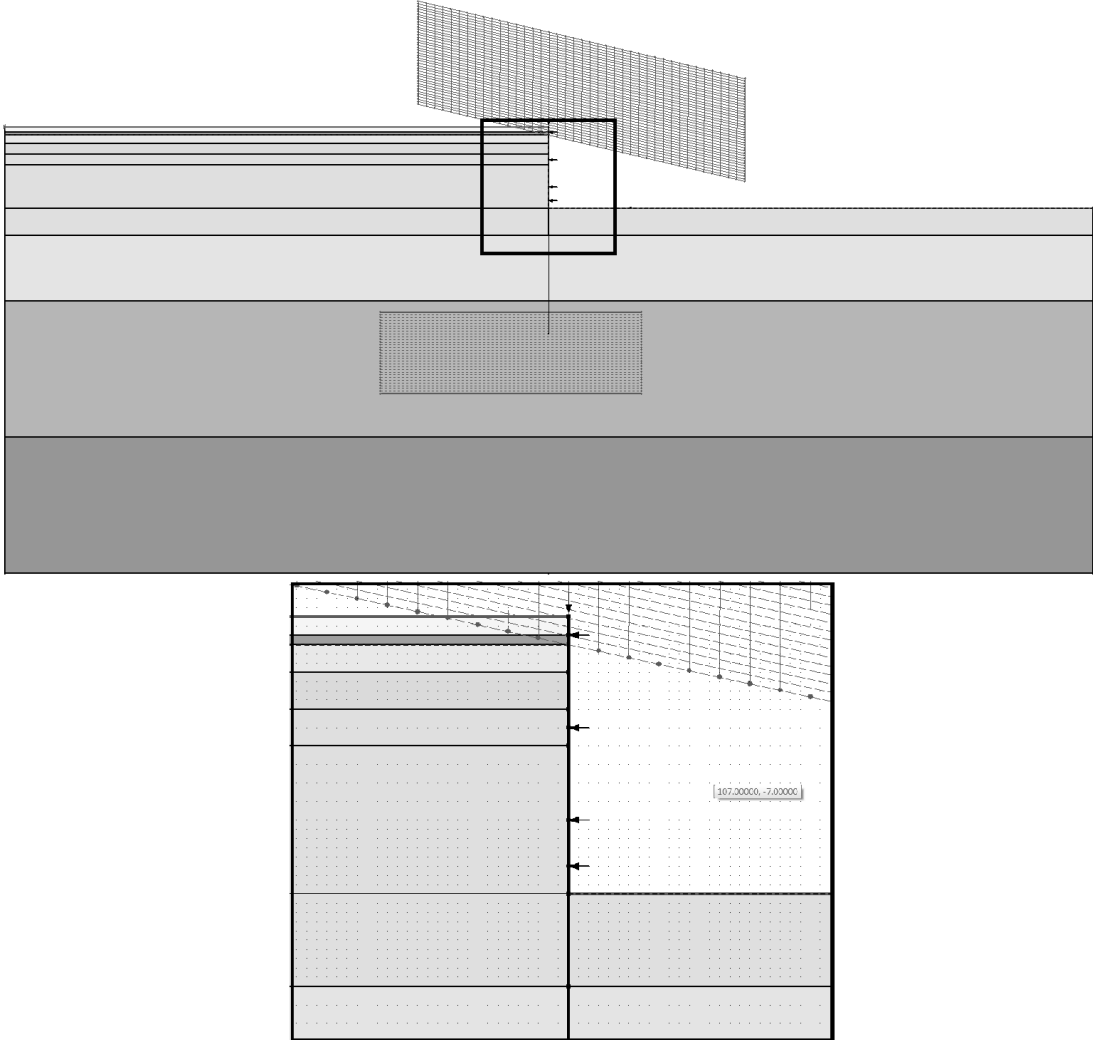


Figure 4:16 - Illustration of geometry in Slope/W

When calculating the *FS* with *Slope/W* point loads are included in the model to simulate the shoring that is used. The magnitude of these point loads are determined through 2D calculations performed in *Plaxis 2D*. The usage of these point loads in the analytical calculations is later validated to some degree by comparing the analytical *FS* and the *FS* calculated in *Plaxis 2D*. The exact values of the extracted point loads (from *Plaxis 2D*) can be seen in Appendix D.

Water

For this case the water level is found at +0.5 m (1.5 m from the surface). The excavation is considered dry in every new excavation step simulating a pump that is used to pump the water out at all times. The drainage type used in *Plaxis 2D* and *Plaxis 3D* is *Undrained B*.

Mesh

The meshing is of great importance when determining the *Factor of Safety*. Therefore the mesh is done in accordance with the software introduction in Section 4.1. Example of meshing quality can be seen in Appendix B.

Parameters

The parameters used for the soil model are presented in Appendix A and the structural parameters in Table 4:3. The dimensioning of the structural parameters has been made in accordance with Ryner, et al. (1996) for the *Västlänken* projects geometrical and material conditions. They are presented in term of how they are inserted in *Plaxis*

The material model chosen in *Plaxis 2D and 3D* is the Hardening Soil model and for the analytical calculations are made in *Slope/W* using the *Morgenstern-Price* method.

Table 4:3 - Parameter specification for the real-life case

Input parameters			
Name	Variable	Value	Unit
Height of slope	H	15	m
Height of sheet pile	H_{sp}	38	m
Water level is at 0.5 meters. During the excavation process the excavated pit is considered dry.			
Soils			
Input parameters for the soil materials can be seen in the Appendix A. The soils are divided into Fill 1, Fill 2 and Clays 1 to 7.			
Plate (Retaining wall)		Isotropic	
Thickness	t	1.0	m
Thickness (cross section)	h	0.22	m
Elasticity modulus	E_1	14.71	GPa
Elasticity modulus	E_2	14.71	GPa
Shear modulus	G	5.658	GPa
Moment of inertia	I	$6.6 \cdot 10^{-5}$	m^4/m
Unit weight	γ	25	kN/m^3
Poisson's ratio	ν	0.3	-
Beam 1 (Wailing Beam 1)		1 (1m)	
Elasticity modulus	E	210	GPa
Area (cross-section)	A	0.06900	m^2
Unit weight	γ	78.50	kN/m^3
Moment of Inertia	I_2	0.0006407	m^4
Moment of Inertia	I_3	0.01673	m^4
Beam 2 (Wailing Beam 2,3,4)		(-4m, -9m, -11.5m)	
Elasticity modulus	E	210	GPa
Area (cross-section)	A	0.1080	m^2
Unit weight	γ	78.50	kN/m^3
Moment of Inertia	I_2	0.002626	m^4
Moment of Inertia	I_3	0.03362	m^4
Anchors (Shoring)			
Elasticity modulus	EA	13.15	GN
Anchor spacing	$L_{spacing}$	10	m
Max, tension	$F_{max, tension}$	22.22	MN
Max, compression	$F_{max, compression}$	19.50	MN
Point loads (For Slope/W)		Load against retaining wall from inside of excavation.	
+1m	PL_1	40.5	kN
-4m	PL_{-4}	677.8	kN
-9m	PL_{-9}	1084	kN
-11.5m	$PL_{-11.5}$	882	kN

5 Results

5.1 Generalised slope

Two-Dimensional calculations

From *Slope/W* resulting *FS* and the positioning of the critical slip surface is given and can be viewed in Figure 5:1.

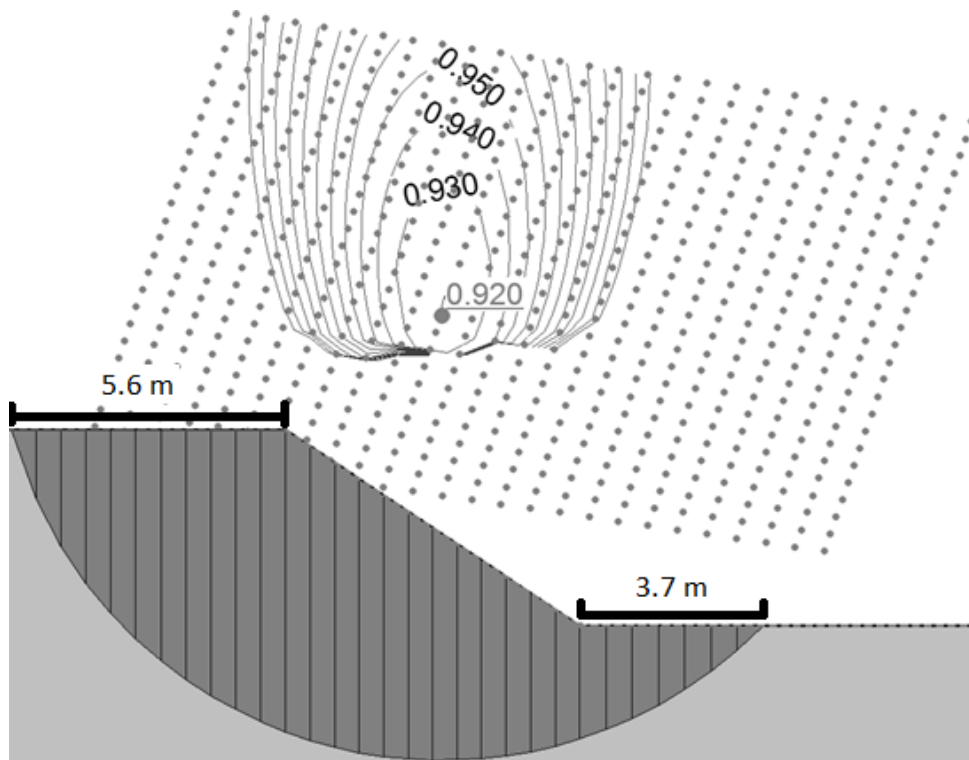


Figure 5:1 – Result generalised slope in Slope/W, $FS = 0.92$

Table 5:1 – Results generalised slope

2-Dimensional analytical results		
<i>Factor of Safety</i>	0.92	-
$Area_{\text{slip surface}}$	55.675	m^2
$M_{\text{Resisting}}$	1752.8	kNm
$M_{\text{Activating}}$	1906.1	kNm
Radius	8.575	m
C (Equation 2:6)	2.793	m

The *FS* calculated in *Plaxis 2D* is 0.93. It is similar to the one obtained from the analytical calculations.

$$FS_{2D-Plaxis} = 0.93$$

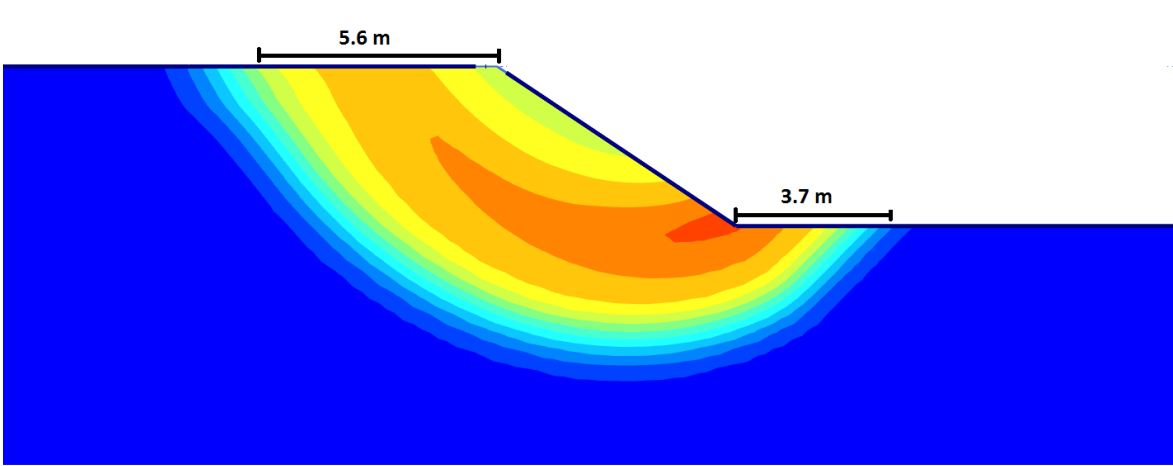


Figure 5:2 – Result, generalised slope *Plaxis 2D*, *FS* = 0.93

The deformation shows a similar pattern as for the analytical calculations when looking at the *Plaxis 2D* results seen in Figure 5:2.

For the 2D-calculations the results are plotted in Figure 5:3. These results do not consider any 3D-effects.

Table 5:2 - Result 2D

Results 2D		
	<i>2D - Analytical</i>	<i>Plaxis 2D</i>
Factor of Safety	0.92	0.93

2D-Calculations with 3D-effects

The results for the 2-Dimensional *FS* are increased with the additional *3D-effects*. In correlation with *CSS report 3:95*, the *Factor of Safety* has been evaluated for a number of different slip surfaces to ensure that the slip surface chosen still is the most critical one even after the increase.

In Figure 2:3 the increased *FS* is plotted for each length. It is presented, in a logarithmic scale.

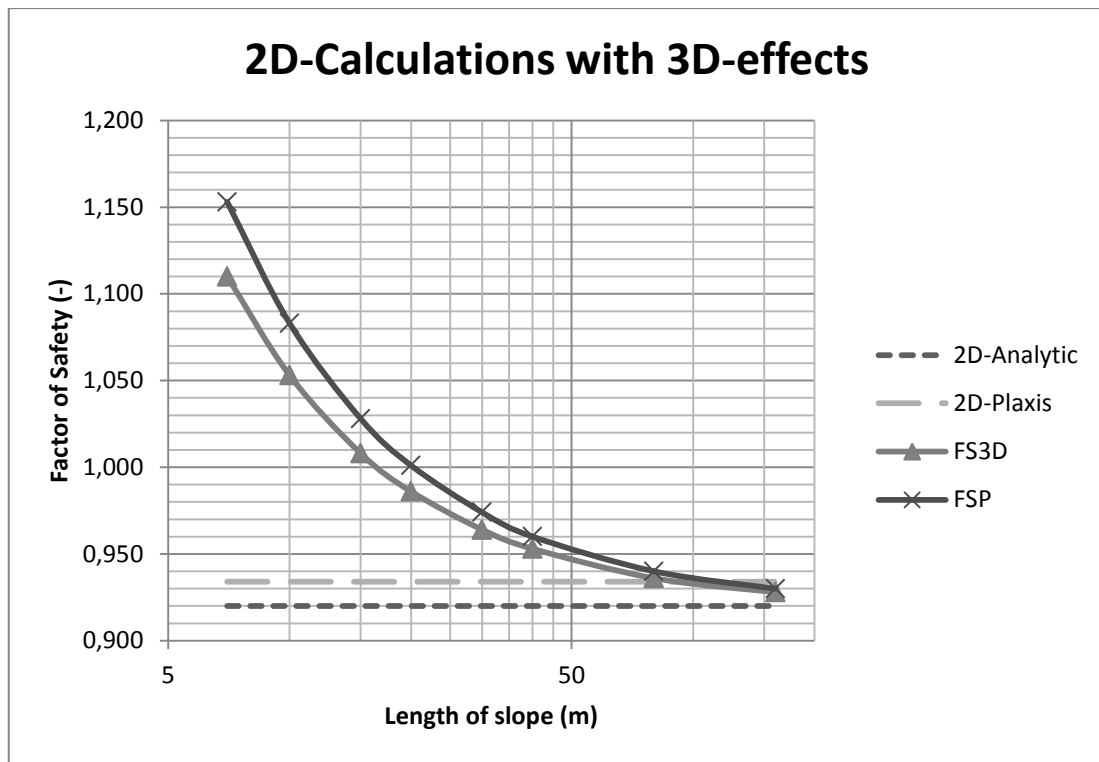


Figure 5:3 – 2D-calculations for the generalised slope

It can be seen that the retaining structure will collapse if calculated analytically in 2D ($FS=0.92$). When considering end surface effects however the system is stable until somewhere between 15 and 20 meters ($FS \geq 1$). This applies for both FS_p and FS_{3-Dim} (FS_p - Planar end surfaces, FS_{3-Dim} - Reduced due to non-planar end surfaces).

Three- Dimensional calculations

3D-models for the different dimensions are evaluated to view the overall 3D-effect for sloped excavations when the different sides interact with each other. Figure 5:4 shows the total deformation of the sloped excavation in plane. There is nothing for any of the modelled dimensions indicating that the slopes cannot be approximated as separate slopes limited by the corners of the excavation. The failure in these models is total stability failure (Figure 5:5), arising at the middle of the sides and not in the corner why the interaction between sides is no problem for these generalised sloped excavations.

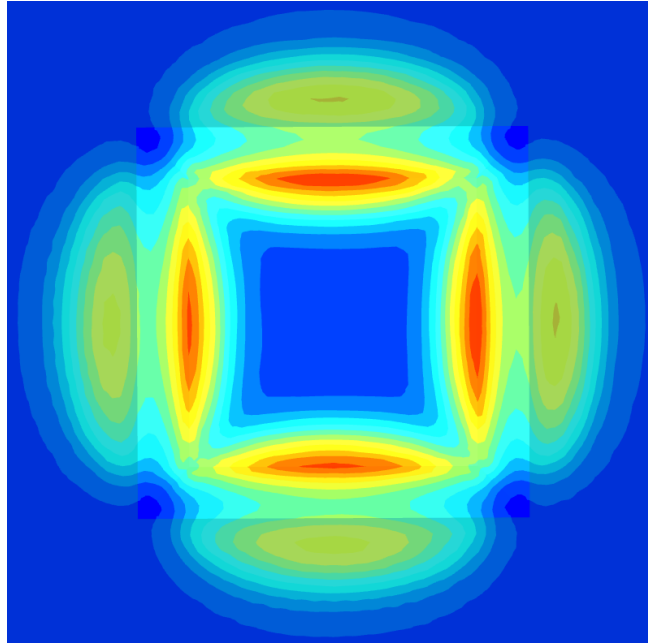


Figure 5:4 – Result, generalised slope Plaxis 3D, 40m (length of slope)

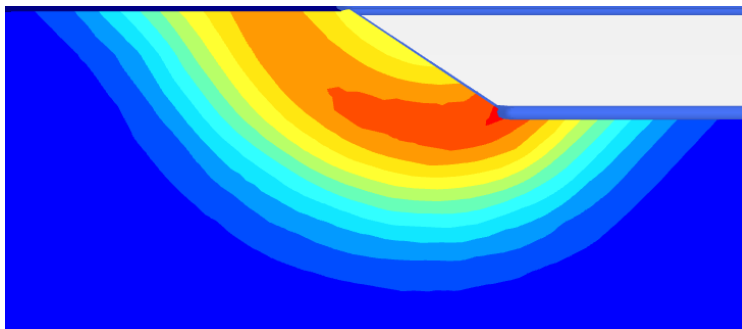


Figure 5:5 – Result, generalised slope Plaxis 3D, 40m (length of slope),
Critical slip surface in the middle of one side

The FS calculated in *Plaxis 3D* is compared to the analytically approximated FS in Figure 5:6. The values are also presented in

Table 5:3.

Studying Figure 5:6 it is apparent that the sloped excavation pits smaller than 15X15 m has a much higher FS in the FE-models than in the analytical calculations. This is thought to be geometrical effects that will be discussed later.

The analytically calculated FS is on the safe side compared to the numerically calculated FS . The difference between FS_p and $FS_{Plaxis\ 3D}$ is presented in percentage in

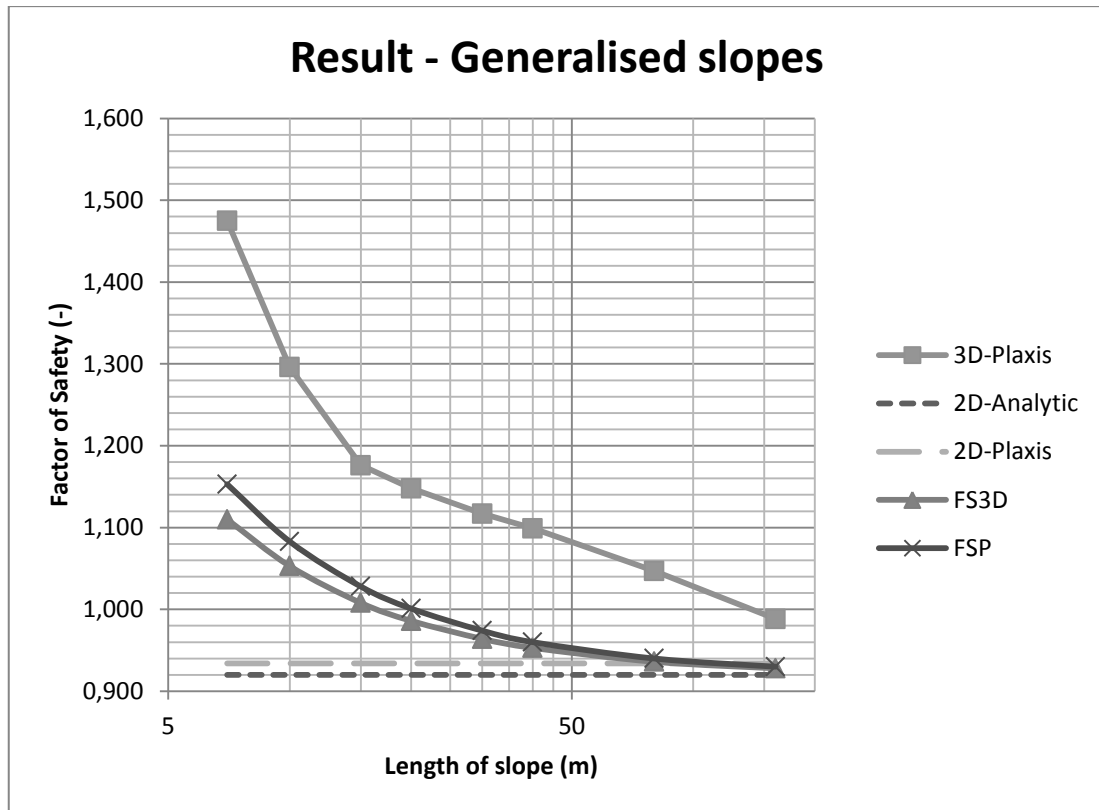


Figure 5:6 - Result summarization - Generalised slopes

Table 5:3 - Result summarization - Generalised slopes

Factor of Safety - all calculation types for different widths of the slope						
Length of slope (m)	2D - Calculation	2D-Plaxis	FS_P	FS_{3D}	$FS_{3D Plaxis}$	Diff. FS_P and $FS_{3D Plaxis}$ (%)
7	0.92	0.93	1.15	1.11	1.48	27.9 %
10	0.92	0.93	1.08	1.05	1.30	19.7 %
15	0.92	0.93	1.03	1.01	1.18	14.4 %
20	0.92	0.93	1.00	0.99	1.15	14.7 %
30	0.92	0.93	0.97	0.96	1.12	14.7 %
40	0.92	0.93	0.96	0.95	1.1	14.5 %
80	0.92	0.93	0.94	0.94	1.05	11.4 %
160	0.92	0.93	0.93	0.93	0.99	6.3 %

5.2 Generalised excavation pit with retaining structure

Two-Dimensional calculations

From *Slope/W* the resulting *FS* and positioning of the critical slip surface is given and can be viewed in Figure 5:7. The shoring has not been considered for the analytical calculations, as discussed in Section 4.1. If the shoring is handled as an internal or external force makes a difference. This was noticed when modelling the later on presented real-life case and is not considered in the generalised case.

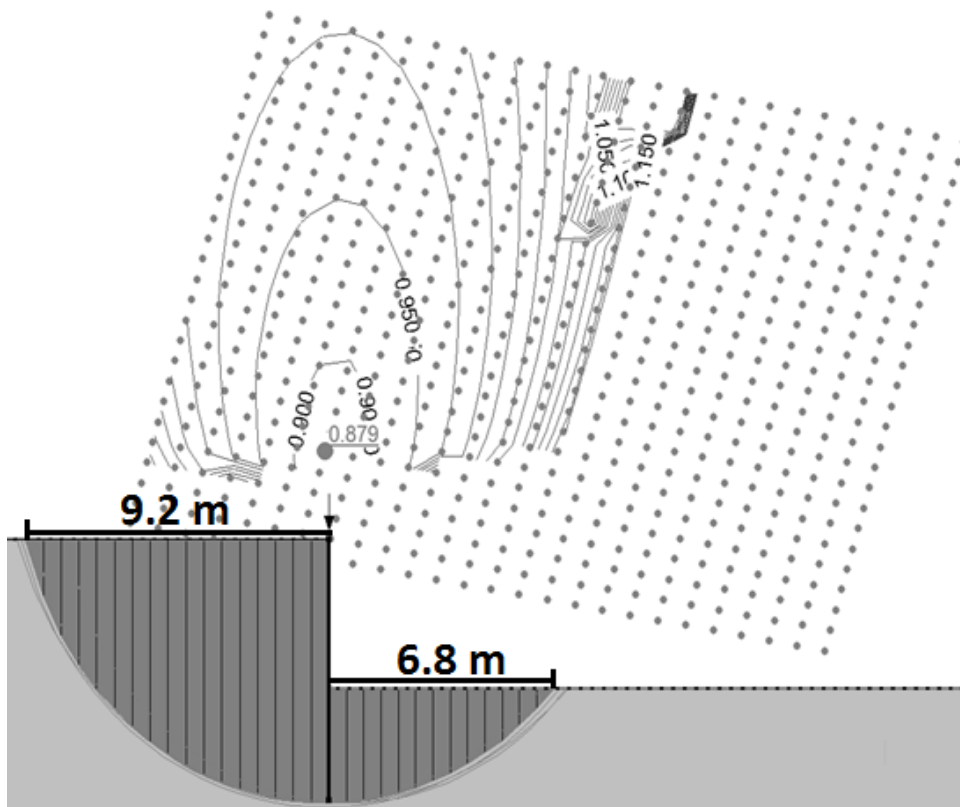


Figure 5:7 – Results Slope/W, *FS*=0.88

Table 5:4 – Results Slope/W

2-Dimensional analytical results		
<i>Factor of Safety</i>	0.88	-
<i>Area</i> _{slip surface}	62.437	m ²
<i>M</i> _{Resisting}	1899.2	kNm
<i>M</i> _{Activating}	2159.8	kNm
<i>Radius</i>	9.360	m
<i>C</i> (Equation 2:6)	2.817	m

The FS calculated in *Plaxis 2D* is 0.93. It is similar to the one obtained from the analytical calculations but with a small difference due to the shoring.

$$FS_{2D-Plaxis} = 0.93$$

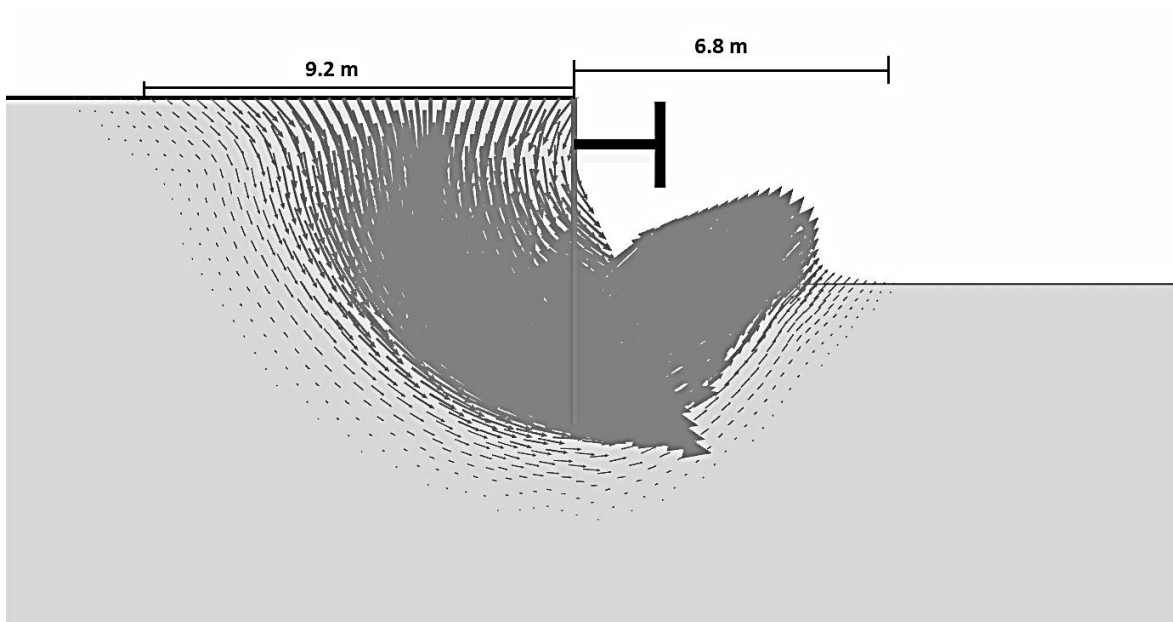


Figure 5:8 – Results Plaxis 2D, $FS=0.93$

The FS for the 2D-calculations are shown in Table 5:5.

Table 5:5 - Result 2D

Results 2D		
	<i>2D - Analytical</i>	<i>Plaxis 2D</i>
<i>Factor of Safety</i>	0.88	0.93

2D-Calculations with 3D-effects

The results for the 2-Dimensional FS are increased with the end surfaces shear forces. In correlation with the *CSS report 3:95*, the FS has been controlled for a number of different slip surfaces to ensure that the slip surface chosen still is the most critical one even after the increase.

After evaluating different slip surfaces it is concluded that the critical slip surface has changed when considering 3D-effects. This updated slip surface is the one presented in Figure 5:7.

In Figure 5:9 the increased 2-Dimensional *FS* is shown for each length, calculated according to the *CSS report 3:95*.

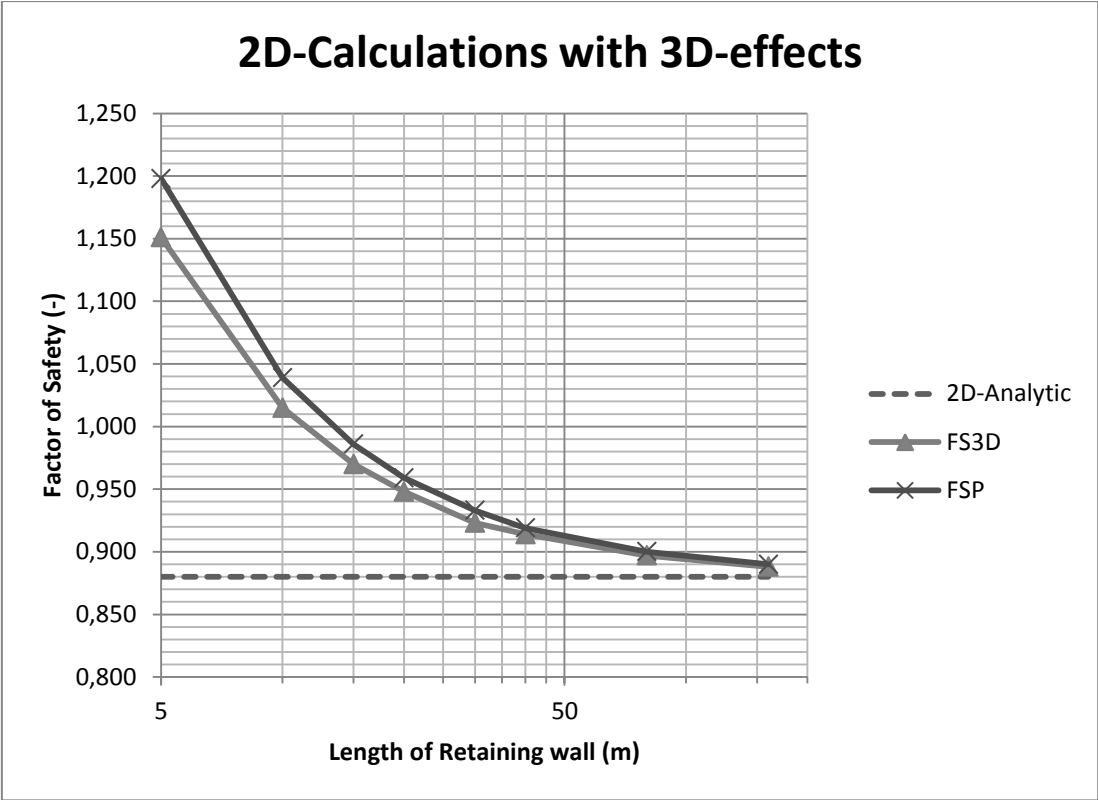


Figure 5:9 – Results for 2D calculations

It can be seen that the retaining structure will collapse if calculated analytically in 2D ($FS=0.88$). When considering end surface effects however the system is stable ($FS \geq 1$) until somewhere between 10 and 15 meters. This applies for both FS_p and FS_{3-Dim} (FS_p - Planar end surfaces, FS_{3-Dim} - Reduced due to non-planar end surfaces).

Three- Dimensional calculations

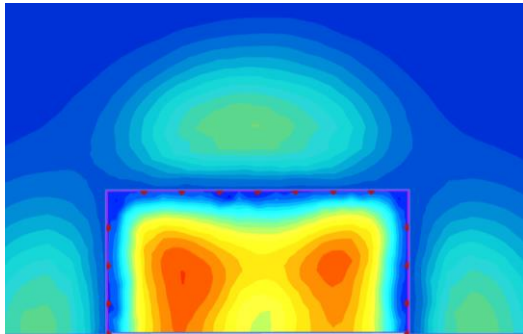
Different dimensions of this generalised case are evaluated to view the 3D-effect for excavations that contain retaining structures. The earlier mentioned limitation in

Plaxis 3D is dealt with by introducing another modelling method and the result for the two different ways of modelling is presented.

Figure 5:10 shows the so called boxed 40x40m excavation with connected retaining structures on all sides and Figure 5:13 show the case with retaining structure along one side and with prescriptions along the others.

For the boxed system, Figure 5:12b) visualise that the structure forces the materials beneath the construction resulting in a different failure mechanism, bottom heave. As mentioned this is due to the structural element in *Plaxis 3D* which is limited to linear-elastic material models, therefore the structure never plasticises. The structures withstand unreasonable big moment especially in the corners. This phenomena is presented more in Appendix E.

a)



b)

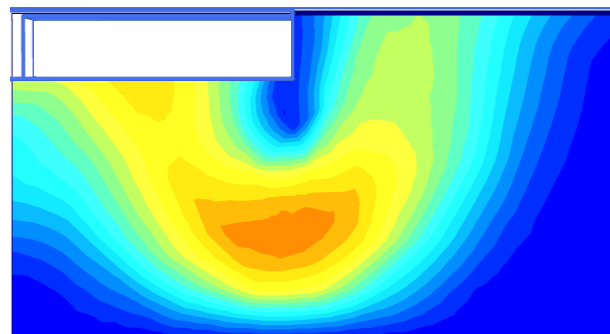


Figure 5:10 a) Resulting total displacement for "boxed" system (seen from above) b) Section showing bottom heave.

The models with prescriptions on the sides do not have the problems from the connection of the structures and as can be seen in Figure 5:13b) it is a total stability failure. As for the sloped excavations both types of models with retaining structure are stable around the corners.

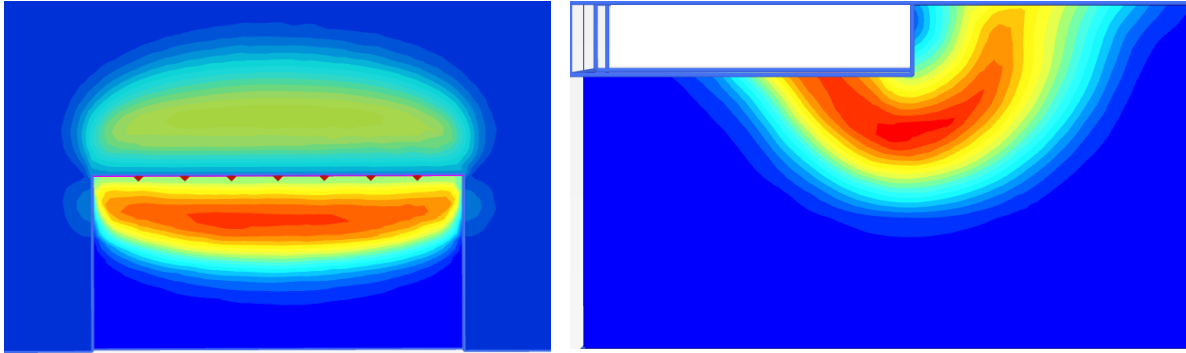


Figure 5:11 – Results Plaxis 3D, Boxed system (Total displacements, seen from above)

In Figure 5:12 the *FS* for the two systems with retaining structure is shown. An infinite long slope modelled in 3D with the same retaining structure is also shown. It can be seen that the system modelled with prescriptions goes towards the 2D-case whereas the boxed does not.

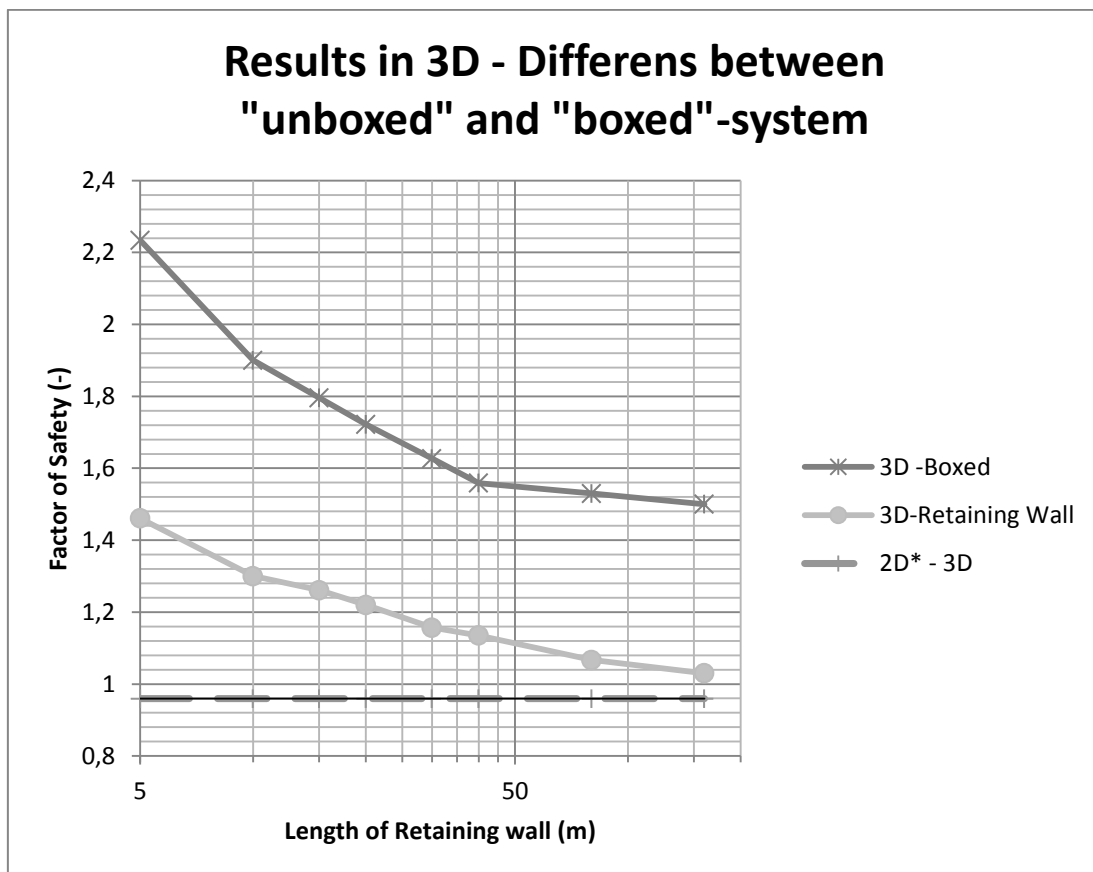


Figure 5:12 – Results Plaxis 3D, Boxed systems compared to systems with one retaining wall with prescriptions

Further on the models will be defined with prescriptions and the FS in the comparisons will be presented from those systems.

Result summarisation – Generalised excavation pit with retaining structure

In Figure 5:13, FS from *Plaxis 3D* for each length is presented along with the analytically calculated FS . There is no distinct deviation in the numerically calculated FS for the smaller geometries as could be seen for the sloped excavations.

As for the sloped excavations the analytically increased FS is on the safe side compared to the numerically calculated FS . The difference between FS_P and $FS_{3DRetaining\ wall}$ is presented in percentage in Table 5:6.

It should be noticed that if the shoring would have been accounted for in the analytical calculations the analytically calculated FS would become equivalent to the FS calculated in *Plaxis 2D*, ($FS=0.93$). Starting at this FS when adding the 3D-effects would give a more accurate comparison with the later on presented 3D-models analysed in *Plaxis 3D*.

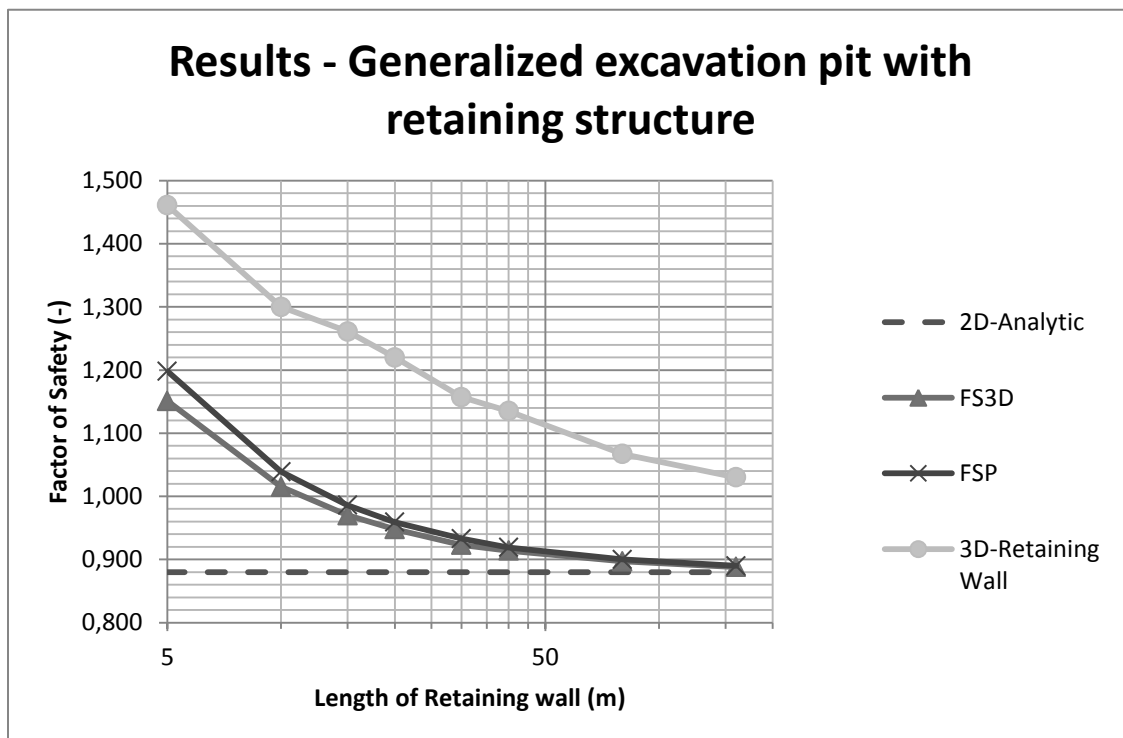


Figure 5:13 – Result for generalised slope with retaining structure

Table 5:6 – Result summarisation for generalised slope with retaining structure

Factor of safety - All calculation types for different length of retaining wall							
Length of slope (m)	2D Analytic	2D Plaxis	FS_P	FS_{3D}	2D* in 3D	FS_{3D} Retaining wall	Diff. FS_P and FS_{3D} Retaining wall (%)
5	0.88	0.93	1.15	1.20	0.96	1.46	18.0 %
10	0.88	0.93	1.02	1.04	0.96	1.30	20.1 %
15	0.88	0.93	0.97	0.99	0.96	1.24	21.8 %
20	0.88	0.93	0.95	0.96	0.96	1.20	21.4 %
30	0.88	0.93	0.92	0.93	0.96	1.16	19.4 %
40	0.88	0.93	0.91	0.92	0.96	1.13	19.0 %
80	0.88	0.93	0.90	0.90	0.96	1.07	15.7 %
160	0.88	0.93	0.89	0.89	0.96	1.03	13.6 %

5.3 Real-life case (*Västlänken* project)

Two- Dimensional calculations

When first modelling the system without consideration to the shoring the analytically calculated FS was lower ($FS \approx 1.1$) than the one calculated in *Plaxis 2D* ($FS=1.33$). The difference was found to be dependent on how the shoring is modelled analytically.

The FS from *Slope/W* and the positioning of the critical slip surface, when considering the shoring, can be viewed in Figure 5:14.

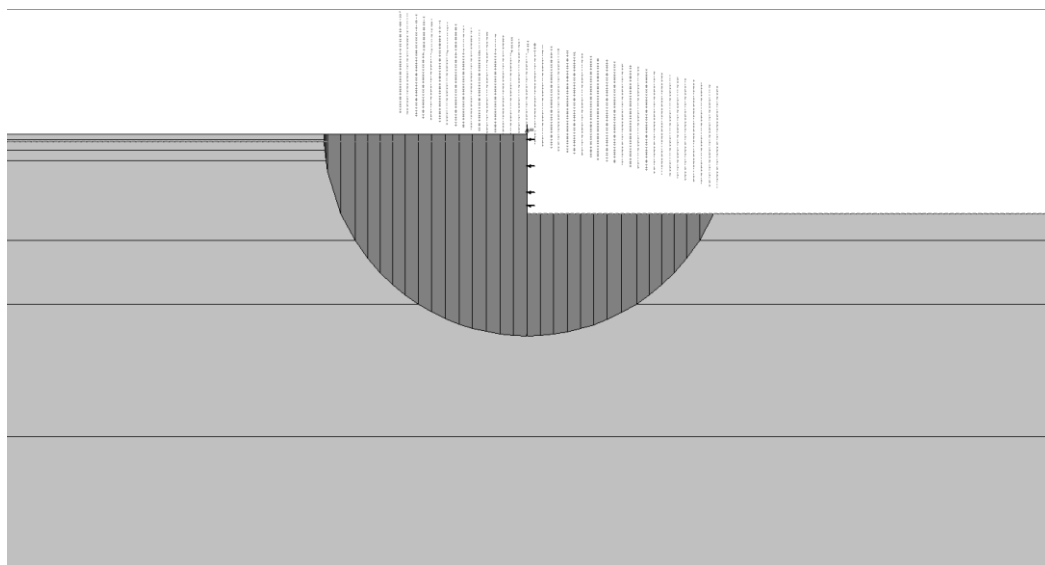


Figure 5:14 – Result Slope/W, $FS=1.34$

Table 5:7 – Results Slope/W

2-Dimensional analytical results		
<i>Factor of Safety</i>	1.34	-
Area _{slip Slope/W}	1722.5	m ²
Area _{slip surface Calc}	1700	m ²
Area _{slip surface Clay}	1585	m ²
M _{Resisting}	194450	kNm
M _{Activating}	145210	kNm
M _{End Surface}	1756679	kNm

The Factor of safety calculated in *Plaxis 2D* is 1.33. It is similar to the one obtained in the analytical calculations.

$$FS_{2D-Plaxis} = 1.33$$

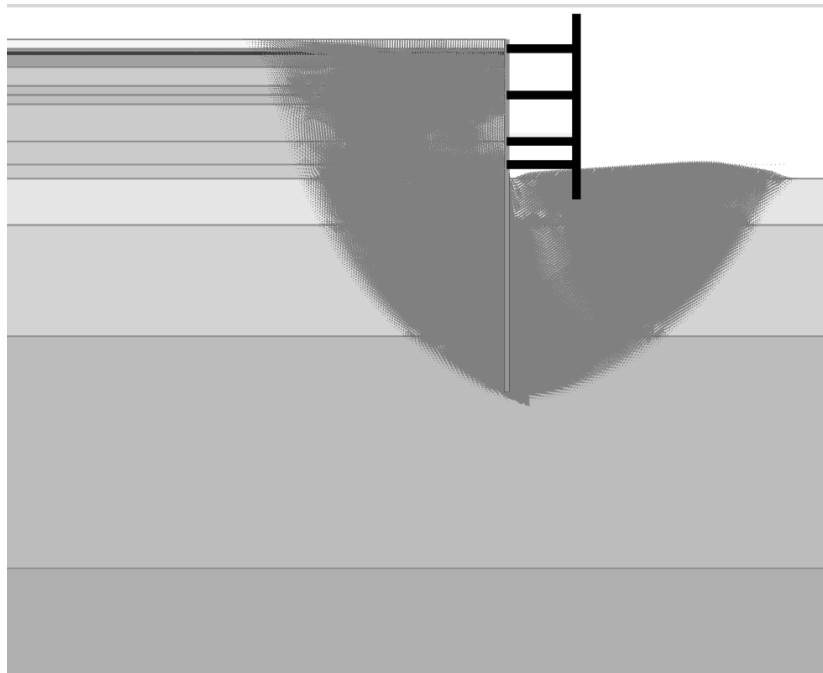


Figure 5:15 – Plaxis 2D, displacement

Table 5:8 - Result 2D, Real-life case

Results 2D		
	<i>2D - Analytical</i>	<i>Plaxis 2D</i>
Factor of Safety	1.34	1.33

2D-Calculations with 3D-effects

The approximated area for each soil layer and the respective average shear force is then used when calculating the end surface moment $M_{\text{End Surface}}$. The difference between the summarised approximated areas for the soil layers and the original area given by Slope/W is less than 1% and therefore considered a good enough approximation.

$M_{\text{End Surface}}$ is then used in Equation 2:1 to calculate the new FS considering end surface effects. In correlation with the *CSS report 3:95*, the FS has been evaluated for a number of different slip surfaces to ensure that the slip surface chosen still is the most critical one even after the increase. The increased 2D FS is shown in Figure 5:16.

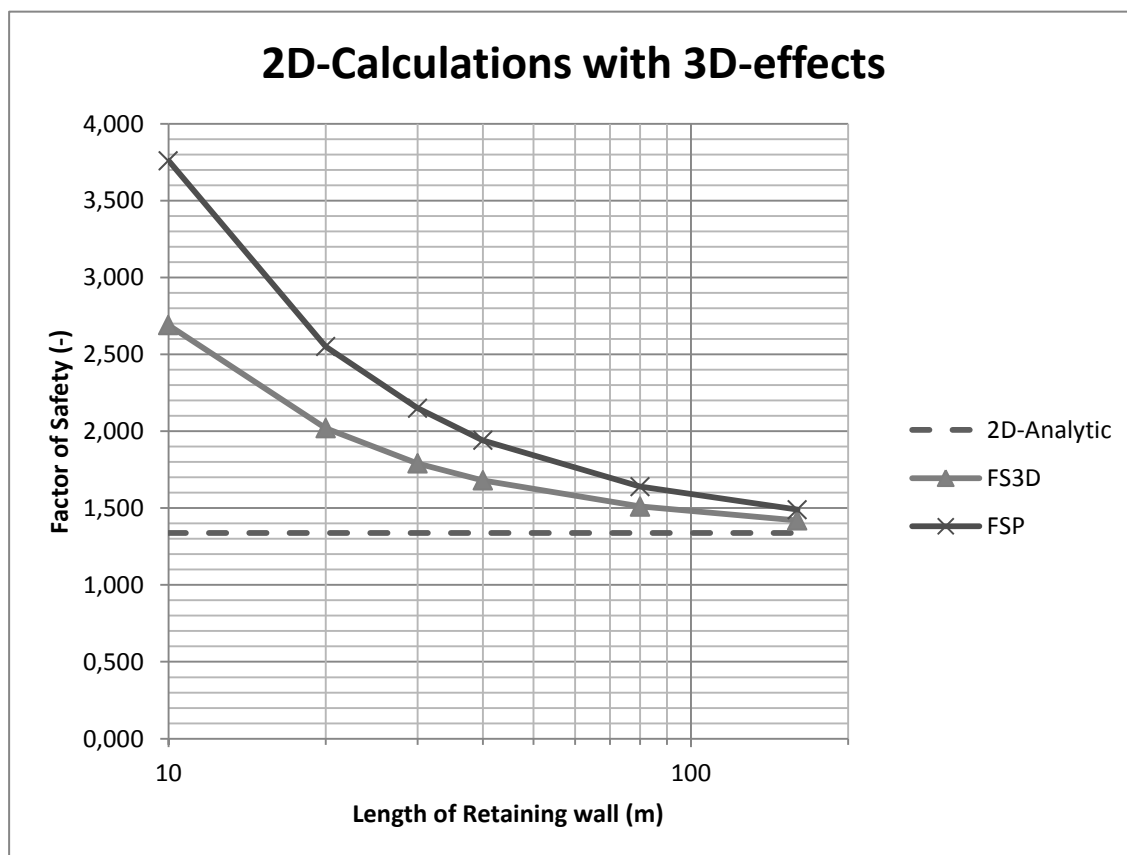


Figure 5:16 – 2D-calculations results with 3D-effects

The FS is unsatisfying if analysed analytically in 2D ($FS=1.34$), When considering end surface effects, sections up to 70 meters still have satisfying FS (above 1.56 in this case). This applies to both planar end surfaces FS_P and FS_{3-Dim} , which is the reduced FS due to non-planar end surfaces.

Three- Dimensional calculations

In Figure 5:16 the $FS_{3D-Retaining\ wall}$ for different lengths of the excavation with the width of 70 m is evaluated and presented in comparison with the analytical FS .

As for both the general cases the analytically increased FS is on the safe side compared to the numerically calculated FS . The difference between FS_P and $FS_{3D-Retaining\ wall}$ is presented in percentage in Table 5:9.

It can also be seen that the 3D-effects decrease drastically for lengths exceeding 40 m. This is thought to be due to geometrical effects that will be discussed later.

It should also be noticed that if one chooses not to consider the shoring and start at $FS=1.1$ the same calculation can be made (for its respective slip surface and area) but it will consequently give a shorter accepted section while still having a satisfying FS .

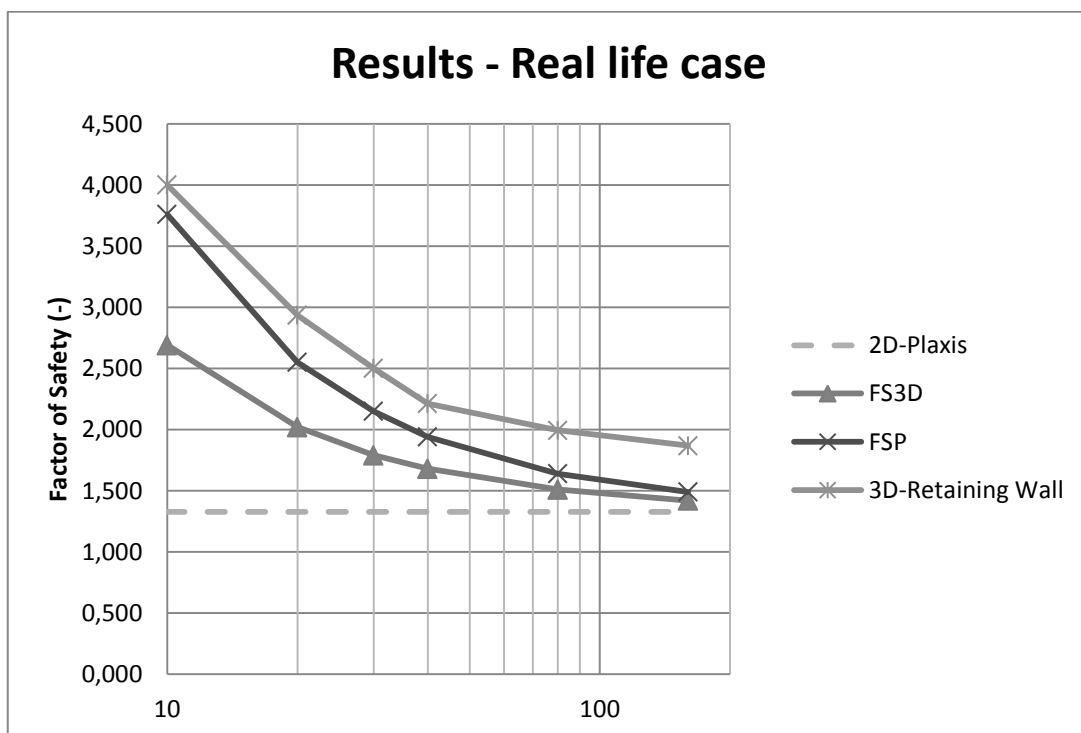


Figure 5:17 – Result visualisation for real-life case

Table 5:9 - Result summarisation for real-life case

Factor of Safety – All calculation types for different length of retaining wall						
Length of slope (m)	2D Analytic	2D Plaxis	<i>FS_P</i>	<i>FS_{3D}</i>	<i>FS_{3D} Retaining wall</i>	Diff. <i>FS_P</i> and <i>FS_{3D} Retaining wall</i> (%)
10	1.34	1.33	2.69	3.76	4.00	6.0 %
20	1.34	1.33	2.02	2.55	2.94	13.1 %
30	1.34	1.33	1.79	2.15	2.54	15.3 %
40	1.34	1.33	1.68	1.94	2.21	12.3 %
80	1.34	1.33	1.51	1.64	1.99	17.8 %
160	1.34	1.33	1.42	1.49	1.87	20.3 %

6 Discussion and Conclusion

6.1 Discussion

The goal with this project has been to evaluate and answer the stated objectives. The goal for us as students has also been to gain a greater level of knowledge into the geotechnical industry and geotechnical FE-modelling.

When analysing the results for the generalised slopes-systems it becomes apparent that in addition to the increase in FS when comparing it to the analytical calculations (with and without considering the 3D-effects), there are also other stabilising phenomena surrounding the corners. This could possibly be some kind of interaction between the different sliding volumes in a 3D-system pushing against each other.

Using the end surface theory to describe the 3D-slope-system is in this case an underestimation of the increased stability compared to the FE-calculations. Obvious in the results is that considering the 3D-effects is a better determination of the FS than not doing so. This is in accordance with the *CSS report 3:95*.

Finally we conclude that the 3D-effects can be applied to a 2D-calculation and get results that come close to the modelled slope-systems for geometries subjected to total stability failure.

The results show that between 15 and 80m the difference between 2D calculations considering 3D-effects and 3D-modeling is similar but with an increase of roughly 14%. This indicates that the approximation with FS_p is on the safe side compared to the FE-calculated FS i.e. there is possibility to account for even more stability in the 2D-calculations. The results indicate the approximation is on the safe side, to generally account for more stability in analytical calculations is by the author's believed to be the case. Since this work has only evaluated one generalised case and one real-life case further investigations are needed with a more complete range of geometries and material parameters.

Sloped excavation pits smaller than 15X15 m has a higher FS in the FE-calculations than the analytical calculations. This is thought to be partly due to stabilising effects around corners but mainly due to the fact that it is no longer the same failure

mechanism presented from the FE-calculations, as for the analytical calculations. The smaller sloped excavation pits give a misleading FS analytically since Slope/W cannot handle symmetry and for small excavations the slip surfaces will interact with the one from the opposite side.

In this work (according to analytical calculations) they start to interact at 12m and below. If this distance from where the slip surface penetrates the bottom is larger than the excavated bottom it should also be considered in the analytical calculations, it is not considered in this comparison but the FS would as the FE-model does increase drastically. This is also depending on a couple of assumptions made in the work, such as assuming that the slope is fixed in the middle.

When the lengths of the sides in the sloped-excavation are larger than 80 meters the factor of safety will become close to the FS of the modelled infinite long slope (2D slope) for the 3D-system. This means that the slope starts to behave like a 2D-case due to the fact that the shear force in the end surfaces can no longer transfer the excessive moment further.

According to the *CSS report 3:95* theories, the excessive moment can be transferred to the nearby masses of the slope section that is being calculated and it is transferred through the shear-force of the end surfaces. If comparing the maximal theoretical length with the maximal length possible from the FE-modelling it is evident that there are additional effects around the corners that either move the boundary of where the corner is thought to be stable (still able to carry the transferred moment from the slope) or that other effects helps absorb the acting moment from the slope.

Treating each side in a square excavation with slopes as a 2D-slope appears to be on the safe side. This conclusion can be drawn after comparing the modelled results to the increased 2D results in this work. Nothing indicates that the corners cannot withstand the transferred moment from the slopes on each side.

The results show that the end-surface forces will influence the FS for some lengths. The FS_p has also shown to be a better approximation than the reduced FS_{3-dim} (with our objectives in mind, compared to our models).

For the questions regarding how well the end surface effects, approximate the FS in systems with retaining structures; the results indicate some interesting things. From the results one can see a distinct pattern along the length of the excavation and the factor of safety. The 2D case modelled in *Plaxis* has a higher FS than the analytical FS for the general models. The reason for this is the fact that the analytical calculations was not considering the forces from the retaining-structure itself other than forcing the critical slip surface below the retaining wall. When introducing a point load at the

level of the wailing beam the 2D-calculations become similar, therefore it is reasonable to consider in the analytical 2D-calculation.

When 2D-methods are used to evaluate how a 3D-system with supporting structures behaves the simplifications and underestimations become apparent. There are many aspects to consider when moving from a 2D-system into an excavation with several sides. In this case the retaining structure forms a boxed-system in the ground. With the additional effects from the stiffness of the construction in mind just using the 3D-effects from the end surface theory is a modest approximation at best.

In the same manner as mentioned above about the additional effects from the corners, which might be more accurately named geometrical effects, the structure affects the total stability in a positive way. This is obvious and is also proved when modelling a construction around all sides of the excavation. The retaining structure works as one connected unit which generates a higher *FS* compared to the models with a retaining structure along one side and prescribed conditions along the others.

The effect that the supporting structures have on total stability is related to what material-model, the structural elements are modelled with and the way they interact. One can conclude that whether the retaining structure is geometrically connected or not there are positive effects brought to the total stability.

Unfortunately *Plaxis 3D* has the limitation of only being able to model plate elements (used for retaining-walls) with a linear-elastic material model. This is why a reliable and reasonable contribution from the structure is impossible to determine.

The “unconnected” case does not consider any of the strength in the structure around the corner but illustrates the stabilising effects of the surrounding soil which also affects the system in a positive way.

When evaluating the results for the *Västlänken* case there are some results to discuss; When first not considering the forces from the wailing beams in the analytical calculations the difference in *FS* between analytical and numerical calculation were unacceptable. When considering these forces as externally acting forces on the sliding soil volume we got close to equivalent *FS*. Evident is that it is advantageous but that it needs further investigation.

From the results presented one can see that a 70x70 m excavation could be possible if the increase in stability from the shoring is accounted for in the analytical calculations (if the sought *FS* is 1.56). For the *Västlänken* excavation there is a high probability that an excavation of 70x70 meters is possible to excavate without accounting for the stability from the connections between the retaining walls.

Throughout this work, FS_p has shown to be a better approximation compared to the FE-calculations. FS_p allows for an excavated geometry of 70x110 m compared to FS_{3-dim} which allows for 70x60m (based on $FS=1.56$).

It should also be noticed that if one chooses not to consider the shoring in the analytical calculation it will consequently give a shorter accepted section for a satisfying FS .

When studying the results from the real-life case, it becomes apparent that the FS increase/decrease drastically before and after 40 m. As mentioned the authors believe this to be a geometrical effect due to that the influence of the resisting moment for sections below 40 meters becomes very large compared to the activating moment. This increase is also apparent in the end surface calculations and therefore believed to be the main factor for this phenomenon.

Finally we can see that the generalised case and our real-life case behave similar. Approximating a 3D-system with 2D end surface theories is thought to be a safe approximation. The numerically calculated FS is probably even higher.

From our extensive work with *Plaxis 3D* some observations are made that require further discussion and attention. It is our conclusion that the one/ones performing modelling in this type of software should always question and try to validate the results. For example it has been observed that a minor change in the detail of the mesh can generate a difference between having a model that is stable and a model that is collapsing.

Plaxis 3D does not allow for a high amount of control when it comes to structural elements; how they interact with other structures and also a number of other problems with structural properties which are not possible with our knowledge to edit in the *Plaxis 3D* software.

Apparent throughout the process of this master's dissertation is the fact that the creation of geotechnical models in *Plaxis 2D* and *3D* is quite easy to do, but the consequences of not knowing the underlying calculations and theories could be quite catastrophic.

6.2 Suggestions for further work

From all the things that we have discussed during this project there are some phenomena and problems that need to be investigated further and could be suitable for further work.

The same model could be modelled in other FE-programs, preferably a program which can model structures better than *Plaxis* allows for. Another thing to look at is how the variation of excavated depth relative chosen depth for the retaining wall impacts the *FS*. The calculated 3D-effects will vary with a change in the area of the critical clip surface which is directly related to the different depth of the retaining structure.

The aim of this work was limited to evaluate cohesion soils. Similar evaluation for friction materials could be performed with the same modelling principles but with different material models and other analytical theories.

For the analytical calculations it would be interesting to further validate the possibility and reasonability of including the shoring as point loads in the analytical total stability calculations. Is including the shoring a more valid case or is there something that happens in *Plaxis* which generates a higher *FS* than the analytical calculations? Without these loads inserted into the analytical calculations the difference is quite significant.

It would be of great interest to measure the effects when the *Västlänken* excavation is constructed in reality. It would also be valuable to compare these measurements to numerical results and evaluate the accuracy of the numerical programs when dealing with these types of soils.

7 Bibliographies

Chowdhury, R., Flentje, P., Bhattacharya, G., (2010). *Geotechnical Slope Analysis*. UK: Taylor & Francis Group.

Engelstad, Ø., (2002). *Götatunneln, slissevegger. Omtale av forskjellige aspekter, løsningsvalg*. Bergmekanikk/Geoteknikk: Fjellsprengningsteknikk – 2002. 26.1-26.24.

Fredlund, D. G., Krahn, J., (1977). Comparison of slope stability methods of analysis. *Canadian geotechnical journal Vol. 14*, 429-439.

Geo-Slope International, (2012). *SLOPE/W 2012 – Slope Stability Analysis*. Available: <http://www.geo-slope.com/products/slopew.aspx>. Last accessed 2014/03

Lee, F.-H., Yong, K.-Y., Quan, K.C., Chee, K.-T., (1998). Effect of corners in strutted excavations: Field monitoring and case histories. *Journal of geotechnical and geoenvironmental engineering 124*, 339–349.

Ottosen, N.S., Ristinmaa, M., (2005). *The Mechanics of Constitutive Modeling*, first edn, Elsevier Science, The Boulevard, Langford Kidlington, Oxford OX5 1GB UK.

Ou, C., Shiau, B., (1998). Analysis of the corner effect on excavation behaviors. *Canadian geotechnical journal Vol. 35*, 532-540.

Persson, H., Sigström, D. (2010). Staged excavation in soft clay supported by a cantilever sheet pile wall, Master's thesis, Division of GeoEngineering, Chalmers University of Technology, SE-412 96 Göteborg, Sweden, Available: <http://publications.lib.chalmers.se/records/fulltext/126038.pdf>

Plaxis, (2013). *Plaxis – Scientific Manual*. Available: <http://www.Plaxis.nl/files/files/3D2013-4-Scientific.pdf>. Last accessed 2014/03

Plaxis Tips (n.d), *Plaxis - Fixities and deformation boundary conditions in PLAXIS 3D*, Available: <http://kb.Plaxis.nl/tips-and-tricks/fixities-and-deformation-boundary-conditions-Plaxis-3d>. Last accessed 2014/04

Plaxis 2D, (2013). *Plaxis 2D – Reference Manual*. Available: <http://www.Plaxis.nl/files/files/2DAnniversaryEdition-2-Reference.pdf>. Last accessed 2014/03

Plaxis 3Da, (2013). *Plaxis 3D – Reference Manual*. Available: <http://www.Plaxis.nl/files/files/2D2013-2-Reference.pdf>. Last accessed 2014/04

Plaxis 3Db, (2013). Plaxis 3D – Material Models Manual. Available:
<http://www.Plaxis.nl/files/files/3D2013-3-Material-Models.pdf>. Last accessed 2014/03

Ristinmaa, M., (n.d). *Beräkningsbaserad materialmodellering Course, lecture notes, Solid Mechanics, Faculty of Engineering, LTH*, Available:
http://www.solid.lth.se/education/courses_swedish/beraekningsbaserad_materialmodellering_fhln05/literature-and-software/. Last accessed 2014/03

Ronaldo, I., (2013). *Plasticity Modeling and Computation*, first edn. Springer-Verlag Berlin Heidelberg. Springer Heidelberg New York Dordrecht London. E-book

Ryner, A., Fredriksson, A., Stille, H., (1996). *Sponthandboken – Handbok för konstruktion och utformning av sponter*. Stockholm.

Skredkommissionen, (1995). Skredkommissionen Rapport 3:95 – *Anvisningar för släntstabilitetsutredningar*. Linköping, IVA Skredkommissionen

Trafikverket, (2011). TK Geo II, *Trafikverkets tekniska krav för geokonstruktioner*. SWE, Trafikverket

Appendix

A - Material parameters

Real-life Case - Hardening soil

Clay-parameters (Hardening Soil material model)

Material		Clay 1	Clay 2	Clay 3
Top	(level)	-1	-3	-5
Bottom	(level)	-3	-5	-13
Drainage-	type	Undrained B	Undrained B	Undrained B
γ_{unsat}	(kN/m ³)	16	16	16
γ_{sat}	(kN/m ³)	16	16	16
C_u	(kPa)	15	15	15
$C_{u,inc}$	(kPa)	0	1,6	1,6
y_{ref}	(level)	---	-3	-3
E_{50}^{ref}	(kPa)	11250	16500	25000
p^{ref}	(kPa)	100	100	100
E_{oed}^{ref}	(kPa)	7500	8300	12300
E_{ur}^{ref}	(level)	23650	36650	53600
m	---	1	1	1
v'_{ur}	---	0,2	0,2	0,2
K_0	---	2,381	1,479	1,086
OCR^*	---	10,17	4,28	2,44
R	---	1	1	1
R_f		0,9	0,9	0,9
$k_x=k_y$	(m/day)	$8,64 \cdot 10^{-5}$	$8,64 \cdot 10^{-5}$	$8,64 \cdot 10^{-5}$
M_0	(MPa)	7,5	7,5	7,5
$M_{0,inc}$	(MPa)	0	0,8	0,8
$y_{ref,M0}$	(MPa)	-3	-3	-3
M_{ul}^{**}	(MPa)	14	33,3	40
$M_{ul,inc}$	(MPa)	9,65	3,35	3,4
$y_{ref,Mul}$	(MPa)	-1	-3	-5
σ'_0^{***}	(kPa)	6	18	48
σ'_c^{***}	(kPa)	61	77	117
C_u	(kPa)	23,5	26	30,5
E_{50}/E_{oed}	(kPa)	1,5	2,0	2,0
$E_{ur}^{ref}/E_{50}^{ref}$	(kPa)	0,48	0,45	0,47

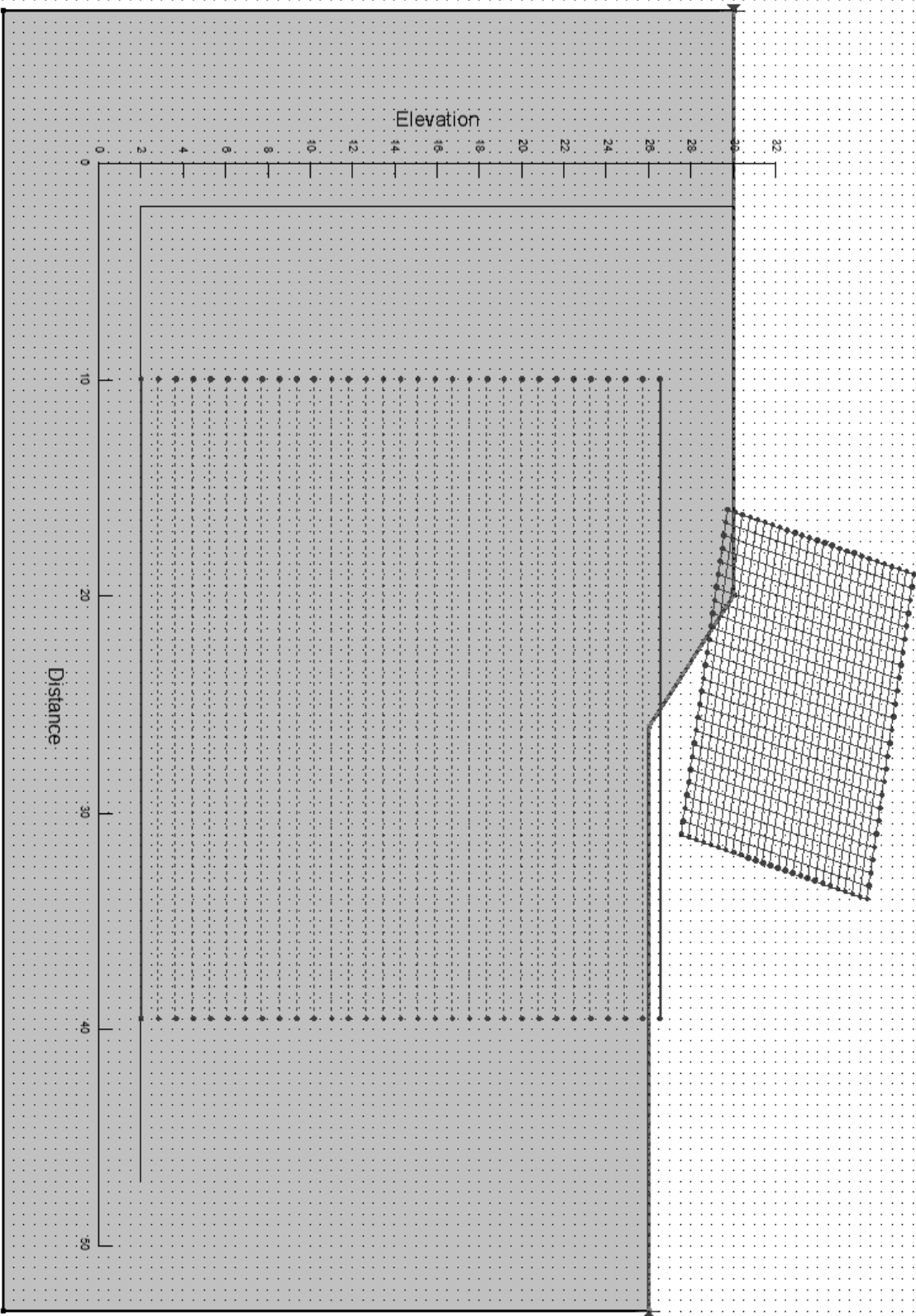
Material		Clay 4	Clay 5	Clay 6	Clay 7
Top	(level)	-13	-18	-30	-55
Bottom	(level)	-18	-30	-55	-80
Drainage-	type	Undrained B	Undrained B	Undrained B	Undrained B
γ_{unsat}	(kN/m ³)	16	16,1	16,5	16,8
γ_{sat}	(kN/m ³)	16	16,1	16,5	16,8
C_u	(kPa)	15	15	15	15
$C_{u,inc}$	(kPa)	1,6	1,6	1,6	1,6
y_{ref}	(level)	-3	-3	-3	-3
E_{50}^{ref}	(kPa)	35000	48500	78000	118000
p^{ref}	(kPa)	100	100	100	100
E_{oed}^{ref}	(kPa)	17500	24300	39100	59100
E_{ur}^{ref}	(level)	75700	105800	185100	299300
m	---	1	1	1	1
v'_{ur}	---	0,2	0,2	0,2	0,2
K_0	---	0,958	0,913	0,743	0,659
OCR^*	---	1,94	1,71	1,50	1,38
R	---	1	1	1	1
R_f		0,9	0,9	0,9	0,9
$k_x=k_y$	(m/day)	$8,64 \cdot 10^{-5}$	$8,64 \cdot 10^{-5}$	$4,32 \cdot 10^{-5}$	$4,32 \cdot 10^{-5}$
M_0	(MPa)	7,5	7,5	7,5	7,5
$M_{0,inc}$	(MPa)	0,8	0,8	0,8	0,8
$y_{ref,M0}$	(MPa)	-3	-3	-3	-3
M_{ul}^{**}	(MPa)	67,2	84,2	127,6	241,8
$M_{ul,inc}$	(MPa)	3,4	3,6	4,6	4,6
$y_{ref,Mul}$	(MPa)	-13	-18	-30	-55
σ'_o^{***}	(kPa)	87	139	256	423
σ'_c^{***}	(kPa)	169	237	385	585
C_u	(kPa)	48,5	60	97	147
E_{50}/E_{oed}	(kPa)	2,0	2,0	2,0	2,0
$E_{ur}^{ref}/E_{50}^{ref}$	(kPa)	0,46	0,46	0,42	0,39

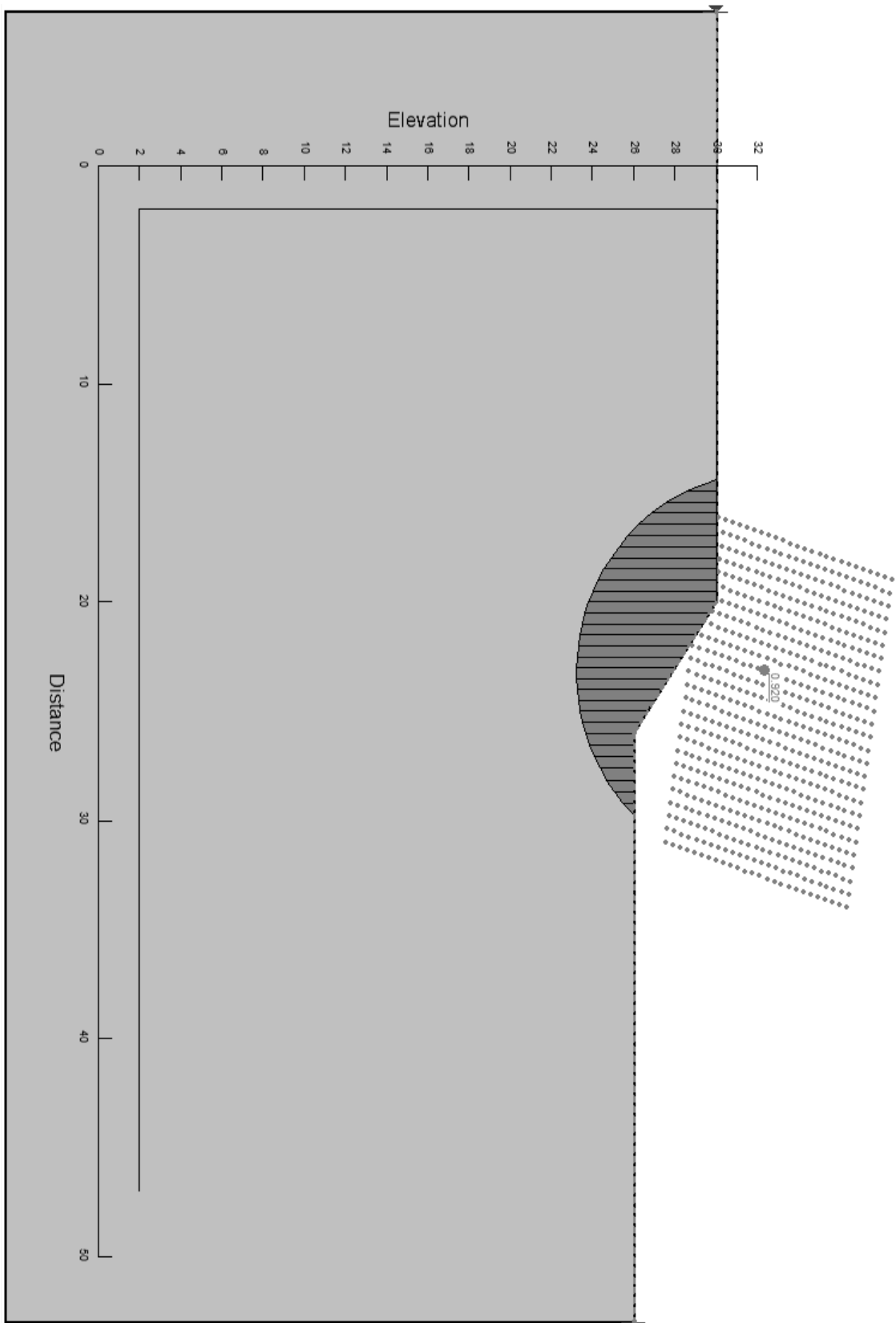
Fill-parameters (Mohr-Coulomb material model)

Material		Fill 1	Fill 2
Top	(level)	2	1
Bottom	(level)	1	-1
Drainage-	type	Drained	Drained
γ_{unsat}	(kN/m ³)	18	17
γ_{sat}	(kN/m ³)	21	21
ϕ'	(°)	38	35
c'	(kPa)	2	2
ψ'	(°)	5	2
E'	(kPa)	45000	20000
E'_{inc}	(kPa)	---	---
γ_{ref}	(level)	---	---
ν'	---	0,2	0,2
K_0	---	0,384	0,426
R	---	1	1
$k_x=k_y$	(m/day)	0,6	0,12

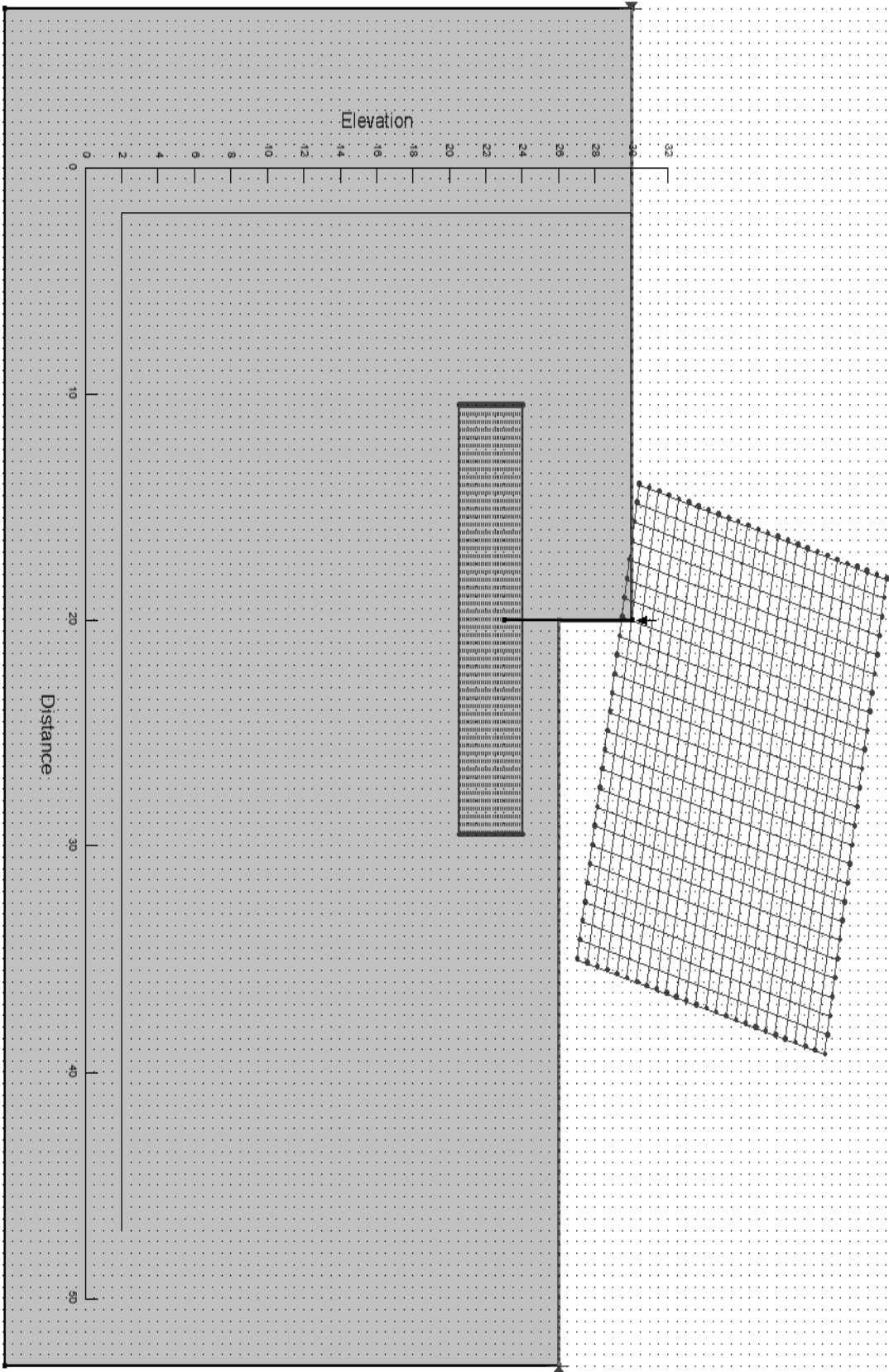
B - Slope results

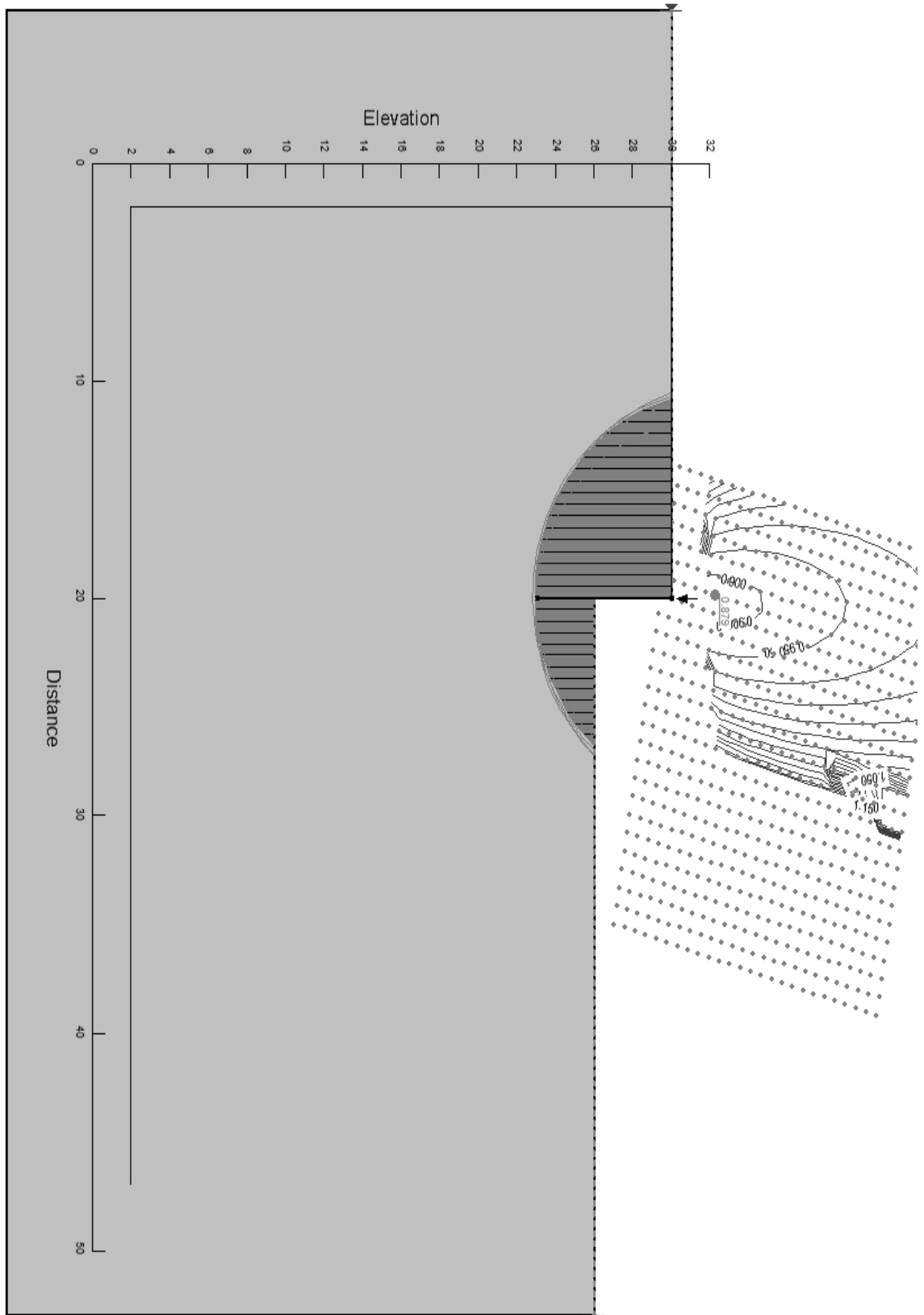
Generalised slope





Generalised slope with retaining structure





Meshing quality

The figure below illustrates the level of resolution that has been used for one of the models in the work. In this model the *Factor of Safety* is not changed with finer level of meshing.

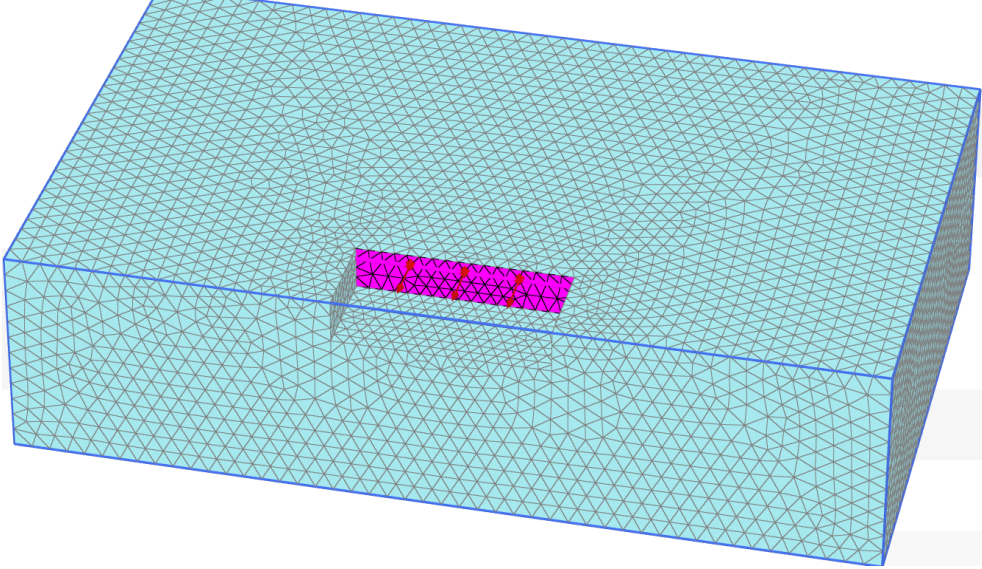


Figure - Illustration of mesh for a 3D-model

For this model the *Plaxis 3D* tool for evaluating meshing quality rates the worst element to 0,53.

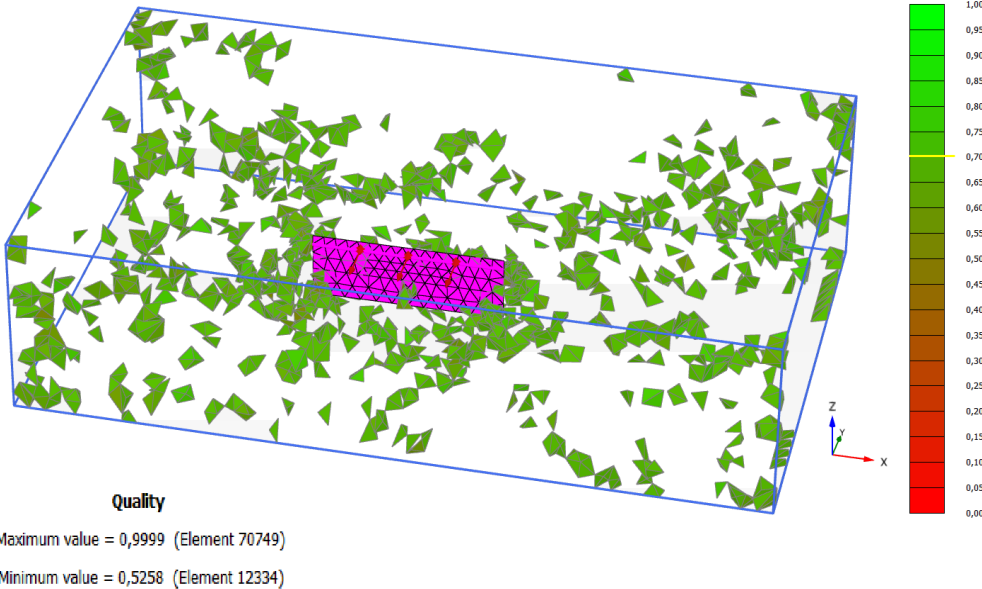
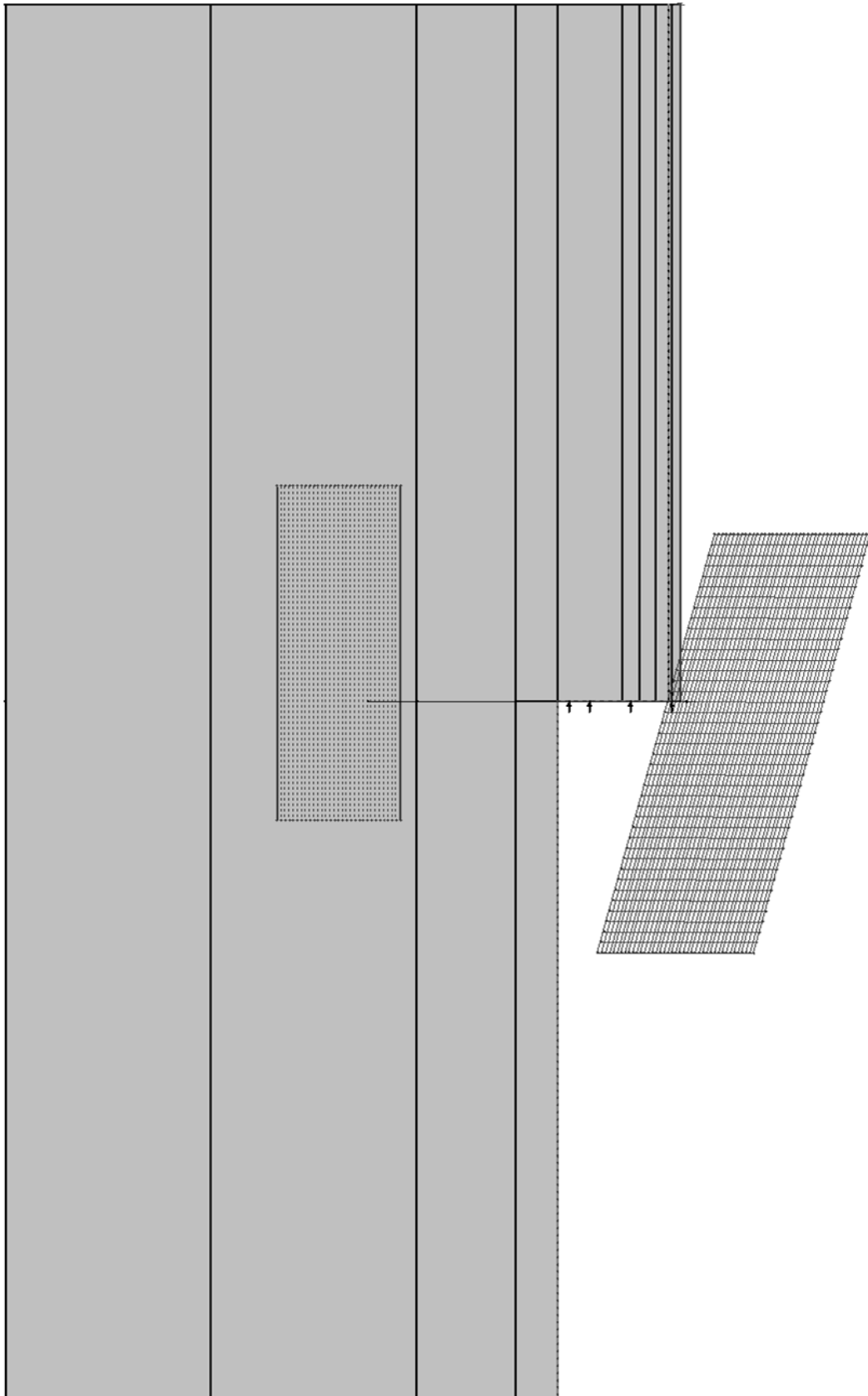
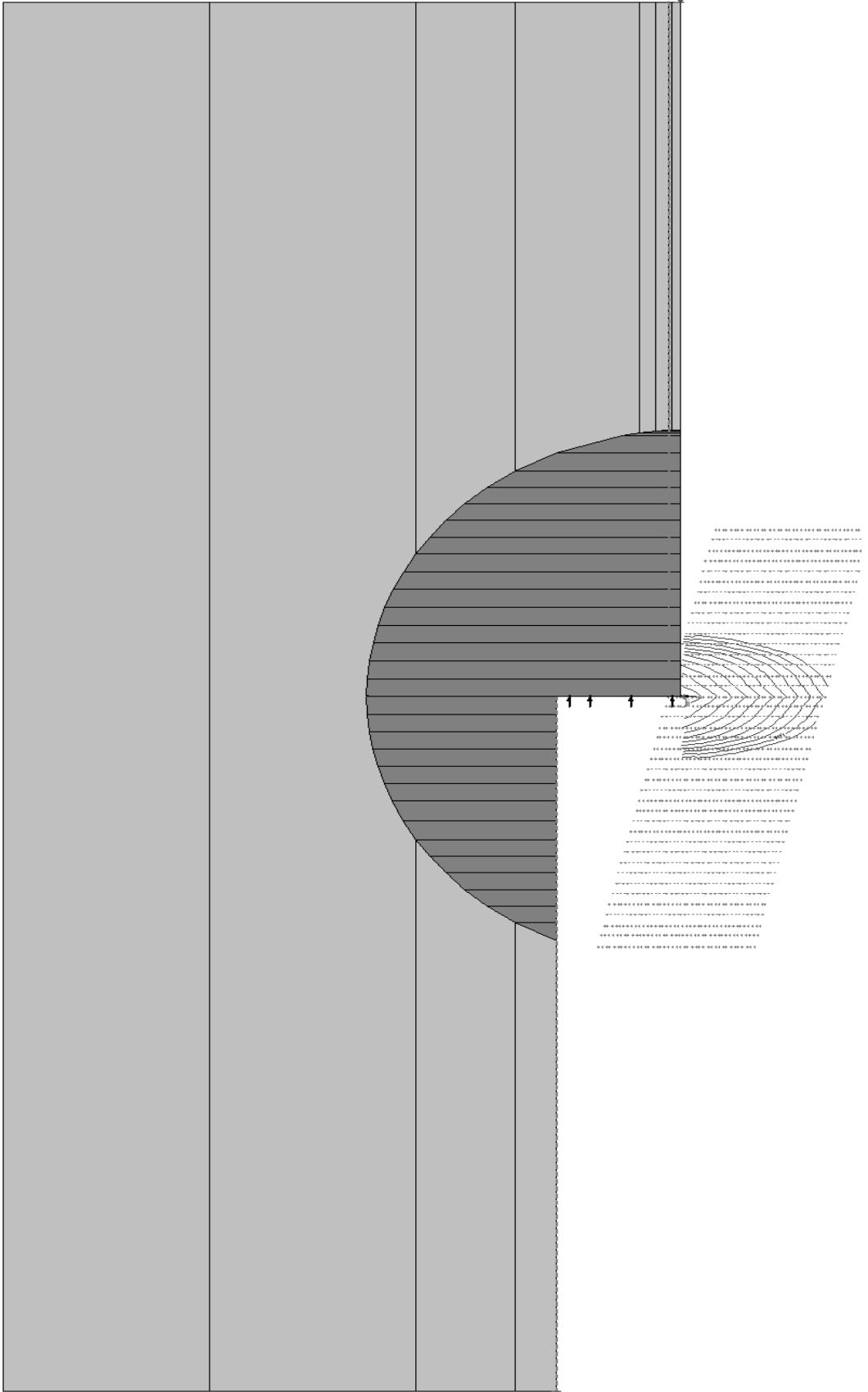


Figure - Illustration of the meshing quality for the same 3D-model

Real-life Case (Västlänken project)





Meshing quality

The figure below illustrates the level of resolution that has been used for one of the models in the work. In this model the *Factor of Safety* is not changed with finer level of meshing.

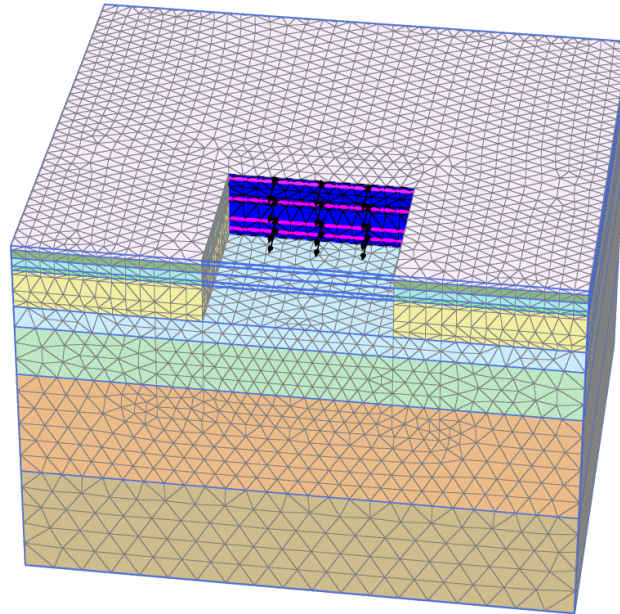


Figure – Meshing performed in Plaxis 3D

For the models the *Plaxis 3D* tool for evaluating meshing quality rates the worst element to 0, 30. This worst case is for the biggest model evaluated and the *Factor of Safety* does not change with finer meshing.

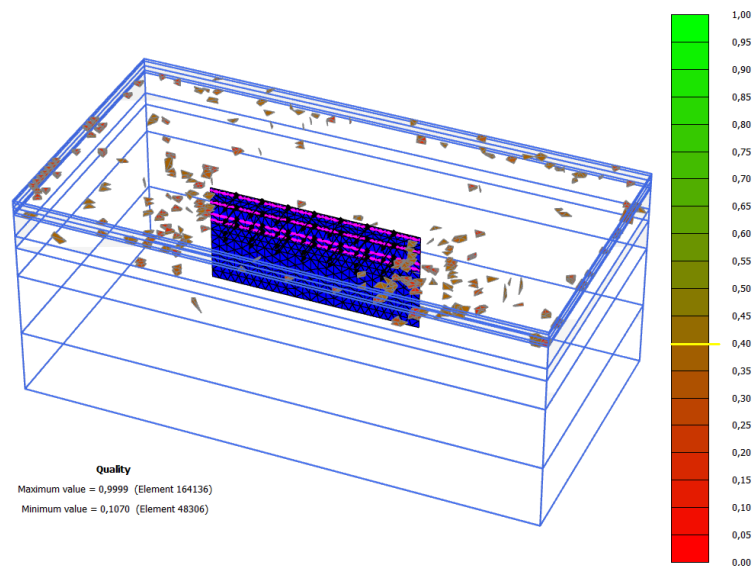
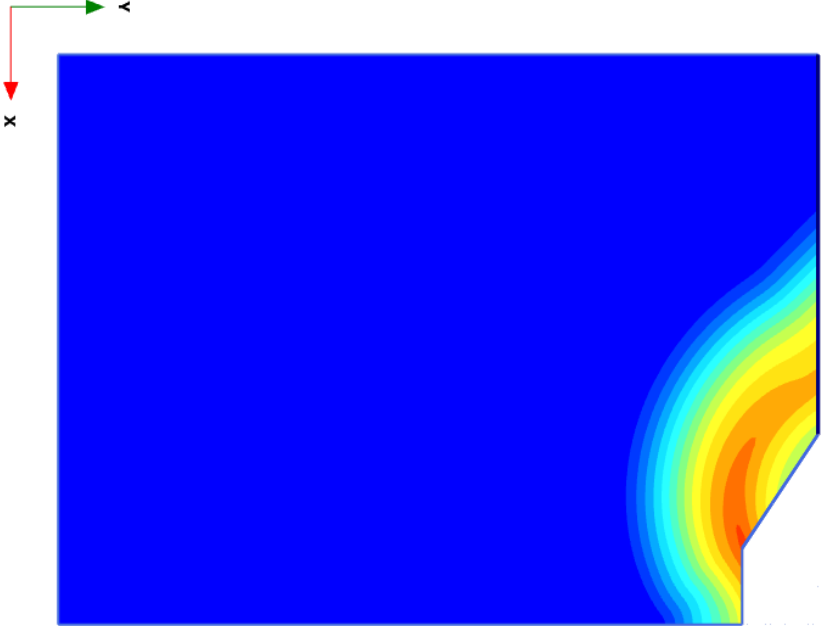
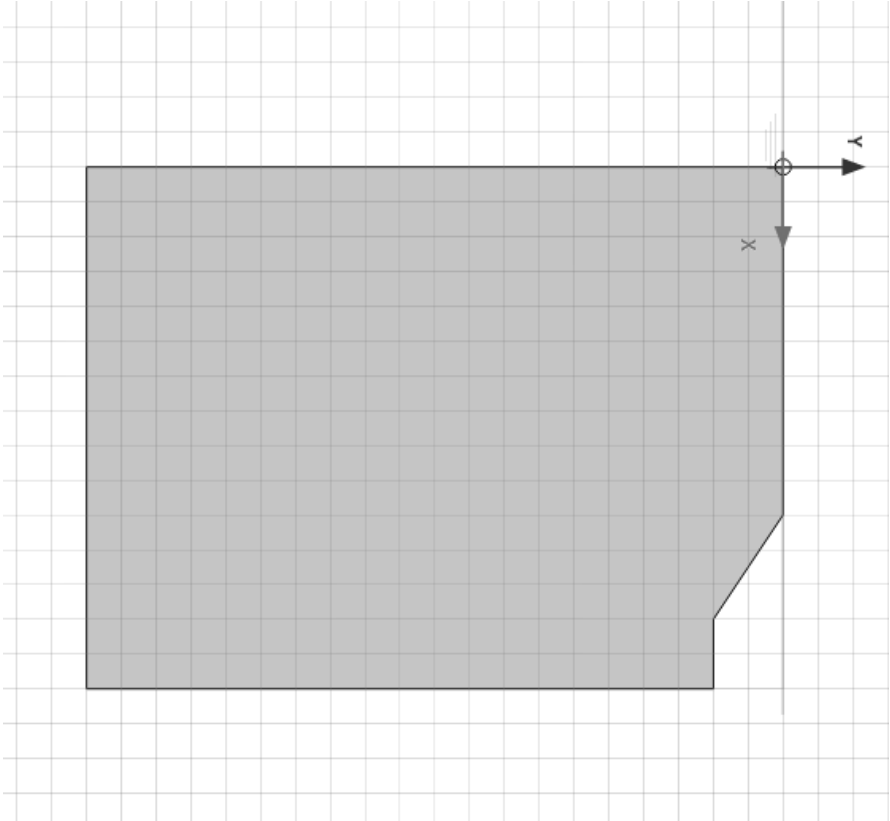


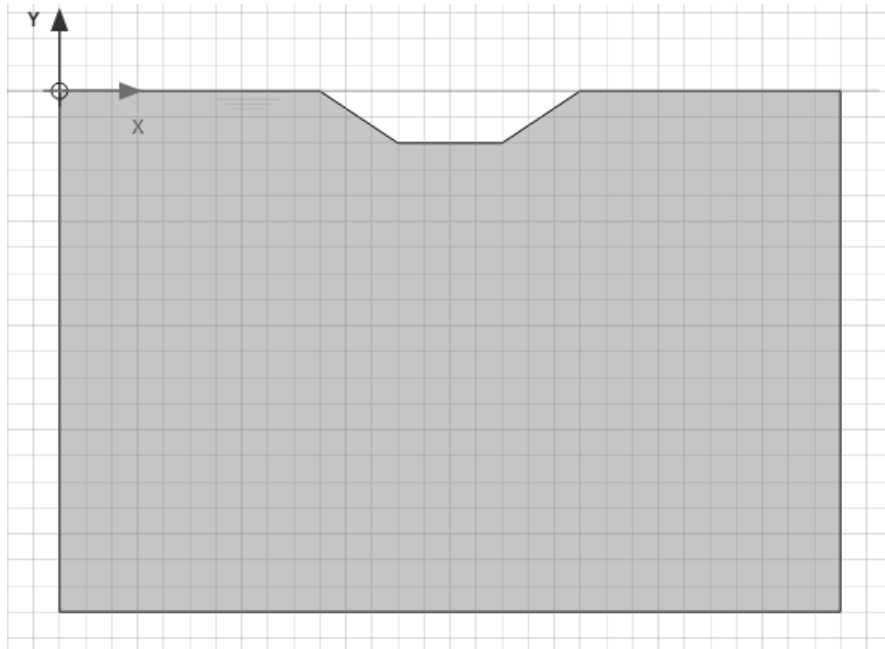
Figure – Meshing quality for worst case model in Plaxis 3D

C - Plaxis 2D Results

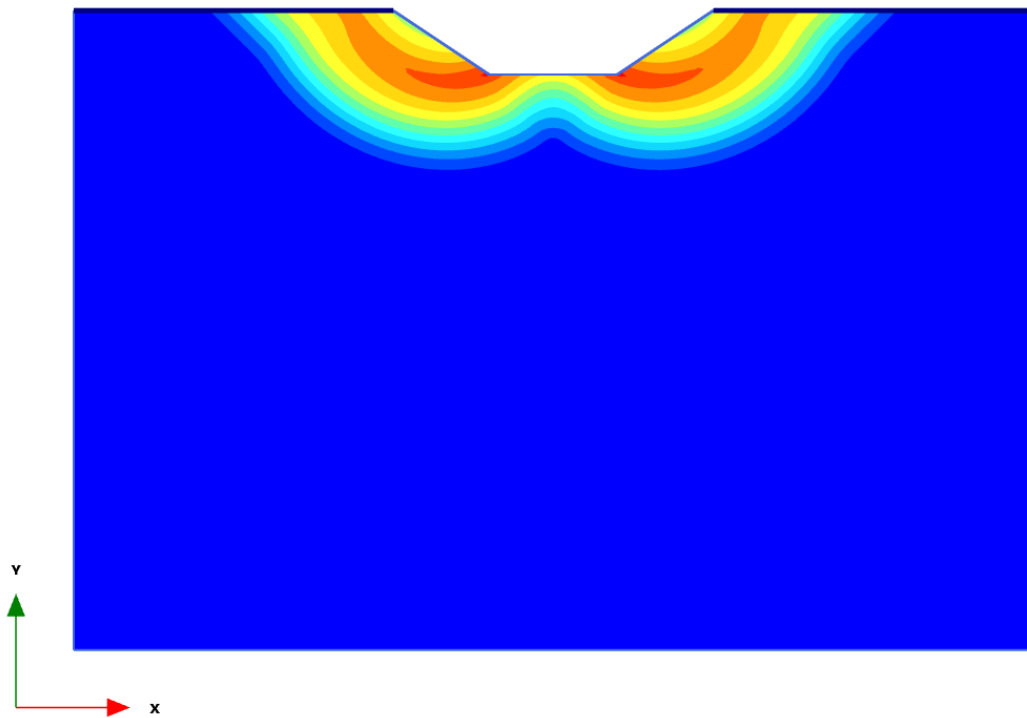
Symmetry validation

FS Half model = 5,19

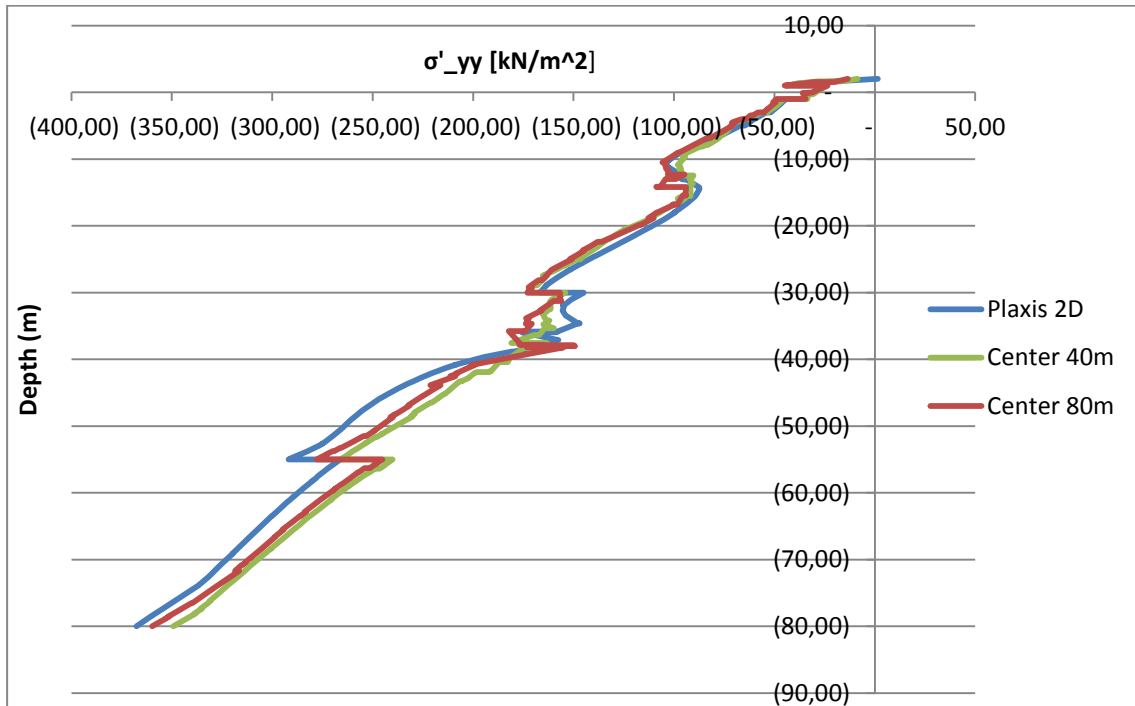




FS Full model = 5,19



D - Real-life case (Västlänken project)



Structural element	X [m]	Y [m]	N [kN]	Rotation [°]	Length [m]	CC [m]
Fixed-end anchor 1-1	3,50E+01	1,00E+00	4,05E+02	0,00E+00	1,70E+01	10
Fixed-end anchor 2-2	3,50E+01	-4,00E+00	6,78E+03	0,00E+00	1,70E+01	10
Fixed-end anchor 3-3	3,50E+01	-9,00E+00	1,08E+04	0,00E+00	1,70E+01	10
Fixed-end anchor 4-4	3,50E+01	-1,15E+01	8,82E+03	0,00E+00	1,70E+01	10

E – Structural elements in Plaxis 3D

The figure below shows the momentum in a) and deformation in b) for the plate element (retaining wall) for one side of the boxed case. As mentioned the structural element it is not plasticising why it withstand unreasonably large moments.

In b) it can be seen that the plate has no deformations in the corners. Instead of plasticising it generates big moments and form a skirt that forces the material under the retaining structure.

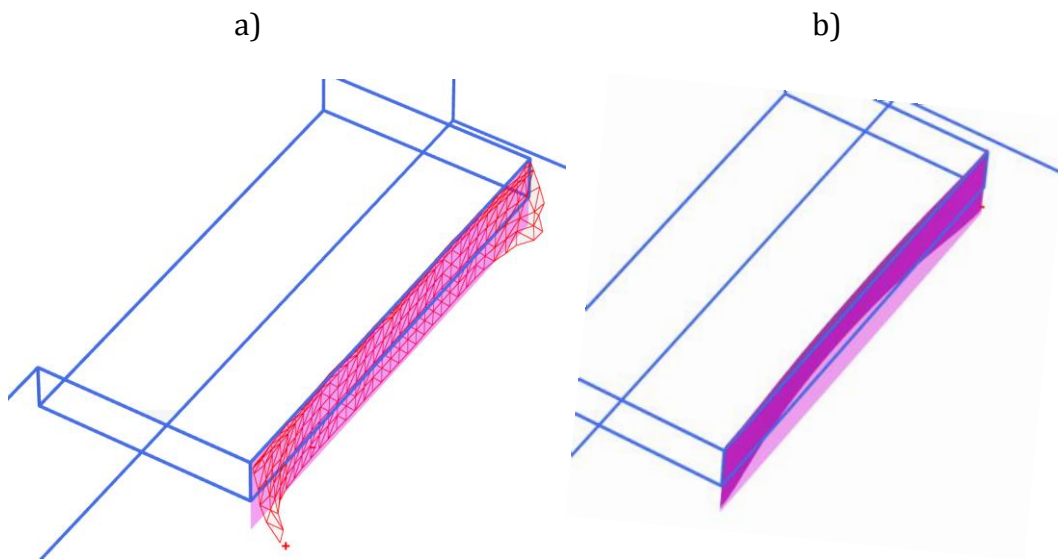


Illustration of the momentum in the plate for the 3D-model seen in Figure 5:10

The moment in the plate for the 3D-model seen in Figure 5:10

	Max	Min
Moment	2599 kNm/m	-334,4 kNm/m

Next figure shows the momentum in a) and deformation in b) for the plate element (retaining wall) for one side of the case with prescription along the other sides. The plate element is not fixed in the corners and do not take any moment.

In b) it can be seen that the plate is allowed to deformations in the corners. Instead of withstanding unreasonable large moment it deforms and allows for a total stability failure.

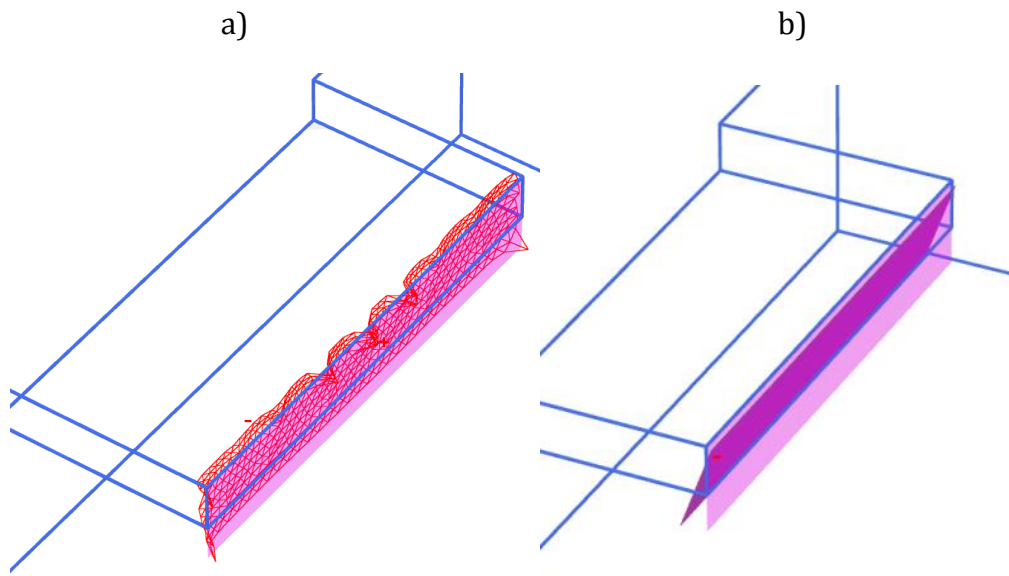


Illustration of the momentum in the plate for the 3D-model seen in Figure 5:11

The moment in the plate for the 3D-model seen in Figure 5:11

	Max	Min
Moment	52,48 kNm/m	-146,5 kNm/m

Reality lays somewhere in between where there is some stiffness to account for from the connections in the supporting structure.